

# **Theory of Steady-State Superradiance**

by

**Minghui Xu**

B.S., Electronic Engineering, Peking University, 2008

M.S., Physics, Peking University, 2011

A thesis submitted to the  
Faculty of the Graduate School of the  
University of Colorado in partial fulfillment  
of the requirements for the degree of  
Doctor of Philosophy  
Department of Physics

2016

This thesis entitled:  
Theory of Steady-State Superradiance  
written by Minghui Xu  
has been approved for the Department of Physics

---

Prof. Murray J. Holland

---

Prof. James K. Thompson

Date \_\_\_\_\_

The final copy of this thesis has been examined by the signatories, and we find that both the content and the form meet acceptable presentation standards of scholarly work in the above mentioned discipline.

Xu, Minghui (Ph.D., Physics)

Theory of Steady-State Superradiance

Thesis directed by Prof. Murray J. Holland

In this thesis, I describe the theoretical development of the superradiant laser, or laser in the extreme bad-cavity regime. In this regime, the cavity decay rate is much greater than the atomic dynamics. The atoms emit photons into the cavity mode superradiantly in steady state. We develop group-theoretic methods that enable us to exactly solve mesoscopic systems with hundreds of atoms. We demonstrate the synchronization of atomic dipoles in steady-state superradiance. With this synchronized system, we propose conditional Ramsey spectroscopy which allows us to observe Ramsey fringes indefinitely, even in the presence of atomic decoherence. Furthermore, we explore manifestations of synchronization in the quantum realm with two superradiant atomic ensembles. We show that two such ensembles exhibit a dynamical phase transition from two disparate oscillators to quantum phase-locked dynamics. Finally, we study the mechanical effect of the light-atom interaction in the steady-state superradiance. We find efficient many-body cooling of atoms. The work described in this thesis lays the theoretical foundation for the superradiant laser and for a potential future of active optical frequency standards.

## Dedication

To Mom, Dad, and Tianxiao

## Acknowledgements

I owe a tremendous thank you to my advisor, Prof. Murray Holland. Murray allowed me to be part of his group in the summer of 2012 when my first-year advisor Chris left JILA. Since then Murray has financially supported me. During the fall semester in 2013, I was stuck in China due to my F1 visa denial. In that semester, Murray did all he could to eventually get me back to the US. He worked through an exhaustive sequence of events, including working closely with lawyers and officials of the University. Under the intervention by Congressman Jared Polis, the situation was eventually reviewed and finally the determination was made that the original decision by the US Embassy was actually made in error. I am now typing the acknowledgements, full of gratitude, also because Murray has been an excellent scientific mentor. Murray lead me to the fruitful project of steady-state superradiance, in which he has keen physical insights and a wealth of creative ideas. He is always available for discussion and providing potential solutions and guidance. On top of all these things, Murray has also been a good friend.

Special thanks to John (a.k.a. Jinx) Cooper. Jinx is a quantum optics guru and has been enthusiastic about steady-state superradiance. Among numerous things that he has taught me, I feel that these two are most important for research. As he always says, “Once you get the physics right, math is simple”, and “Do not trust anything unless you derive it by yourself”. There is a good example for the latter. Jinx was acknowledged by J. D. Jackson in the Classical Electrodynamics (a standard graduate textbook) because he found quite a few improvements when he taught that class.

I would like to thank the faculty here at the University of Colorado. I am especially grateful to Chris Greene, Ana Maria Rey, Juan Restrepo, Victor Gurarie, Lijun Chen, Oliver Dewolfe,

Michael Hermele, James Thompson, and Jun Ye. I benefited a lot from interactions with them.

Here are even more people who helped me understand physics: David Tieri, Effie Fine, Stefan Schütz, Giovanna Morigi, Dominic Meiser, Tony Lee, Ching-Kit Chan, Jose D’Incao, Bihui Zhu, Victor Colussi, Peiru He, Athreya Shankar, Zhexuan Gong, Alexey Gorshkov, Michael Foss-Feig, Johannes Schachenmayer, and Kaden Hazzard. Special thanks to David. He has been a super nice officemate and extremely helpful.

## Contents

<b>Chapter</b>	
<b>1</b> Introduction	<b>1</b>
<b>2</b> The superradiant laser	<b>5</b>
2.1 Dicke superradiance . . . . .	5
2.2 Laser theory in a nutshell . . . . .	9
2.3 Steady state superradiance . . . . .	14
<b>3</b> Group-theoretic methods for solving the laser equation	<b>22</b>
3.1 Lindbladian in terms of generators of the $SU(4)$ group . . . . .	22
3.2 Generalized Dicke states . . . . .	25
3.3 Calculating observables . . . . .	28
3.4 Transform to the angular-momentum basis representation . . . . .	29
3.5 Further simplifying: $U(1)$ symmetry and quantum jump . . . . .	32
<b>4</b> A new perspective on steady state superradiance	<b>35</b>
4.1 Synchronization of atomic dipoles . . . . .	35
4.2 Probing the synchronization with Ramsey spectroscopy . . . . .	37
4.3 Robustness of the synchronization . . . . .	42
4.4 Conditional Ramsey spectroscopy with synchronized atoms . . . . .	42

<b>5</b>	Quantum synchronization of two ensembles of superradiant atoms	<b>47</b>
5.1	Setup . . . . .	48
5.2	Mean-field picture . . . . .	49
5.3	Quantum signatures of the synchronization . . . . .	50
<b>6</b>	Supercooling of atoms based on steady-state superradiance	<b>59</b>
6.1	Cavity cooling in the strong coupling regime . . . . .	59
6.2	Supercooling . . . . .	63
<b>7</b>	Summary and outlook	<b>78</b>
	<b>Bibliography</b>	<b>79</b>
	<b>Appendix</b>	
<b>A</b>	Adiabatic elimination	<b>89</b>
<b>B</b>	$SU(4)$ generators and $\lambda$ -matrices	<b>91</b>
<b>C</b>	$ S, M\rangle\langle S, M' $ representation	<b>93</b>

## Tables

### Table

3.1	The action of the $SU(4)$ superoperators on the elements of the fundamental representation $u, d, s, c$ . . . . .	26
-----	---	----

## Figures

### Figure

2.1	Source: Ref. [42]. Comparison between the general characteristics of ordinary fluorescence and superradiance experiment. (a) Ordinary spontaneous emission is essentially isotropic with exponential decaying intensity (time constant $\tau_{\text{sp}}$ ). (b) Superradiance is anisotropic with an emission occurring in a short burst of duration $\sim \tau_{\text{sp}}/N$ . . . . .	6
2.2	Dicke states of $N$ two-level atoms. $S$ denotes the symmetrizer with respect to atomic labels. . . . .	7
2.3	Schematic for implementing the incoherent pumping in a three-level configuration. The coherent driving laser is indicated by the green-dashed arrow and spontaneous decay into the excited state $ e\rangle$ is indicated by the orange-dotted arrow. . . . .	10
2.4	Numerical simulation (blue dashed line) of a bad cavity laser. Left panel: Atom-atom correlation as a function of time. Right panel: Spectrum of the laser light (red solid line is the fit to Lorentzian). The parameters are $N = 200$ , $C = 0.2$ , $w = 18\gamma$ , $T_2^{-1} = 2\gamma$ , $\kappa = 2500\gamma$ . . . . .	19
2.5	Source: Ref. [93]. Power as a function of pump rate $w$ and atom number $N$ . The rapid buildup of power above threshold $w \sim \gamma$ can be seen as well as the decrease of emitted power for too strong a pump. The dashed line shows the boundary of the region of collective emission. . . . .	19

- 2.6 Source: Ref. [93]. (a) Linewidth vs  $w$  and  $N$ . The white dashed lines indicate (from left to right) the spontaneous decay rate  $\gamma$ , the inhomogeneous relaxation rate  $T_2$ , and the maximum pump rate  $w = NC\gamma$ . (b) is a cut through (a) for  $N = 10^6$  atoms. 21
- 3.1 (a) Young tableau for determining the irreducible representations contained in the direct product representation of the  $SU(2)$  group for  $N = 4$ . The dimension for  $S = 2, 1, 0$  is 5, 3, 1 respectively, and  $n_s = 1, 3, 2$ , so the total Hilbert space dimension is  $5 \times 1 + 3 \times 3 + 1 \times 2 = 2^4$  as expected. (b) ‘‘Pascal’s triangle’’ to evaluate  $n_S$  in an iterative way for any  $N$  (the case considered in (a) is the fourth row down from the top). (c) Pyramid representation of the density operator in the  $|S, M\rangle$  representation for  $N = 4$ . Each layer of the pyramid represents the block matrix for each  $S$ . . . . . 31
- 4.1 (a) Ramsey spectroscopy where atoms are coupled collectively to a cavity and pumped individually with incoherent rate  $w$ . (b) Ramsey sequence showing preparation in state  $|g\rangle$  (pseudospins pointing down to the south pole of the Bloch sphere), the  $\pi/2$   $y$ -axis rotation from the south pole to the equator, precession around the equator, and second  $\pi/2$   $x$ -axis rotation, after which the  $z$ -axis projection carries information about the cosine of the accumulated phase. . . . . 38
- 4.2 Calculations of Eq. (4.1) using  $SU(4)$  theory in Chapter 3 with  $N = 250$ ,  $\Gamma_C = 0.2/T_1$ ,  $T_2 = T_1$ , and  $w = N\Gamma_C/2$ . (a) Ramsey fringes with synchronized atoms (red solid line) versus  $T$ . Conventional Ramsey fringes (blue dashed line) for the same  $T_1$  and  $T_2$ . (b) During the interrogation time, the atomic inversion  $\langle \hat{\sigma}_j^z \rangle$  (blue dashed line), spin-spin correlation  $\langle \hat{\sigma}_j^+ \hat{\sigma}_k^- \rangle$  (red solid line),  $\langle \hat{\sigma}_j^+ \hat{\sigma}_k^- \rangle - \langle \hat{\sigma}_j^+ \rangle \langle \hat{\sigma}_k^- \rangle$  (red dotdashed line) and  $\langle \hat{\sigma}_j^+ \hat{\sigma}_k^z \rangle / (\langle \hat{\sigma}_j^+ \rangle \langle \hat{\sigma}_k^z \rangle)$  (green dotted line). . . . . 39
- 4.3 The decay rate  $\lambda$  of the visibility of Ramsey fringes at  $\Gamma_C = 0.2/T_1$  and  $T_2 = T_1$  as a function of repumping for  $N = 200$  and as a function of  $N$  for  $w = N\Gamma_C/2$  (Inset). The dots are numerical solutions of Eq. (4.1), and the solid blue line is the semiclassical approximation for comparison. . . . . 40

- 4.4 (a) The decay rate of the visibility of the Ramsey fringes as a function of standard deviation of the  $g$  factor at  $\Gamma_C = 0.2/T_1$ ,  $T_2 = T_1$ , and  $w = N\Gamma_C/5$  for  $N = 250$  atoms. (b) The decay rate of the visibility of the Ramsey fringes as a function of number of atoms at  $\Gamma_C = 0.2/T_1$ ,  $T_2 = T_1$ ,  $w = N\Gamma_C/5$ , and  $\Delta g/\bar{g} = 0.2$ .  $\Gamma_C$  in both (a) and (b) is defined using the mean of the  $g$  distribution,  $\bar{g}$ . Statistics are accumulated by sampling  $g$  from a Gaussian distribution. The dots are average values for 100 runs, and error bars represent the standard deviations. . . . . 43
- 4.5 Quantum state diffusion calculations of conditional Ramsey fringes subject to continuous homodyne measurement of the cavity output field for  $N = 10$  and  $w = N\Gamma_C/2$ . The blue dashed lines are the ensemble average for reference. (a) A typical Ramsey fringe for a single experimental trial (red solid line). (b) Histograms are the statistics of the positions of zero crossings of each fringe for 4000 trials. The blue solid lines are fitted Gaussian distributions with variance of  $T\Gamma_C$  centered on the zero crossing of the ensemble average. . . . . 45
- 5.1 Two ensembles of driven two-level atoms coupled to a single-mode cavity field. The atoms in ensemble  $A$  are detuned above the cavity resonance (dashed line). Ensemble  $B$  contains atoms detuned below the cavity resonance by an equivalent amount. . . . 48
- 5.2 Steady state value of population inversion  $\langle \hat{\sigma}_1^z \rangle$ , spin-spin coherence within each ensemble  $\langle \hat{\sigma}_1^+ \hat{\sigma}_2^- \rangle$  and correlation between ensembles  $\langle \hat{\sigma}_{A1}^+ \hat{\sigma}_{B1}^- \rangle$  as a function of detuning. Red dots are exact numerical calculation by applying the  $SU(4)$  group theory. Blue lines are semiclassical results based on solutions to Eq. (5.7) to (5.9). . . . . 52
- 5.3 Steady-state relative phase precession for two ensembles as a function of detuning at  $w = N\gamma_C/2$  for  $N = 100$  (blue dashed line),  $N = 500$  (purple dot dashed line) and  $N = 10^6$  (red solid line). The straight dotted line is  $\delta = \Delta$ . . . . . 53

- 5.4 (a) Nonequilibrium phase diagram of the quantum synchronization represented by  $\Gamma$  (in units of  $\gamma_C$ ) on the  $w$ - $\delta$  parameter plane, where the dissipative coupling  $N\gamma_C$  ( $N = 10^4$ ) is fixed. An abrupt peak is observed at the boundary between the synchronized and unsynchronized phases. (b) As for (a) but on the  $w$ - $N\gamma_C$  parameter plane. . . . . 54
- 5.5 Finite size scaling behavior of the quantum criticality for  $\delta = N\gamma_C/2$ . For  $N \rightarrow \infty$ , the critical pump rate is  $w_c = \delta$ . The red dots show the offset between the critical pump rate  $w_N$  for finite  $N$  and  $w_c$ . The blue squares show  $\Gamma$  (in units of  $\gamma_C$ ) at  $w_N$ . Both exhibit linear scalings on the log-log plot. . . . . 56
- 5.6 Classical correlation and quantum discord between one atom in ensemble A and one atom in ensemble B. The blue dashed line is based on semiclassical approximation described in the paper. The red dots are exact numerical calculations. There are 30 atoms in each ensemble. The comparison between these two lines indicates the “quantumness” of correlations present in our system. . . . . 57
- 6.1 An atom with velocity  $v$  is moving freely along the cavity axis. The atom coherently scatters the photons of the transverse laser into the cavity mode. The frequency of the laser  $\omega_L$  is red detuned from the cavity resonance frequency  $\omega_c$  by  $\Delta_c$ . Due to Doppler effect, the atom will scatter more photons into the direction along which it moves. . . . . 60

- 6.2 Atoms with ultranarrow transition  $|g\rangle \leftrightarrow |e\rangle$  are confined to the axis of a standing-wave mode of an optical cavity. Different implementations of pumping may be considered [12, 93]. In the simplest scenario shown, a transition is driven from the ground state  $|g\rangle$  to an auxiliary state  $|a\rangle$  that rapidly decays to the excited state  $|e\rangle$ . In this way  $|a\rangle$  can be adiabatically eliminated and a two-state pseudospin description in the  $\{|g\rangle, |e\rangle\}$  subspace used, with repumping corresponding to an effective rate  $w$  from  $|g\rangle$  to  $|e\rangle$ . If the repumping laser is directed normal to the cavity axis, the absorption does not modify the momentum. Momentum recoil is induced by the on-axis component of the wavevector  $\vec{k}'$  of the dipole radiation pattern for the  $|a\rangle \leftrightarrow |e\rangle$  transition. . . . . 63
- 6.3 Time evolution of the average momentum square (red dots) evaluated from 4000 trajectories simulated by integrating Eqs. (6.28) and (6.32) for 1 atom (a), 20 atoms (b), and 60 atoms (c). The blue solid line is a fit to an exponential decay. The parameters are  $\Delta = \kappa/2 = 100$ ,  $\gamma_C = 0.1$ , and  $\omega_r = 0.25$ . The repumping rates are chosen such that the average atomic population inversion in all cases is the same [ $w = 0.15$  (a), 0.28 (b), 1.3 (c)]. Insets show the momentum statistics. The blue solid line is a fit to a Gaussian distribution. . . . . 69
- 6.4 (a) Cooling rate (in units of the single atom cooling rate  $R_S$ ) as a function of atom number. (b) Final momentum width ( $\Delta p = \sqrt{\langle p^2 \rangle}$ , blue squares) and spin-spin correlation (red dots) as a function of atom number. The parameters are the same as those in Fig. 6.3. . . . . 71
- 6.5 (a) Final momentum width as a function of  $\gamma_C$  for 40 atoms. The parameters are  $\Delta = \kappa/2 = 200$ ,  $w = N\gamma_C/4$ , and  $\omega_r = 0.25$ . (b) Final momentum width as a function of repumping strength for 40 atoms without ( $k' = 0$ , blue squares) and with recoil associated with repumping ( $k' = k$ , red dots). The parameters are  $\Delta = \kappa/2 = 200$ ,  $\gamma_C = 0.5$ , and  $\omega_r = 0.25$ . . . . . 73

# Chapter 1

## Introduction

Our era has seen quantum physics beginning to enable new technologies with unprecedented capabilities, *e.g.*, optical lattice clocks with stability at the  $10^{-18}$  level [9, 49], small quantum processors implementing Shor’s factoring algorithm [82, 144], and quantum teleportation over 100 kilometers [84, 145]. The light-matter interaction has been a valuable resource for probing and controlling quantum systems, and for synthesizing new quantum states. It is therefore the basis for many quantum technologies such as quantum computation, communication, simulation, sensing and metrology.

Cavity quantum electrodynamics (QED) represents a particularly important system for applications in quantum physics. First, cavity output photons are information carriers. It was shown that cavity fields could be used to probe the Mott insulator to superfluid phase transition [94] and to detect topological order and statistics of anyonic excitations [58]. Second, cavity dissipation provides the source to dissipatively control quantum systems. Based on the idea of quantum reservoir engineering [29], it was shown that an atomic ensemble coupled to a decaying cavity mode could be driven dissipatively to the targeted spin-squeezed state [25]. The cavity dissipation can also be used for the feedback control of quantum systems [138] and for cooling the objects coupled to the cavity [108, 141]. Third, cavity mediated interactions give rise to interesting quantum many-body states, *e.g.*, crystallinity and frustration with Bose-Einstein condensates in a multimode cavity [38], frustration and glassiness with cavity-confined spin systems [39], and to the Dicke quantum spin glass of atoms and photons with atomic qubits coupled to discrete cavity modes [119]. In this thesis,

it will be shown that the cavity-mediated dissipative coupling leads to synchronization states of atomic dipoles [140, 142]. Last, optical cavities are ideal for conversion between the stationary gate qubits and flying qubits (photons), which is essential for quantum networks. Quantum gates can be implemented in optical cavities with high fidelities [15]. An elementary quantum network of single atoms in optical cavities has been demonstrated [109]. Therefore, an important theme of current research in quantum physics is to explore how engineered photon fields interacting with quantum systems could be harnessed to probe and control the system, synthesize new quantum states, and process quantum information. Over the past decade, cavity QED has been expanded to new physical systems, such as atoms coupled to chiral bosonic waveguides [102], nitrogen-vacancy (NV) centers in diamond coupled with photonic structures [21], quantum dots in photonic crystals [124], and superconducting qubits coupled with an inductance/capacitance resonator [146]. This will not only advance quantum technologies, but also allow for better understanding of quantum many-body physics and fundamental questions in quantum mechanics.

The laser is a typical cavity QED system. Since its first demonstration in 1960 [85], the laser has had a profound impact on fundamental science research and has found widespread applications in society in general. Lasers typically operate in the good cavity regime of cavity QED where the linewidth of the cavity is much narrower than the bandwidth of the gain medium [95]. The atoms generate a coherent electromagnetic field in the cavity by means of stimulated emission [113].

An important application of lasers is as a stable local oscillator for optical atomic clocks [83]. The precision currently achievable by atomic clocks is remarkable; for example, the accuracy and instability of state-of-the-art optical lattice clocks lies in the realm of  $10^{-18}$  [9, 49]. The pursuit of even more stability is motivated by the potential benefit to a wide range of fields in the physical and natural sciences, facilitating progress in diverse areas such as; redefinition of the system of physical units in terms of time [14], clock-based geodesy [20], gravitational wave detection [40], and tests of fundamental physics and cosmology [6, 26]. Atomic clock developments have also enabled spin-off applications, including precision measurements [111], quantum state control [77], and investigations of quantum many-body physics [88, 106].

Such lasers rely on stabilization against reference cavities. The most advanced such laser realized to date has been achieved at JILA and reaches linewidths about 40mHz corresponding to quality factors of  $Q > 10^{15}$  [22]. The principal limiting factor in the way of further improvements of these local oscillators is thermal vibrations of the dielectric coatings on the cavity mirrors [65]. To overcome this technical challenge, researchers have proposed an alternate approach using an active system based on steady state superradiance on a clock transition to create an even more stable light source [18, 93].

As shown in Ref. [93], a steady-state superradiant laser is a possible system to consider for generating millihertz linewidth light. It was demonstrated in a recent proof of principle experiment using a two-photon Raman transition [12]. In the regime of steady-state superradiance, the cavity decay is much faster than all other processes. Therefore, the cavity mode plays the role of a dissipative collective coupling for the atoms that leads to the synchronization of atomic dipoles [140, 142]. The emergence of a macroscopic collective dipole induces an extremely narrow linewidth for the generated light [93, 140]. The optimal parameters are in the weak-coupling regime of cavity QED [95] [single-atom cooperativity parameter  $C < 1$ , see definition in Eq. (2.50)], that is opposite to the strong-coupling situation usually considered. Narrow-linewidth superradiant lasers require weak-dipole atoms (*e.g.* using intercombination lines or other forbidden transitions) confined in a high-finesse optical cavity.

In this thesis, I provide comprehensive studies of the steady-state superradiance. The thesis is structured as follows:

- Chapter 2 introduces Dicke superradiance, laser theory, and features of steady state superradiance. We emphasize that the superradiant laser is indeed collective spontaneous emission in steady state.
- Chapter 3 describes novel group-theoretic methods to efficiently solve the laser equation. The method may be applied to a wide variety of applications for simulating open quantum systems with large system size.

- Chapter 4 presents our new perspective on steady state superradiance: the synchronization of atomic dipoles. This offers an alternative understanding of the narrow linewidth of the superradiant laser. By demonstrating the synchronization effect, we propose conditional Ramsey spectroscopy with synchronized atoms. This could have important consequences for atomic clocks.
- Chapter 5 studies quantum synchronization with two ensembles of superradiant atoms. We show quantum synchronization as a dynamical phase transition. Quantum fluctuations and quantum correlations are found to be important, shedding light on current understanding of the quantum aspects of synchronization.
- Chapter 6 proposes to utilize steady-state superradiance for the efficient cooling of atoms. The temperature limit is determined by a modified atomic linewidth rather than the cavity linewidth as in normal cavity assisted cooling. The cooling rate is enhanced by the superradiance. The new cooling scheme is dubbed “supercooling”. It represents a first example of many-body laser cooling.
- Chapter 7 concludes the thesis and discusses the potential future of active optical standards.

## Chapter 2

### The superradiant laser

#### 2.1 Dicke superradiance

Superradiance is a fundamental quantum optical phenomenon in the photon emission process by many emitters. It was first predicted by Robert H. Dicke [28] in the context of spontaneous emission. Consider a gas of atoms (or molecules) initially prepared in the excited state decaying by spontaneous emission to a lower state. In a dilute atomic system, the photon emission by each atom can be considered as independent. As shown in Fig. 2.1(a), the emission obeys an exponential decay law (decay time constant  $\tau_{\text{sp}}$ ) and the radiation pattern is essentially isotropic. These features are notably changed when the atomic ensemble becomes dense enough. As shown in Fig. 2.1(b), the atomic ensemble starts to radiate photons much faster and stronger than the emission of independent atoms, and that radiation occurs in a well defined direction depending on the geometry of the atoms [42].

This phenomenon was termed “superradiance” by Dicke in 1954. Essentially, it is due to the indiscernibility of atoms with respect to the photon emission. This causes constructive interference in the photon emission by the ensemble. The intensity becomes proportional to the square of the number of atoms  $N$ . In the above case [Fig. 2.1(b)], when the wavelength of light is much greater than the separation of atoms, the atoms interact with the light in a collective and coherent way. As the emission begins, the quantum fluctuation of the vacuum field acts on independent atoms, and an order appears in the atomic ensemble which can be defined as phase-locking of the atomic dipoles. As a result, the atoms emit light as a high intensity pulse, with rate  $\propto N^2$  and short

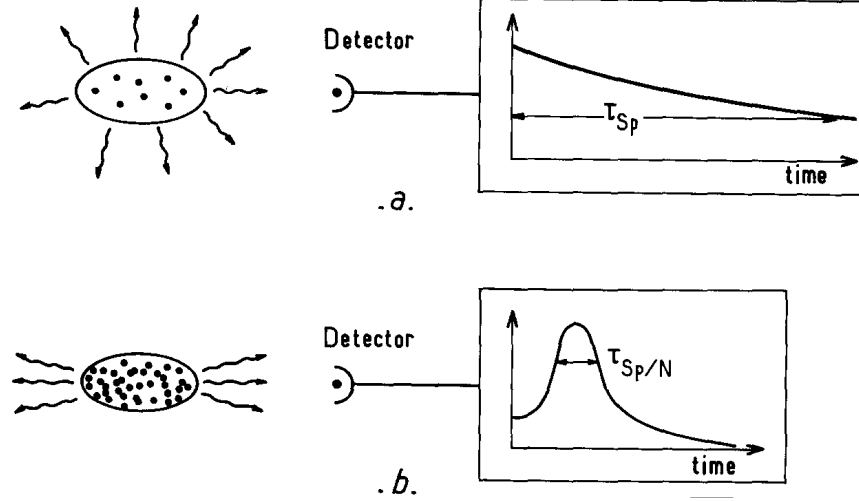


Figure 2.1: Source: Ref. [42]. Comparison between the general characteristics of ordinary fluorescence and superradiance experiment. (a) Ordinary spontaneous emission is essentially isotropic with exponentially decaying intensity (time constant  $\tau_{sp}$ ). (b) Superradiance is anisotropic with an emission occurring in a short burst of duration  $\sim \tau_{sp}/N$ .

duration of the order of  $\tau_{sp}/N$ .

Since Dicke's original work [28], superradiance has been extensively studied and demonstrated in a wide variety of physical systems [42]. More recently, it was demonstrated in quantum dots [114], NV centers [62], and atoms trapped along a photonic crystal waveguide [37]. In spite of the complications of different physical situations, the essential mechanism of superradiance is pretty simple.

To illustrate the key aspects of superradiance, it is easiest to introduce the permutation invariant atomic states. Consider an ensemble of  $N$  two level atoms, identified by the indices  $1, 2, \dots, j, \dots, N$ . The upper level and lower level of atom  $j$  are represented as  $|e\rangle_j$  and  $|g\rangle_j$  respectively. All the atoms are prepared in the upper level at time 0 so that

$$|\psi(0)\rangle = |e\rangle_1 |e\rangle_2 \dots |e\rangle_N. \quad (2.1)$$

We make the basic assumption that the atoms are indiscernible with respect to the photon emission or absorption process in the subsequent evolution. Therefore, the system must remain in a Hilbert subspace invariant to atomic permutations. Note that the two-level atom can be described as a

fictitious pseudospin-1/2 system with  $|e\rangle$  and  $|g\rangle$  being the spin up and down state respectively. So the  $N$ -atom permutation invariant state is isomorphous to a symmetrical superposition of  $N$  spin-1/2 states [42], which are the familiar angular momentum eigenstates  $|J, M\rangle$  with  $J = N/2$  and  $M = -N/2, -N/2 + 1, \dots, N/2 - 1, N/2$ . There are  $N + 1$  such states, see Fig. 2.2. Due to their application in superradiance, these states are also referred to as Dicke states. Note that  $J + M$  is the number of atoms in the excited state. So the state in which all atoms are excited may be written as  $|\psi(0)\rangle = |N/2, N/2\rangle$ .

Symmetrical state of  $N$  two-level identical atoms

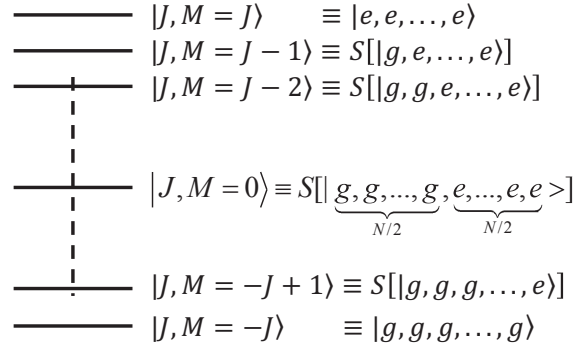


Figure 2.2: Dicke states of  $N$  two-level atoms.  $S$  denotes the symmetrizer with respect to atomic labels.

To define the electric dipole of  $j$ -th atom, we introduce the atomic raising and lowering operators

$$\hat{\sigma}_j^+ = |e\rangle_j \langle g|_j, \quad \hat{\sigma}_j^- = |g\rangle_j \langle e|_j, \quad (2.2)$$

and the atomic population inversion operators

$$\hat{\sigma}_j^z = |e\rangle_j \langle e|_j - |g\rangle_j \langle g|_j. \quad (2.3)$$

These are Pauli matrices and obey the well-known commutation relations

$$[\hat{\sigma}_i^+, \hat{\sigma}_j^-] = \delta_{ij} \hat{\sigma}_j^z, \quad [\hat{\sigma}_i^z, \hat{\sigma}_j^\pm] = \pm 2\delta_{ij} \hat{\sigma}_j^\pm. \quad (2.4)$$

The dipole operator for the  $j$ -th atom is

$$\mathcal{D}_j = (\hat{\sigma}_j^+ + \hat{\sigma}_j^-) D \hat{\epsilon}, \quad (2.5)$$

where  $D$  is the electric dipole matrix element of the  $|e\rangle \leftrightarrow |g\rangle$  transition and  $\hat{\epsilon}$  is the normalized vector along the polarization direction.

Under the condition of Dicke superradiance, individual dipoles may phase-lock. It is natural to assume that  $N$  atoms behave like a macroscopic dipole resulting from the sum of all  $N$  individual dipoles

$$\hat{\mathcal{D}} = \sum_{j=1}^N \hat{\mathcal{D}}_j = (\hat{J}^+ + \hat{J}^-)D\hat{\epsilon}, \quad (2.6)$$

where we have introduced the collective operators

$$\hat{J}^{\pm} = \sum_{j=1}^N \hat{\sigma}_j^{\pm}. \quad (2.7)$$

Recalling that the rate of photon emission by a single atom is proportional to  $\langle \hat{\sigma}_j^+ \hat{\sigma}_j^- \rangle$ , we naturally generalize this to get the superradiant photon emission rate [42],

$$W_S \propto \langle \hat{J}^+ \hat{J}^- \rangle. \quad (2.8)$$

For the Dicke state  $|J, M\rangle$ , we immediately get

$$W_S \propto (J + M)(J - M + 1). \quad (2.9)$$

We have used

$$\hat{J}^{\pm}|J, M\rangle = \sqrt{(J \mp M)(J \pm M + 1)}|J, M \pm 1\rangle. \quad (2.10)$$

From Eq. (2.9), we can see that the photon emission rate increases from  $N$  for  $M = N/2$  (fully excited) to  $\frac{1}{2}N(\frac{1}{2}N + 1)$  for  $M = 0$  (half excited). Therefore, the photon emission rate strongly increases when the system cascades down the ladder of the  $|J, M\rangle$  states as shown in Fig. 2.2. The maximum rate of emission is proportional to  $N^2$  for  $M = 0$ .

The  $N^2$  scaling of the photon emission rate is directly related to the build up of correlations between atomic dipoles, which is the very essence of Dicke superradiance. By using Eq. (2.7) and permutation symmetry, we can rewrite Eq. (2.8) as

$$\langle \hat{J}^+ \hat{J}^- \rangle = \left\langle \sum_{i=1}^N \hat{\sigma}_i^+ \sum_{j=1}^N \hat{\sigma}_j^- \right\rangle = N \langle \hat{\sigma}_i^+ \hat{\sigma}_i^- \rangle + N(N-1) \langle \hat{\sigma}_i^+ \hat{\sigma}_j^- \rangle. \quad (2.11)$$

There are  $N$  terms  $\langle \hat{\sigma}_i^+ \hat{\sigma}_i^- \rangle$  representing the population in the excited state and  $N(N - 1)$  cross terms  $\langle \hat{\sigma}_i^+ \hat{\sigma}_j^- \rangle$  that represent the atomic correlations. These correlations are reminiscent of the spin-spin correlations appearing in a ferromagnetic system. In order for the superradiance to manifest, the atom-atom correlation, measured by  $\langle \hat{\sigma}_i^+ \hat{\sigma}_j^- \rangle$ , should be nonzero.

It is easy to get

$$\langle J, M | \hat{\sigma}_i^+ \hat{\sigma}_j^- | J, M \rangle = \frac{J^2 - M^2}{N(N - 1)}. \quad (2.12)$$

Therefore, the atom-atom correlation increases from 0 to a maximum value of  $1/4$  when  $M$  goes from  $N/2$  to zero and decreases to 0 when  $M = -N/2$ .

## 2.2 Laser theory in a nutshell

As noted by Serge Haroche in Ref. [42],

“One of the interests in superradiance study lies in its close connection with the physics of laser emission. *A superradiant medium is indeed nothing but a mirrorless laser pumped in a percussional way at time  $t = 0$ .* The superradiant phase-locking of the dipoles belonging to different atoms thus exhibits a strong relationship with the ordering process by which the atoms in a laser amplifier acquire a common phase and start emitting coherently.”

In this section, I provide a simple theory of the laser. The basis of laser action is stimulated emission of radiation. If a net population inversion of atoms is maintained, the electromagnetic field will be amplified. As lasing takes place, atoms lose their inversion. Some mechanism must be provided to pump them back up again so as to maintain the population inversion. Note that by coherent drive, the atom will never achieve population inversion regardless of the pump strength [36]. This is because coherent drive involves both atomic excitation and deexcitation. Therefore, a laser requires the incoherent repumping of the atoms (see below for a possible implementation).

I use the simplest possible laser model as the basis for my analysis. The well-known model [44] accounts for a single-mode electromagnetic field in a cavity interacting with  $N$  identical two-level atoms in terms of the Jaynes-Cummings Hamiltonian [95], and for the irreversible photon escape (atomic and cavity decay) and atomic decoherence in terms of Liouville operators. The above

model is treated in terms of the following quantum master equation for the atom plus field density operator  $\hat{\rho}$ :

$$\frac{d}{dt}\hat{\rho} = \frac{1}{i\hbar}[\hat{H}, \hat{\rho}] + \kappa\mathcal{L}[\hat{a}]\hat{\rho} + \sum_{j=1}^N \gamma\mathcal{L}[\hat{\sigma}_j^-]\hat{\rho} + \frac{1}{2T_2}\mathcal{L}[\hat{\sigma}_j^z]\hat{\rho} + w\mathcal{L}[\hat{\sigma}_j^+]\hat{\rho} \quad (2.13)$$

where  $\mathcal{L}[\hat{O}]\hat{\rho} = (2\hat{O}\hat{\rho}\hat{O}^\dagger - \hat{O}^\dagger\hat{O}\hat{\rho} - \hat{\rho}\hat{O}^\dagger\hat{O})/2$  is the Lindbladian superoperator [80] describing the incoherent processes. The Hamiltonian  $\hat{H}$  is

$$\hat{H} = \hbar\omega_a \sum_{j=1}^N \hat{\sigma}_j^+ \hat{\sigma}_j^- + \hbar\omega_c \hat{a}^\dagger \hat{a} + \frac{\hbar g}{2} \sum_{j=1}^N (\hat{a}^\dagger \hat{\sigma}_j^- + \hat{\sigma}_j^+ \hat{a}), \quad (2.14)$$

where  $\omega_a$  and  $\omega_c$  are the atomic transition frequency and the frequency of the cavity mode respectively, and  $g$  is the single atom-cavity coupling strength. Here,  $\hat{a}$  and  $\hat{a}^\dagger$  are the annihilation and creation operators for cavity photons. Note that the Hamiltonian has been specified in the dipole and rotating wave approximations. The cavity dissipation with power decay rate  $\kappa$  is described by  $\kappa\mathcal{L}[\hat{a}]\hat{\rho}$ . The atomic spontaneous emission with rate  $\gamma$  is described by  $\gamma\mathcal{L}[\hat{\sigma}_j^-]\hat{\rho}$ . The incoherent repumping takes the atoms from the ground state to the excited state incoherently and is modeled as inverse spontaneous emission with rate  $w$  (term  $w\mathcal{L}[\hat{\sigma}_j^+]\hat{\rho}$ ). The additional dephasing of the atomic dipole is modeled phenomenologically as a  $T_2$  process and is described by  $\frac{1}{2T_2}\mathcal{L}[\hat{\sigma}_j^z]\hat{\rho}$ . Note that the Liouvillian is derived in the usual Born-Markov approximation [81], assuming weak system-reservoir coupling and delta-correlation of the reservoir.

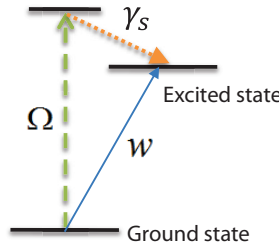


Figure 2.3: Schematic for implementing the incoherent pumping in a three-level configuration. The coherent driving laser is indicated by the green-dashed arrow and spontaneous decay into the excited state  $|e\rangle$  is indicated by the orange-dotted arrow.

Since incoherent pumping generates population inversion in a two-level system, it is induced by the system coupling to a negative-temperature reservoir and therefore can only be implemented

using auxiliary atomic levels. A typical approach is coherently driving a transition from the ground state  $|g\rangle$  to a third state that rapidly decays to the excited state  $|e\rangle$ , as shown in Fig. 2.3. In the limit of large  $\gamma_s$ , this will lead to an effective incoherent pumping rate  $w = |\Omega|^2/\gamma_s$ .

It turns out that simple mean-field theory of Eq. (2.13) can reveal a great deal about the properties of a laser. The complete set of quantum Langevin equations according to Eq. (2.13) in the reference frame rotating at frequency  $\omega$  [36]

$$\frac{d}{dt}\hat{a} = -\frac{1}{2}(\kappa + 2i\omega_c - 2i\omega)\hat{a} - \frac{iNg}{2}\hat{S}^- + \hat{F}^a, \quad (2.15)$$

$$\frac{d}{dt}\hat{S}^- = -\frac{1}{2}(\Gamma + 2i\omega_a - 2i\omega)\hat{S}^- + \frac{ig}{2}\hat{a}\hat{S}^z + \hat{F}^-, \quad (2.16)$$

$$\frac{d}{dt}\hat{S}^z = -(w + \gamma)(\hat{S}^z - d_0) + ig(\hat{a}^\dagger\hat{S}^- - \hat{a}\hat{S}^+) + \hat{F}^z, \quad (2.17)$$

where  $\Gamma \equiv w + \gamma + 2/T_2$  is the generalized single-atom decoherence and  $d_0 = (w - \gamma)/(w + \gamma)$  characterizes the atomic inversion that would be obtained for a single-atom in the absence of the cavity. We have defined the collective operators,

$$\hat{S}^\pm = \frac{1}{N} \sum_{k=1}^N \hat{\sigma}_k^\pm, \quad \hat{S}^z = \frac{1}{N} \sum_{k=1}^N \hat{\sigma}_k^z. \quad (2.18)$$

The quantum noise operators  $\hat{F}^\mu$  have zero mean and second-order correlations given by

$$\langle \hat{F}^\mu(t) \hat{F}^\nu(t') \rangle = 2D^{\mu\nu} \delta(t - t'). \quad (2.19)$$

The diffusion matrix elements  $D^{\mu\nu}$  can be obtained [36]

$$\begin{aligned} 2D^{aa^\dagger} &= \kappa, & 2D^{+-} &= \frac{1}{N} \left( w + \frac{1}{T_2} (1 + \langle \hat{S}^z \rangle) \right) \\ 2D^{-+} &= \frac{1}{N} \left( \gamma + \frac{1}{T_2} (1 - \langle \hat{S}^z \rangle) \right), & 2D^{+z} &= -\frac{2w}{N} \langle \hat{S}^+ \rangle \\ 2D^{z+} &= \frac{2\gamma}{N} \langle \hat{S}^+ \rangle, & 2D^{-z} &= \frac{2\gamma}{N} \langle \hat{S}^- \rangle \\ 2D^{z-} &= -\frac{2w}{N} \langle \hat{S}^- \rangle, & 2D^{zz} &= \frac{2\gamma}{N} (1 + \langle \hat{S}^z \rangle) + \frac{2w}{N} (1 - \langle \hat{S}^z \rangle). \end{aligned} \quad (2.20)$$

From Eq. (2.20), we can see that the noise is  $1/\sqrt{N}$  smaller than the deterministic terms in the quantum Langevin equation. To zeroth order, we can discard the noise terms and arrive at the

mean-field equations of motion

$$\frac{d}{dt}a_0 = -\frac{1}{2}(\kappa + 2i\omega_c - 2i\omega)a_0 - \frac{iNg}{2}S_0^-, \quad (2.21)$$

$$\frac{d}{dt}S_0^- = -\frac{1}{2}(\Gamma + 2i\omega_a - 2i\omega)S_0^- + \frac{ig}{2}a_0S_0^z, \quad (2.22)$$

$$\frac{d}{dt}S_0^z = -(w + \gamma)(S_0^z - d_0) + ig(a_0^*S_0^- - a_0S_0^+), \quad (2.23)$$

where the 0 subscript denotes the mean value, *e.g.*  $\langle \hat{a} \rangle = a_0$ .

A closed-form solution of Eqs. (2.21)–(2.23) can be obtained in steady-state by setting the left hand sides to zero. We find from Eq. (2.22) and Eq. (2.23)

$$S_0^z = \frac{d_0}{1 + \frac{g^2|a_0|^2}{w+\gamma} \frac{2\Gamma}{\Gamma^2+4(\omega_a-\omega)^2}} \quad (2.24)$$

for the steady-state population inversion. Plugging it to Eq. (2.21), we have

$$a_0 \left( 1 - \frac{Ng^2}{(\kappa + 2i\omega_c - 2i\omega)(\Gamma + 2i\omega_a - 2i\omega)} \frac{d_0}{1 + \frac{g^2|a_0|^2}{w+\gamma} \frac{2\Gamma}{\Gamma^2+4(\omega_a-\omega)^2}} \right) = 0. \quad (2.25)$$

There are two solutions for the average photon number  $|a_0|^2$ ,

$$a_0 = 0, \quad (2.26)$$

and

$$|a_0|^2 = \frac{w + \gamma}{g^2} \frac{\Gamma^2 + 4(\omega_a - \omega)^2}{2\Gamma} \left( \frac{d_0Ng^2}{(\kappa + 2i\omega_c - 2i\omega)(\Gamma + 2i\omega_a - 2i\omega)} - 1 \right). \quad (2.27)$$

In Eq. (2.27), for  $|a_0|^2$  to be real, we need to have

$$\omega = \frac{\kappa\omega_a + \Gamma\omega_c}{\kappa + \Gamma}, \quad (2.28)$$

that is the laser frequency  $\omega$  is the weighted average of the cavity frequency and atomic frequency.

Plugging Eq. (2.28), into Eq. (2.27), we can get a simple expression when  $|\omega_c - \omega_a| \ll \kappa + \Gamma$

$$|a_0|^2 \approx \frac{(w + \gamma)\Gamma}{2g^2} \left( \frac{d_0Ng^2}{\kappa\Gamma} - 1 \right) = n_0(\mathcal{G} - 1), \quad (2.29)$$

where  $n_0 = \frac{(w+\gamma)\Gamma}{2g^2}$  is called the saturation photon number and  $\mathcal{G} = \frac{Ng^2}{\kappa\Gamma}d_0$  is called the generalized cooperativity parameter. Clearly, the second solution is only possible if  $\mathcal{G} > 1$ .  $\mathcal{G}$  can be varied

by changing the repumping  $w$ . The behavior of the system is completely different depending on whether  $\mathcal{G}$  is greater than or less than 1, and there is a threshold at  $\mathcal{G} = 1$ . Below the threshold,  $\mathcal{G} < 1$ ,  $a_0 = 0$ . There is no mean coherent field established. Above the threshold, when  $\mathcal{G} > 1$ , a mean coherent photon field arises. More importantly, we emphasize that a nonzero collective atomic dipole  $S_0^-$  develops, which is a signature of atomic dipole phase locking.

As introduced in Chapter 1, one of the most important properties of the laser is its spectral linewidth. Indeed, one impetus to develop a useful form of quantum optical theory came from the need to understand the properties of laser light. Here, I follow Haken's phase diffusion method [43, 44] to provide a closed-form solution to obtain the spectral linewidth of the laser light.

Differentiating Eq. (2.15) with respect to time and substituting Eqs. (2.15) – (2.16) we obtain

$$\ddot{\hat{a}} = -\frac{1}{2}(\kappa + \Gamma)\dot{\hat{a}} - \frac{\kappa\Gamma}{4}\hat{a} + \frac{Ng^2}{4}\hat{a}\hat{S}^z + \hat{F}, \quad (2.30)$$

where

$$\hat{S}^z = \int_0^t dt' e^{-(w+\gamma)(t-t')} \left( (w + \gamma) + \hat{F}^z - \frac{2}{N} \left( \frac{d}{dt} (\hat{a}^\dagger \hat{a}) + \kappa \hat{a}^\dagger \hat{a} - \hat{a}^\dagger \hat{F}^a - \hat{F}^{a\dagger} \hat{a} \right) \right), \quad (2.31)$$

and

$$\hat{F} = \frac{\Gamma}{2}\hat{F}^a - \frac{iNg}{2}\hat{F}^- + \hat{F}^a. \quad (2.32)$$

The annihilation operator  $\hat{a}$  is decomposed according to

$$\hat{a} = (a_0 + \hat{r})e^{i\hat{\phi}}. \quad (2.33)$$

Above threshold, amplitude fluctuations are small so that  $\hat{r}$  can be neglected. We then obtain for the two time correlation function of the field amplitude

$$\langle \hat{a}^\dagger(t)\hat{a}(0) \rangle = a_0^2 \langle e^{i[\hat{\phi}(t) - \hat{\phi}(0)]} \rangle. \quad (2.34)$$

After substituting Eq. (2.33) into Eq. (2.30), we take the imaginary part to first order in products of operators, and find,

$$\ddot{\hat{\phi}} = -\frac{1}{2}(\kappa + \Gamma)\dot{\hat{\phi}} + \frac{1}{a_0}\text{Im}[\hat{F}], \quad (2.35)$$

where a factor of  $e^{-i\phi}$  has been absorbed into  $\hat{F}$ . Equation (2.35) is then integrated, assuming that  $(\kappa + \Gamma)$  is large, to arrive at

$$\hat{\phi}(t) - \hat{\phi}(0) = \frac{2}{a_0(\kappa + \Gamma)} \int_0^t dt' \text{Im} \left[ \frac{\Gamma}{2} \hat{F}^a - \frac{iNg}{2} \hat{F}^- \right]. \quad (2.36)$$

Since  $\hat{F}^a$  and  $\hat{F}^-$  are Gaussian, we can use

$$\langle e^{i[\hat{\phi}(t) - \hat{\phi}(0)]} \rangle = e^{-\frac{1}{2} \langle [\hat{\phi}(t) - \hat{\phi}(0)]^2 \rangle}. \quad (2.37)$$

Therefore, we use Eq. (2.36), along with Eqs. (2.20) to find

$$\langle (\hat{\phi}(t) - \hat{\phi}(0))^2 \rangle = \frac{(\mathcal{G}/d_0 + 1)}{2(\mathcal{G} - 1)} \frac{\Gamma}{(w + \gamma)} \frac{g^2 \kappa}{(\kappa + \Gamma)^2} t, \quad (2.38)$$

so that the linewidth  $\Delta\nu$  in the unit of Hz is given by

$$\Delta\nu = \frac{(\mathcal{G}/d_0 + 1)}{2(\mathcal{G} - 1)} \frac{\Gamma}{(w + \gamma)} \frac{g^2 \kappa}{(\kappa + \Gamma)^2}. \quad (2.39)$$

Lasers typically operate in the good cavity regime of cavity QED where the linewidth of the cavity is much narrower than the bandwidth of the gain medium, *i.e.*,  $\kappa \ll \Gamma$ . In this case,

$$\begin{aligned} \Delta\nu &\approx \frac{\mathcal{G}/d_0 + 1}{2(\mathcal{G} - 1)} \frac{\kappa}{(w + \gamma)\Gamma/g^2} = \frac{\mathcal{G}/d_0 + 1}{4} \frac{\kappa}{|a_0|^2} = \frac{1}{4} \frac{S_0^z + 1}{S_0^z} \frac{\kappa}{|a_0|^2} \\ &\propto \frac{\kappa}{|a_0|^2}. \end{aligned} \quad (2.40)$$

This is the famous Schawlow-Townes linewidth for laser [113]. In a good-cavity laser, the macroscopic phase information that is associated with the coherence of the generated radiation is encoded in the light field.

### 2.3 Steady state superradiance

Fritz Haake made an important connection between Dicke superradiance and bad-cavity laser.

As he wrote in Ref. [13]

As has already been pointed out by Dicke the ‘‘coherence brightening’’ occurs practically exclusively in the axial direction for such a pencil-shaped arrangement. Emission of radiation does take place in non axial directions, too, but to a much

lesser extent and essentially unfavored by cooperative effects. It may therefore be looked upon as an incoherent loss mechanism for the atoms. The latter artifice greatly reduces the complexity of the problem, for it leaves us with the axial modes only as dynamical field variables. *As a device which further simplifies the problem, we quantize the electromagnetic field with respect to the volume of the cavity. . . .* The escape of photons through the non mirrored end face of the pencil into the radiation field is taken care of as a loss mechanism for the field mode in the cavity.

*What we have just described as our model of a superradiant system is nothing but the well-known simplest possible laser model. . . .* However, we have to solve the laser master equation in a limit that, for good reasons, has hardly ever been considered in laser theory. We are here concerned with a low-quality cavity. . . . In contrast to the laser, the superradiant device must not be designed to lock the photons in the cavity but rather to release them as fast as they can escape according to the velocity of light. Moreover, again as opposed to what is typical for a laser, the incoherent atomic decay process must be so slow that the individual atomic dipoles do not get out of phase with each other before they can involve themselves cooperatively in the interaction with the field mode.

Haake's statement can be made quantitative by a "superradiance master equation" that was first derived in Ref. [13]. It describes the cooperative decay of atomic excitations without allowing for any feedback of the field on the atoms.

Let us consider the laser equation Eq. (2.13) in the bad cavity regime, or the superradiant limit. In this limit, the cavity decay rate  $\kappa$  is much faster than any other time scale. Therefore, it allows for an expansion in powers of  $\kappa^{-1}$  and the elimination of the field variable (see Appendix A). To this end, we start with the quantum Langevin equation for the cavity field according to the quantum master equation Eq. (2.13) in the rotating frame of the cavity frequency,

$$\frac{d}{dt}\hat{a} = -\frac{\kappa}{2}\hat{a} - i\Delta\hat{a} - i\frac{g}{2}\hat{J}^- + \sqrt{\kappa}\hat{\xi}_\kappa(t), \quad (2.41)$$

where  $\Delta = \omega_c - \omega_a$  and  $\hat{\xi}_\kappa$  is the quantum white noise originating from the cavity output with  $\langle \hat{\xi}_\kappa(t)\hat{\xi}_\kappa^\dagger(t') \rangle = \delta(t-t')$ . The formal solution to Eq. (2.41) is

$$\hat{a}(t) = e^{-(\kappa/2+i\Delta)\Delta t}\hat{a}(t_0) - i\frac{g}{2}\int_0^{\Delta t} ds e^{-(\kappa/2+i\Delta)s}\hat{J}^-(t-s) + \hat{\mathcal{F}}(t), \quad (2.42)$$

where  $\hat{\mathcal{F}}(t) = \sqrt{\kappa}\int_0^{\Delta t} ds e^{-(\kappa/2+i\Delta)s}\hat{\xi}_\kappa(t-s)$  is the noise term and  $\Delta t = t - t_0$ . Under the approximation of coarse graining, the first term on the right-hand side of Eq. (2.42) vanishes, and it is

shown in Appendix A that

$$\langle \hat{\mathcal{F}}(t) \hat{\mathcal{F}}^\dagger(t') \rangle \approx \frac{\kappa}{\kappa^2/4 + \Delta^2} \delta(t - t'). \quad (2.43)$$

It would be convenient to choose  $\hat{\mathcal{F}}(t) = -i \frac{\sqrt{\gamma_C}}{g/2} \hat{\xi}(t)$ , with

$$\gamma_C = \frac{g^2 \kappa/4}{\kappa^2/4 + \Delta^2}. \quad (2.44)$$

Furthermore, the integral in Eq. (2.42) can be expanded in powers of  $1/(\kappa/2 + i\Delta)$  (see Appendix A). As a result we obtain

$$\hat{a}(t) \approx \frac{-i \frac{g}{2} \hat{J}^-}{\kappa/2 + i\Delta} + \hat{\mathcal{F}}(t) + \mathcal{O}[(\kappa/2 + i\Delta)^{-2}]. \quad (2.45)$$

Because we are interested in the deep bad-cavity regime as motivated above, the expansion can be truncated in lowest order. This yields the ‘‘superradiance master equation’’.

$$\frac{d}{dt} \hat{\rho} = \frac{1}{i\hbar} \left[ -\frac{\hbar\gamma_\Delta}{2} \hat{J}^+ \hat{J}^-, \hat{\rho} \right] + \gamma_C \mathcal{L}[\hat{J}^-] \hat{\rho} + \sum_{j=1}^N \gamma \mathcal{L}[\hat{\sigma}_j^-] \hat{\rho} + \frac{1}{2T_2} \mathcal{L}[\hat{\sigma}_j^z] \hat{\rho} + w \mathcal{L}[\hat{\sigma}_j^+] \hat{\rho}, \quad (2.46)$$

where

$$\gamma_\Delta = \frac{g^2 \Delta/2}{\kappa^2/4 + \Delta^2}. \quad (2.47)$$

Before discussing the physics of Eq. (2.46), a proof is given of the superradiance master equation by comparing the equations of motion for spins (*i.e.*  $\hat{\sigma}_j^-, \hat{\sigma}_j^z$ ) derived from Eq. (2.46) and Eq. (2.13) in the large  $\kappa$  limit. The complete set of equations of motion for spins according to Eq. (2.46) is

$$\begin{aligned} \frac{d}{dt} \hat{\sigma}_j^- &= -\left(\frac{w}{2} + \frac{1}{T_2}\right) \hat{\sigma}_j^- - i \frac{\gamma_\Delta}{2} \hat{\sigma}_j^z \cos(k\hat{x}_j) \hat{J}^- + \frac{\gamma_C}{2} \hat{\sigma}_j^z \cos(k\hat{x}_j) \hat{J}^- \\ &\quad + \sqrt{\gamma_C} \hat{\sigma}_j^z \cos(k\hat{x}_j) \hat{\xi} - \sqrt{w} \hat{\sigma}_j^z \hat{\xi}_j^\dagger + \sqrt{\frac{2}{T_2}} (\hat{\xi}_j^{z\dagger} - \hat{\xi}_j^z) \hat{\sigma}_j^-, \\ \frac{d}{dt} \hat{\sigma}_j^z &= w(1 - \hat{\sigma}_j^z) + 2\text{Re} \left[ (i\gamma_\Delta - \gamma_C) \hat{\sigma}_j^+ \hat{J}^- \right] \cos(k\hat{x}_j) \\ &\quad - 2\sqrt{\gamma_C} (\hat{\sigma}_j^+ \hat{\xi} + \hat{\xi}^\dagger \hat{\sigma}_j^-) \cos(k\hat{x}_j) + 2\sqrt{w} (\hat{\sigma}_j^+ \hat{\xi}_j^\dagger + \hat{\xi}_j \hat{\sigma}_j^-), \end{aligned} \quad (2.48)$$

where  $\hat{\xi}_j$  and  $\hat{\xi}_j^z$  are the independent repumping noise and  $T_2$  dephasing noise for each atom, respectively. While the same set of equations according to Eq. (2.13) is

$$\begin{aligned} \frac{d}{dt} \hat{\sigma}_j^- &= -\left(\frac{w}{2} + \frac{1}{T_2}\right) \hat{\sigma}_j^- + i \frac{g}{2} \hat{\sigma}_j^z \hat{a} \cos(k\hat{x}_j) - \sqrt{w} \hat{\sigma}_j^z \hat{\xi}_j^\dagger + \sqrt{\frac{2}{T_2}} (\hat{\xi}_j^{z\dagger} - \hat{\xi}_j^z) \hat{\sigma}_j^-, \\ \frac{d}{dt} \hat{\sigma}_j^z &= w(1 - \hat{\sigma}_j^z) - ig \hat{\sigma}_j^+ \hat{a} \cos(k\hat{x}_j) + ig \hat{a}^\dagger \hat{\sigma}_j^- \cos(k\hat{x}_j) + 2\sqrt{w} (\hat{\sigma}_j^+ \hat{\xi}_j^\dagger + \hat{\xi}_j \hat{\sigma}_j^-). \end{aligned} \quad (2.49)$$

Plugging Eq. (2.45) into Eq. (2.49) results in a set of equations identical to Eq. (2.48). Consequently, the superradiance master equation describes the same spin dynamics of atoms as Eq. (2.13) in the large  $\kappa$  limit.

From the superradiance master equation Eq. (2.46), we see two new terms coming from the elimination of the photon field:

- $\gamma_C \mathcal{L}[\hat{J}^-] \hat{\rho}$  term

This is a Lindbladian term with decay operator being the collective operator  $\hat{J}^-$ . Therefore, this term gives rise to the collective photon emission by the atoms into the cavity mode.

We can expand this term as

$$\gamma_C \mathcal{L}[\hat{J}^-] \hat{\rho} = \gamma_C \sum_{j=1}^N \mathcal{L}[\hat{\sigma}_j^-] \hat{\rho} + \gamma_C \sum_{i \neq j} \frac{1}{2} (2\hat{\sigma}_i^- \hat{\rho} \hat{\sigma}_j^+ - \hat{\rho} \hat{\sigma}_j^+ \hat{\sigma}_i^- - \hat{\sigma}_j^+ \hat{\sigma}_i^- \hat{\rho}).$$

Therefore, this collective decay term introduces spontaneous decay of atoms into the cavity mode with rate  $\gamma_C$  and dissipative coupling between atoms. The dissipative coupling is essential for the build up of atom-atom correlations  $\langle \hat{\sigma}_i^+ \hat{\sigma}_j^- \rangle$  and thus the superradiant emission.

- $\frac{1}{i\hbar} [-\frac{\hbar\gamma\Delta}{2} \hat{J}^+ \hat{J}^-, \hat{\rho}]$  term

This is a Hamiltonian term with the Hamiltonian  $-\frac{\hbar\gamma\Delta}{2} \hat{J}^+ \hat{J}^-$ . This term introduces the coherent coupling between atoms and the energy shift of atom  $j$  by  $-\hbar\gamma\Delta/2$ . The underlying mechanism of this energy shift is formally similar to that of the Lamb shift [81], that is, the interaction of atoms with off-resonant light modes through emission and absorption of virtual photons. When  $\Delta = 0$ , the energy shift disappears. An intuitive way to understand this energy shift in the dispersive limit ( $\Delta \gg \kappa$ ) is to view it as a Stark shift due to vacuum fluctuations of the cavity field.

It is the collective decay term that gives rise to the superradiance. To focus on the superradiant behavior of atoms in the bad-cavity laser, we consider the case  $\Delta = 0$  in this section. As a result,

$\gamma_C = g^2/\kappa$ . In this case, we rename  $\gamma_C$  to  $\Gamma_C = C\gamma$ . Here,

$$C = \frac{g^2}{\kappa\gamma} \quad (2.50)$$

is the so-called single-atom cooperativity parameter of the cavity [64]. It is a dimensionless parameter that describes the ratio of atomic photon emission rate into the cavity mode as enhanced by the cavity finesse to atomic photon emission rate into the free space.

A remarkable feature of the superradiant limit of the laser is its linewidth property. According to the linewidth formula for laser Eq. (2.39), in the bad cavity limit, *i.e.*,  $\kappa \gg \Gamma$ ,

$$\Delta\nu \approx \frac{\mathcal{G}/d_0 + 1}{2(\mathcal{G} - 1)} \frac{\Gamma}{w + \gamma} \Gamma_C. \quad (2.51)$$

In the limit that  $w \gg \gamma$ ,  $1/T_2$ ,  $d_0 \approx 1$  and  $\Gamma \approx w + \gamma$ , this can be further simplified to

$$\Delta\nu \approx \frac{\mathcal{G} + 1}{2(\mathcal{G} - 1)} \Gamma_C \approx \frac{1 + S_0^z}{2(1 - S_0^z)} C\gamma. \quad (2.52)$$

The linewidth formula in the superradiant limit Eq. (2.52) differs qualitatively from the Schawlow-Townes linewidth for good-cavity laser [113]. As the cavity linewidth  $\kappa$  drops out of the linewidth formula Eq. (2.52), the coherence property of the bad cavity laser does not depend on the cavity linewidth. By comparing Eq. (2.40) and Eq. (2.52), we reach the conclusion that the coherence is stored in the photons for the good cavity laser but is stored in the atoms for the bad-cavity laser.

To validate the above discussion about the superradiance emission by atoms in the bad cavity laser, we employ the methods described in Chapter 3 to numerically solve the laser master equation Eq. (2.13) in the bad-cavity limit. As shown in Fig. 2.4, we find the build-up of atom-atom correlations  $\langle \hat{\sigma}_i^+ \hat{\sigma}_j^- \rangle$  in steady state, which is a signature of superradiance. Furthermore, the linewidth of the laser light shown in Fig. 2.4 is Lorentzian and proportional to  $C\gamma$ , which is consistent with the prediction of Eq. (2.52).

Therefore, the superradiant decay of an ensemble of atoms in steady state can be described realistically in terms of the simplest possible laser model Eq. (2.13) in the bad cavity limit. In 2009, Meiser *et. al.* proposed to use a clock transition of strontium atoms in an optical cavity

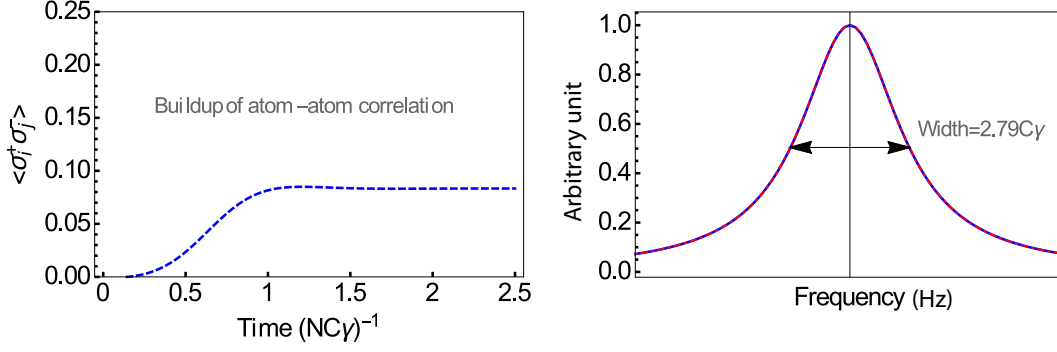


Figure 2.4: Numerical simulation (blue dashed line) of a bad cavity laser. Left panel: Atom-atom correlation as a function of time. Right panel: Spectrum of the laser light (red solid line is the fit to Lorentzian). The parameters are  $N = 200$ ,  $C = 0.2$ ,  $w = 18\gamma$ ,  $T_2^{-1} = 2\gamma$ ,  $\kappa = 2500\gamma$ .

as a possible realization of such model [93]. The motivation here was to generate an ultranarrow linewidth laser source by using atoms with extremely small spontaneous emission rate  $\gamma$  and a bad cavity with  $C \ll 1$ . In this system, the weak radiative power due to small  $\gamma$  of the clock transition (for example, for  $10^6$  fully inverted  $^{87}\text{Sr}$  atoms the power of the spontaneous emitted light is of the order  $10^{-16}$  W) is not of major concern. This is due to the fact that the photon emission rate is boosted by the superradiance and scales favorably with atom number. Below I will give detailed discussion of the proposal.

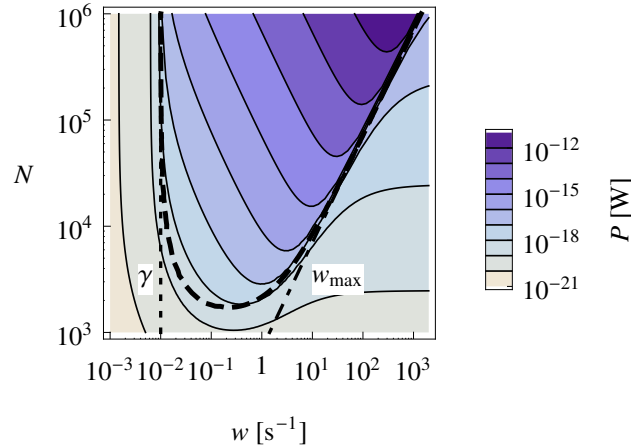


Figure 2.5: Source: Ref. [93]. Power as a function of pump rate  $w$  and atom number  $N$ . The rapid buildup of power above threshold  $w \sim \gamma$  can be seen as well as the decrease of emitted power for too strong a pump. The dashed line shows the boundary of the region of collective emission.

Consider  $N$  ultracold two-level  $^{87}\text{Sr}$  atoms confined in an optical cavity. The lasing transition is the ultranarrow clock transition from  $^3P_0$  to  $^1S_0$  with extremely weak dipole matrix element of the intercombination transition of order  $10^{-5}ea_0$ . Here  $e$  is the electron charge and  $a_0$  is the Bohr radius. The linewidth  $\gamma$  is about  $0.01 \text{ s}^{-1}$ . The atoms are located in a high- $Q$  optical cavity with cavity decay rate  $\kappa = 1 \text{ MHz}$ . The atoms are confined along the axis of the cavity mode in a 1D optical lattice at antinodes of the field, so that the atom-cavity coupling  $g$  is uniform to good approximation. For a bad cavity, the single-atom cooperativity parameter  $C \approx 0.15$  and  $g \approx 37 \text{ s}^{-1}$ . The  $T_2$  dephasing time can be pushed to  $T_2 \sim 1 \text{ s}$  in modern optical lattice clock experiment [9]. The repumping rate  $w$  can be widely tuned from 0 to the values of order  $10^4 \text{ s}^{-1}$ .

According to the parameters, the proposed system is thus an extreme case of a bad cavity laser. It has astounding potential linewidth of  $\sim C\gamma = 1 \text{ mHz}$  according to Eq. (2.52). For reference, the most stable conventional laser based on stabilization against carefully designed passive cavities achieve linewidth  $\sim 40 \text{ mHz}$  [22].

In such a laser, the atoms emit light collectively. As shown in Fig. 2.5, the resulting power is of order  $10^{-12} \text{ W}$  for  $10^6$  atoms, which would be large enough to be technological relevant. We can also identify two lasing thresholds from Fig. 2.5. In the first threshold  $w \sim \gamma$ , the repumping is large enough so that the atoms get population inverted and start lasing. For the second threshold, the repumping is so large that the atoms get fully inverted and the coherence between atoms is destroyed. This threshold is given by  $w = NC\gamma$ . The maximum power is achieved at  $w = NC\gamma/2$ , where  $\langle \hat{\sigma}_j^z \rangle = 1/2$ . A minimum number of atoms is necessary to have superradiance emission. Assuming  $T_2\gamma \ll 1$ , it is found that  $N_{\text{critical}} = 2/C\gamma T_2$ . Physically, this means that there must be enough atoms for the system to be in the collective strong coupling regime.

As has been discussed, the most striking feature of this laser is its ultranarrow linewidth. Fig. 2.6 shows the linewidth as a function of  $w$  and  $N$ . The leftmost dashed line in Fig. 2.6(a) is  $\gamma$  corresponding to the threshold for collective behavior. When the pump strength  $w$  passes through that threshold the linewidth gets rapidly smaller with increasing  $w$ . When  $w$  reaches  $T_2^{-1}$ , indicated by the second dashed line, essentially all atoms are phase locked together. From that point on the

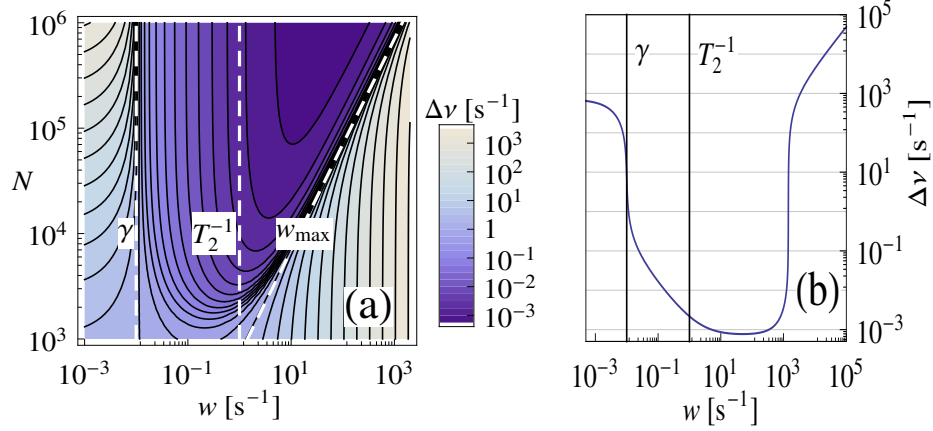


Figure 2.6: Source: Ref. [93]. (a) Linewidth vs  $w$  and  $N$ . The white dashed lines indicate (from left to right) the spontaneous decay rate  $\gamma$ , the inhomogeneous relaxation rate  $T_2$ , and the maximum pump rate  $w = NC\gamma$ . (b) is a cut through (a) for  $N = 10^6$  atoms.

pump noise due to  $w$  grows in proportion to the size of the collective spin vector. Therefore the linewidth is approximately constant and is given by  $\sim C\gamma$ . The actual numerical factor in front of  $C\gamma$  does not change much as a function of  $w$ . When  $w$  increases beyond  $NC\gamma$ , indicated by the third dashed line, the collective dipole is destroyed and the linewidth increases rapidly until it is eventually given by  $w$ . It is important to note that the parameters for achieving the maximum output power and the small linewidth are compatible with each other.

## Chapter 3

### Group-theoretic methods for solving the laser equation

The laser equation Eq. (2.13) is a quantum master equation in the Lindblad form [80] under the Born and Markov approximations [81]. It describes the time evolution of a paradigmatic quantum optical system, *i.e.*, an open quantum system of  $N$  two-level atoms (analogous to pseudo-spin-1/2 systems or qubits) symmetrically coupled to a single-mode photon field. In this chapter, we show that the laser equation can be efficiently simulated by applying group theoretic methods to the quantum master equation. This is important since many examples in quantum optics fall into this class, such as cavity QED, atoms coupled to chiral bosonic waveguides [102], nitrogen-vacancy (NV) centers in diamond coupled with photonic structures [21], quantum dots in photonic crystal [124], and superconducting qubits coupled with inductance/capacitance resonator [146]. The method described in this chapter will find numerous applications for simulating open quantum systems with large system size.

#### 3.1 Lindbladian in terms of generators of the $SU(4)$ group

In general, for all but the smallest system sizes, exact analytic solutions to Eq. (2.13) are intractable. Various approximation methods have been introduced, *e.g.* perturbation theories [61], mean-field approaches [30, 98], cumulant expansions [91, 92, 93], linear response theories [25] and  $c$ -number Langevin equations [7, 69]. However, it is often necessary to benchmark approximate methods with exact numerical solutions. Existing numerical simulation approaches, such as the quantum Monte Carlo method [24, 33, 104], scale exponentially with the underlying dimensionality

of the Hilbert space. Therefore, treating any appreciable system size is extremely difficult. It should be emphasized that the fully-symmetrical Dicke states [28] do not suffice as a reduced basis since basis vectors with mixed symmetry are required.

It has been realized that because of the permutation symmetry with respect to the exchange of spins in Eq. (2.13), the number of independent elements of the atomic density matrix is  $(N+1)(N+2)(N+3)/6$  [74]. This leads to a tremendous reduction of the number of required basis states needed to provide an exact solution of the master equation (from exponential to  $N^3$ ). The permutation symmetry also lead to Hartmann's development of generalized Dicke states [46], which are fully symmetrical states in the Liouvillian space. Furthermore, Hartmann found that the Lindbladian in the laser equation can be expressed in terms of the generators of the  $SU(4)$  group. For this purpose, 18 superoperators  $\mathcal{O}_+$ ,  $\mathcal{O}_-$  and  $\mathcal{O}_3$  where  $\mathcal{O} \in \{\mathcal{Q}, \Sigma, \mathcal{M}, \mathcal{N}, \mathcal{U}, \mathcal{V}\}$  are defined

$$\begin{aligned}
\mathcal{Q}_{\pm}\rho &:= \sum_{j=1}^N \sigma_j^{\pm} \rho \sigma_j^{\mp} \quad , \quad \mathcal{Q}_3\rho := \frac{1}{4} \sum_{j=1}^N (\sigma_j^3 \rho + \rho \sigma_j^3) \\
\Sigma_{\pm}\rho &:= \sum_{j=1}^N \sigma_j^{\pm} \rho \sigma_j^{\pm} \quad , \quad \Sigma_3\rho := \frac{1}{4} \sum_{j=1}^N (\sigma_j^3 \rho - \rho \sigma_j^3) \\
\mathcal{M}_{\pm}\rho &:= \sum_{j=1}^N \sigma_j^{\pm} \rho \frac{1 + \sigma_j^3}{2} \quad , \quad \mathcal{M}_3\rho := \frac{1}{2} \sum_{j=1}^N \sigma_j^3 \rho \frac{1 + \sigma_j^3}{2} \\
\mathcal{N}_{\pm}\rho &:= \sum_{j=1}^N \sigma_j^{\pm} \rho \frac{1 - \sigma_j^3}{2} \quad , \quad \mathcal{N}_3\rho := \frac{1}{2} \sum_{j=1}^N \sigma_j^3 \rho \frac{1 - \sigma_j^3}{2} \\
\mathcal{U}_{\pm}\rho &:= \sum_{j=1}^N \frac{1 + \sigma_j^3}{2} \rho \sigma_j^{\mp} \quad , \quad \mathcal{U}_3\rho := \frac{1}{2} \sum_{j=1}^N \frac{1 + \sigma_j^3}{2} \rho \sigma_j^3 \\
\mathcal{V}_{\pm}\rho &:= \sum_{j=1}^N \frac{1 - \sigma_j^3}{2} \rho \sigma_j^{\mp} \quad , \quad \mathcal{V}_3\rho := \frac{1}{2} \sum_{j=1}^N \frac{1 - \sigma_j^3}{2} \rho \sigma_j^3.
\end{aligned} \tag{3.1}$$

Although this list, Eq. (3.1), contains 18 operator definitions, only 15 of them are independent (it is possible to write  $\mathcal{N}_3$ ,  $\mathcal{U}_3$ ,  $\mathcal{V}_3$  in terms of the others). One can also demonstrate that the 15 remaining superoperators are linear combinations of the familiar Gell-Mann matrices that are the generators of the  $SU(4)$  group,  $\lambda_1, \dots, \lambda_{15}$  (see Appendix B).

In order to see how the superoperators [Eq. (3.1)] are related to generators of the  $SU(4)$  group (Gell-Mann matrices), consider first the fundamental one atom case. We interpret the  $2 \times 2$

density matrix as a  $4 \times 1$  vector in the representing vector space (*i.e.* Liouville space).

$$\begin{pmatrix} a & c \\ d & b \end{pmatrix} \rightarrow \begin{pmatrix} a \\ c \\ d \\ b \end{pmatrix}. \quad (3.2)$$

The relations are then given by [143]

$$\begin{aligned} \mathcal{Q}_\pm &\rightarrow \frac{1}{2}(\lambda_9 \pm i\lambda_{10}) \quad , \quad \mathcal{Q}_3 \rightarrow \frac{1}{4}\lambda_3 + \frac{1}{4\sqrt{3}}\lambda_8 + \sqrt{\frac{1}{6}}\lambda_{15} \\ \Sigma_\pm &\rightarrow \frac{1}{2}(\lambda_6 \pm i\lambda_7) \quad , \quad \Sigma_3 \rightarrow -\frac{1}{4}\lambda_3 + \frac{\sqrt{3}}{4}\lambda_8 \\ \mathcal{M}_\pm &\rightarrow \frac{1}{2}(\lambda_4 \pm i\lambda_5) \quad , \quad \mathcal{M}_3 \rightarrow \frac{1}{4}\lambda_3 + \frac{\sqrt{3}}{4}\lambda_8 \\ \mathcal{N}_\pm &\rightarrow \frac{1}{2}(\lambda_{11} \pm i\lambda_{12}) \quad , \quad \mathcal{N}_3 \rightarrow -\frac{1}{4}\lambda_3 + \frac{1}{4\sqrt{3}}\lambda_8 + \sqrt{\frac{1}{6}}\lambda_{15} \\ \mathcal{U}_\pm &\rightarrow \frac{1}{2}(\lambda_1 \pm i\lambda_2) \quad , \quad \mathcal{U}_3 \rightarrow \frac{1}{2}\lambda_3 \\ \mathcal{V}_\pm &\rightarrow \frac{1}{2}(\lambda_{13} \pm i\lambda_{14}) \quad , \quad \mathcal{V}_3 \rightarrow -\frac{1}{2\sqrt{3}}\lambda_8 + \sqrt{\frac{1}{6}}\lambda_{15}. \end{aligned} \quad (3.3)$$

The commutation relations of the superoperators are given in both Ref. [46] and [101]. The  $SU(4)$  group has three Casimir operators, one of which is quadratic in the generators, and the others are of higher order. The quadratic Casimir operator  $\mathcal{C}_1$  can be expressed in terms of superoperators

$$\mathcal{C}_1 = \sum_{\mathcal{O}} (\mathcal{O}_- \mathcal{O}_+ + \mathcal{O}_3) + \mathcal{U}_3^2 + \frac{1}{3}(\mathcal{U}_3 + 2\Sigma_3)^2 + \frac{1}{6}(3\mathcal{Q}_3 - 2\mathcal{U}_3 - \Sigma_3)^2. \quad (3.4)$$

We can also identify six  $SU(2)$  subalgebras,

$$[\mathcal{O}_+, \mathcal{O}_-] = 2\mathcal{O}_3, \quad [\mathcal{O}_3, \mathcal{O}_\pm] = \pm\mathcal{O}_\pm, \quad (3.5)$$

so that it is useful to define six corresponding quadratic superoperators  $\mathcal{O}^2 = \mathcal{O}_- \mathcal{O}_+ + \mathcal{O}_3^2 + \mathcal{O}_3$ , which commute with  $\mathcal{O}_3$ .

The Lindblad operators in the laser equation Eq. (2.13) can be written compactly with

superoperators  $\mathcal{O}_{+,-,3}$

$$\begin{aligned} \frac{1}{2} \sum_{j=1}^N (2\hat{\sigma}_j^\pm \rho \hat{\sigma}_j^\mp - \rho \hat{\sigma}_j^\mp \hat{\sigma}_j^\pm - \hat{\sigma}_j^\mp \hat{\sigma}_j^\pm \rho) &= -\frac{N}{2} \pm \mathcal{Q}_3 + \mathcal{Q}_\pm, \\ \frac{1}{2} \sum_{j=1}^N (2\hat{\sigma}_j^z \rho \hat{\sigma}_j^z - 2\rho) &= 4\mathcal{M}_3 - 2\mathcal{Q}_3 - 2\Sigma_3 - N. \end{aligned} \quad (3.6)$$

The completeness of  $\mathcal{O}_{+,-,3}$  implies that an arbitrary full-symmetrical Hamiltonian can be expressed by them. Therefore, the Hamiltonian term in Eq. (2.13) can be rewritten as

$$\begin{aligned} \frac{1}{i\hbar} [H, \rho] &= \frac{1}{i\hbar} [\hbar\omega_c \hat{a}^\dagger \hat{a}, \rho] - 2i\omega_a \Sigma_3 \rho - i\frac{g}{2} [\hat{a}(\mathcal{M}_+ + \mathcal{N}_+) \rho + \hat{a}^\dagger(\mathcal{M}_- + \mathcal{N}_-) \rho] \\ &\quad + i\frac{g}{2} [(\mathcal{U}_+ + \mathcal{V}_+) \rho \hat{a}^\dagger + (\mathcal{U}_- + \mathcal{V}_-) \rho \hat{a}]. \end{aligned} \quad (3.7)$$

### 3.2 Generalized Dicke states

The generalized Dicke states are the fully symmetric representation of the  $SU(4)$  group. Transcribing notation from the four-flavor quark model, a model with the same symmetry structure, the fundamental representation is given by  $u = |1\rangle\langle 1|$ ,  $d = |0\rangle\langle 0|$ ,  $s = |1\rangle\langle 0|$ , and  $c = |0\rangle\langle 1|$  (up, down, strange, and charm). For the fully symmetric case, the normalized basis is:

$$P_{\alpha,\beta,\gamma,\delta} = \frac{\alpha!\beta!\gamma!\delta!}{N!} \sum_{\mathcal{P}} \mathcal{P} [u^\alpha d^\beta s^\gamma c^\delta], \quad (3.8)$$

where  $\mathcal{P}$  denotes all possible permutations and  $\alpha + \beta + \gamma + \delta = N$ . Therefore, the number of the basis is  $(N+1)(N+2)(N+3)/6$ . Note that only basis states with  $\gamma = \delta = 0$  have non-vanishing trace of unity.

Although it is perfectly fine to use any three of  $\alpha, \beta, \gamma, \delta$  to label the generalized Dicke states, Hartmann uses three quantum numbers [46] associated with  $SU(2)$  subalgebras [cf. Eq. (3.5)]. To specify such quantum numbers, we derive the following relations using the definition of the basis states in Eq. (3.8) and the action of the superoperators on the fundamental representation shown

	$u$	$d$	$s$	$c$		$u$	$d$	$s$	$c$		$u$	$d$	$s$	$c$
$\mathcal{Q}_+$	0	$u$	0	0	$\mathcal{M}_+$	0	0	0	$u$	$\mathcal{U}_+$	0	0	$u$	0
$\mathcal{Q}_-$	$d$	0	0	0	$\mathcal{M}_-$	$c$	0	0	0	$\mathcal{U}_-$	$s$	0	0	0
$\mathcal{Q}_3$	$\frac{1}{2}u$	$-\frac{1}{2}d$	0	0	$\mathcal{M}_3$	$\frac{1}{2}u$	0	0	$-\frac{1}{2}c$	$\mathcal{U}_3$	$\frac{1}{2}u$	0	$-\frac{1}{2}s$	0
$\Sigma_+$	0	0	0	$s$	$\mathcal{N}_+$	0	$s$	0	0	$\mathcal{V}_+$	0	$c$	0	0
$\Sigma_-$	0	0	$c$	0	$\mathcal{N}_-$	0	0	$d$	0	$\mathcal{V}_-$	0	0	0	$d$
$\Sigma_3$	0	0	$\frac{1}{2}s$	$-\frac{1}{2}c$	$\mathcal{N}_3$	0	$-\frac{1}{2}d$	$\frac{1}{2}s$	0	$\mathcal{V}_3$	0	$-\frac{1}{2}d$	0	$\frac{1}{2}c$

Table 3.1: The action of the  $SU(4)$  superoperators on the elements of the fundamental representation  $u, d, s, c$

in Table 3.1

$$\begin{aligned}
\mathcal{Q}_- \mathcal{Q}_+ P_{\alpha,\beta,\gamma,\delta} &= (\alpha + 1) \beta P_{\alpha,\beta,\gamma,\delta} \quad , \quad \mathcal{Q}_3 P_{\alpha,\beta,\gamma,\delta} = \frac{1}{2}(\alpha - \beta) P_{\alpha,\beta,\gamma,\delta} \\
\Sigma_- \Sigma_+ P_{\alpha,\beta,\gamma,\delta} &= (\gamma + 1) \delta P_{\alpha,\beta,\gamma,\delta} \quad , \quad \Sigma_3 P_{\alpha,\beta,\gamma,\delta} = \frac{1}{2}(\gamma - \delta) P_{\alpha,\beta,\gamma,\delta} \\
\mathcal{M}_- \mathcal{M}_+ P_{\alpha,\beta,\gamma,\delta} &= (\alpha + 1) \delta P_{\alpha,\beta,\gamma,\delta} \quad , \quad \mathcal{M}_3 P_{\alpha,\beta,\gamma,\delta} = \frac{1}{2}(\alpha - \delta) P_{\alpha,\beta,\gamma,\delta} \\
\mathcal{N}_- \mathcal{N}_+ P_{\alpha,\beta,\gamma,\delta} &= (\gamma + 1) \beta P_{\alpha,\beta,\gamma,\delta} \quad , \quad \mathcal{N}_3 P_{\alpha,\beta,\gamma,\delta} = \frac{1}{2}(\gamma - \beta) P_{\alpha,\beta,\gamma,\delta} \\
\mathcal{U}_- \mathcal{U}_+ P_{\alpha,\beta,\gamma,\delta} &= (\alpha + 1) \gamma P_{\alpha,\beta,\gamma,\delta} \quad , \quad \mathcal{U}_3 P_{\alpha,\beta,\gamma,\delta} = \frac{1}{2}(\alpha - \gamma) P_{\alpha,\beta,\gamma,\delta} \\
\mathcal{V}_- \mathcal{V}_+ P_{\alpha,\beta,\gamma,\delta} &= (\delta + 1) \beta P_{\alpha,\beta,\gamma,\delta} \quad , \quad \mathcal{V}_3 P_{\alpha,\beta,\gamma,\delta} = \frac{1}{2}(\delta - \beta) P_{\alpha,\beta,\gamma,\delta} .
\end{aligned} \tag{3.9}$$

We can now define the quantum number associated with the six  $SU(2)$  subalgebras. By requesting, as usual, that  $\mathcal{O}^2 P_{\alpha,\beta,\gamma,\delta} = o(o + 1) P_{\alpha,\beta,\gamma,\delta}$  and  $\mathcal{O}_3 P_{\alpha,\beta,\gamma,\delta} = o_3 P_{\alpha,\beta,\gamma,\delta}$ , we obtain

$$\begin{aligned}
q &= \frac{1}{2}(\alpha + \beta) \quad , \quad q_3 = \frac{1}{2}(\alpha - \beta) \\
\sigma &= \frac{1}{2}(\gamma + \delta) \quad , \quad \sigma_3 = \frac{1}{2}(\gamma - \delta) \\
m &= \frac{1}{2}(\alpha + \delta) \quad , \quad m_3 = \frac{1}{2}(\alpha - \delta) \\
n &= \frac{1}{2}(\beta + \gamma) \quad , \quad n_3 = \frac{1}{2}(\gamma - \beta) \\
u &= \frac{1}{2}(\alpha + \gamma) \quad , \quad u_3 = \frac{1}{2}(\alpha - \gamma) \\
v &= \frac{1}{2}(\beta + \delta) \quad , \quad v_3 = \frac{1}{2}(\delta - \beta) .
\end{aligned} \tag{3.10}$$

Note that  $q + \sigma = m + n = u + v = N/2$ .

Hartmann chooses  $q, q_3, \sigma_3$  to characterize the generalized Dicke states [46]. Note that  $\alpha, \beta, \gamma, \delta$  can be expressed in terms of  $q, q_3, \sigma_3$ ,

$$\begin{aligned}\alpha &= q + q_3 & , & & \beta &= q - q_3 \\ \gamma &= \sigma + \sigma_3 & , & & \delta &= \sigma - \sigma_3 ,\end{aligned}\tag{3.11}$$

where  $\sigma = N/2 - q$ . From  $q = (\alpha + \beta)/2$ , we conclude that  $q$  ranges from 0 to  $N/2$  in steps of  $1/2$  unit. From the  $SU(2)$  subalgebras, we conclude that  $q_3$  ranges from  $-q$  to  $q$  in steps of 1 and  $\sigma_3$  ranges from  $-\sigma$  to  $\sigma$  in steps of 1. Therefore, we denote  $P_{\alpha, \beta, \gamma, \delta}$  by  $P_{q, q_3, \sigma_3}$  with

- $q$ :  $\mathcal{Q}^2 P_{q, q_3, \sigma_3} = q(q+1)P_{q, q_3, \sigma_3}$ ,  $q = 0, 1/2, \dots, N/2$
- $q_3$ :  $\mathcal{Q}_3 P_{q, q_3, \sigma_3} = q_3 P_{q, q_3, \sigma_3}$ ,  $q_3 = -q, -q+1, \dots, q$
- $\sigma_3$ :  $\Sigma_3 P_{q, q_3, \sigma_3} = \sigma_3 P_{q, q_3, \sigma_3}$ ,  $\sigma_3 = -\sigma, -\sigma+1, \dots, \sigma$  ( $\sigma = N/2 - q$ ).

It is straightforward to determine actions of all the raising and lowering superoperators on  $P_{q, q_3, \sigma_3}$ ,

$$\begin{aligned}\mathcal{Q}_{\pm} P_{q, q_3, \sigma_3} &= (q \mp q_3) P_{q, q_3 \pm 1, \sigma_3}, \\ \Sigma_{\pm} P_{q, q_3, \sigma_3} &= (\sigma \mp \sigma_3) P_{q, q_3, \sigma_3 \pm 1}, \\ \mathcal{M}_{\pm} P_{q, q_3, \sigma_3} &= (m \mp m_3) P_{q \pm 1/2, q_3 \pm 1/2, \sigma_3 \pm 1/2}, \\ \mathcal{N}_{\pm} P_{q, q_3, \sigma_3} &= (n \mp n_3) P_{q \mp 1/2, q_3 \pm 1/2, \sigma_3 \pm 1/2}, \\ \mathcal{U}_{\pm} P_{q, q_3, \sigma_3} &= (u \mp u_3) P_{q \pm 1/2, q_3 \pm 1/2, \sigma_3 \mp 1/2}, \\ \mathcal{V}_{\pm} P_{q, q_3, \sigma_3} &= (v \mp v_3) P_{q \mp 1/2, q_3 \pm 1/2, \sigma_3 \mp 1/2}.\end{aligned}\tag{3.12}$$

We note that the fully symmetrical basis are also eigenstates of the quadratic Casimir operator  $\mathcal{C}_1$  with common eigenvalue  $3N(N+4)/8$ .

In order to solve the laser equation Eq. (2.13), we expand the density matrix as

$$\rho = \sum_{q, q_3, \sigma_3, m, n} C_{q, q_3, \sigma_3}^{m, n} P_{q, q_3, \sigma_3} |m\rangle \langle n|,\tag{3.13}$$

where  $C_{q, q_3, \sigma_3}^{m, n}$  are complex coefficients, and  $|n\rangle$  is the photon Fock state. Combining Eqs. (3.6) and (3.7) with the action rules of the  $SU(4)$  superoperators on the basis states Eq. (3.12) gives a closed

solution of the laser equation Eq. (2.13). In general, this can be solved analytically or numerically with standard methods. With generalized Dicke states, the numerical complexity with respect to the atom number reduces from exponential to  $N^3$ .

### 3.3 Calculating observables

Having established the procedure for determining the time evolution of  $\rho$ , it is now important to describe how to calculate physical observables. We begin with the trace given by:

$$\text{Tr}[\rho] = \sum_{m,q3} C_{N/2,q3,0}^{m,m} = 1, \quad (3.14)$$

which is an invariant during evolution to represent probability conservation. Average values  $\langle a \rangle$  and  $\langle a^\dagger a \rangle$  are found analogously. For the spin-operators, we provide the following examples up to quadratic order:

$$\begin{aligned} \langle \sigma_j^z \rangle &= 2\text{Tr}[\mathcal{Q}_3 \rho] / N, \\ \langle \sigma_j^z \sigma_k^z \rangle &= (4\text{Tr}[(\mathcal{Q}_3^2 - \Sigma_3^2) \rho] - N) / [N(N-1)], \\ \langle \sigma_j^\pm \rangle &= \text{Tr}[(\mathcal{M}_\pm + \mathcal{N}_\pm) \rho] / N, \\ \langle \sigma_j^+ \sigma_k^- \rangle &= \text{Tr}[\mathcal{V}_-(\mathcal{M}_- + \mathcal{N}_-) \rho - \mathcal{Q}_- \rho] / [N(N-1)], \end{aligned} \quad (3.15)$$

where  $j \neq k$ .

For coherence properties it is necessary to calculate products of operators evaluated at different times. Of particular interest are the first-order and second-order correlations, which can be found by applying the quantum regression theorem [95]:

$$\begin{aligned} \langle \hat{O}_1(t+\tau) \hat{O}_2(t) \rangle &= \text{Tr} \left[ \hat{O}_1 e^{\mathcal{L}\tau} [\hat{O}_2 \rho(t)] \right], \\ \langle \hat{O}_1(t) \hat{O}_1(t+\tau) \hat{O}_2(t+\tau) \hat{O}_2(t) \rangle &= \text{Tr} \left[ \hat{O}_2 e^{\mathcal{L}\tau} [\hat{O}_2 \rho(t) \hat{O}_1] \hat{O}_1 \right], \end{aligned} \quad (3.16)$$

where  $e^{\mathcal{L}\tau}[\rho]$  is the time propagation from Eq. (2.13) starting with the initial density matrix  $\rho$ . For example, in order to obtain the first-order correlation of  $\hat{O}_1$  and  $\hat{O}_2$ , one takes  $\hat{O}_2 \rho(t)$  as an initial condition, time evolves it for  $\tau$  according to Eq. (2.13), applies  $\hat{O}_1$ , and computes the trace. A

similar procedure follows for the second-order correlation. In this way, field quantities,  $\langle a^\dagger(t+\tau)a(t) \rangle$  and  $\langle a^\dagger(t)a^\dagger(t+\tau)a(t+\tau)a(t) \rangle$  are directly calculated. For spin-coherence, the required expressions are:

$$\begin{aligned} \sum_{j,k=1}^N \langle \sigma_j^+(t+\tau)\sigma_k^-(t) \rangle &= \text{Tr} [(\mathcal{M}_+ + \mathcal{N}_+)e^{\mathcal{L}\tau}[(\mathcal{M}_- + \mathcal{N}_-)\rho(t)]], \\ \sum_{j,j',k,k'=1}^N \langle \sigma_j^+(t)\sigma_{j'}^+(t+\tau)\sigma_k^-(t+\tau)\sigma_{k'}^-(t) \rangle &= \\ \text{Tr} [\mathcal{V}_-(\mathcal{M}_- + \mathcal{N}_-)e^{\mathcal{L}\tau}[\mathcal{V}_-(\mathcal{M}_- + \mathcal{N}_-)\rho(t)]] &. \end{aligned} \quad (3.17)$$

### 3.4 Transform to the angular-momentum basis representation

Although at this point we have provided a theoretical framework that is complete and provides exact and efficient solutions to the general quantum master equation, it is often inconvenient to work in the  $P_{q,q_3,\sigma_3}$  representation of the density operator. For example, it can be a nontrivial procedure to characterize the many-body spin-state in this representation by quantifying the degree of entanglement, which is derived from a functional (*i.e.*  $\text{Tr}[\rho \log(\rho)]$ ). For this reason, we illustrate now the procedure for efficiently projecting the density operator from the  $SU(4)$  basis representation onto the usual representation of density matrices formed from the Hilbert space basis vectors [143]. These Hilbert space basis vectors are specified by the angular momentum eigenket  $|S, M\rangle$ , where  $S = N/2, N/2 - 1, \dots, (1/2 \text{ or } 0)$  is the total spin and  $M = -S, -S+1, \dots, S$  is the spin-projection. Note that  $S$  also labels the symmetry of the states, e.g.  $S = N/2$  corresponds to the fully symmetrical Dicke states.

In order to illustrate how this projection is done, it is instructive for us to first examine explicitly the  $N = 2$  case where the Hilbert space is 4 dimensional. Two spins form a symmetric triplet state and an antisymmetric singlet state, corresponding to total spin  $S = 1$  and  $S = 0$

respectively. In this case, the complete density matrix from Eq. (3.13) for given  $m, n$  is

$$\begin{array}{l} |1, 1\rangle \\ |1, 0\rangle \\ |1, -1\rangle \\ |0, 0\rangle \end{array} \begin{pmatrix} \langle 1, 1| & \langle 1, 0| & \langle 1, -1| & \langle 0, 0| \\ C_{1,1,0}^{m,n} & \frac{C_{1/2,1/2,1/2}^{m,n}}{\sqrt{2}} & C_{0,0,1}^{m,n} & 0 \\ \frac{C_{1/2,1/2,-1/2}^{m,n}}{\sqrt{2}} & \frac{C_{1,0,0}^{m,n} + C_{0,0,0}^{m,n}}{2} & \frac{C_{1/2,-1/2,1/2}^{m,n}}{\sqrt{2}} & 0 \\ C_{0,0,-1}^{m,n} & \frac{C_{1/2,-1/2,-1/2}^{m,n}}{\sqrt{2}} & C_{1,-1,0}^{m,n} & 0 \\ 0 & 0 & 0 & \frac{C_{1,0,0}^{m,n} - C_{0,0,0}^{m,n}}{2} \end{pmatrix}.$$

Notice that the resulting matrix is block diagonal in the  $S = 1$  and  $S = 0$  subspaces (a  $3 \times 3$  block and a  $1 \times 1$  block). In addition, the complex coefficients contributing to the matrix element for  $|S, M\rangle\langle S, M'|$  all satisfy  $q_3 + \sigma_3 = M$  and  $q_3 - \sigma_3 = M'$ . Finally, the trace is simply  $\sum_{q_3=-1}^1 C_{1,q_3,0}^{m,n} = 1$ .

These results can be systematically extended to higher  $N$ . For any  $N$ , the density matrix is block diagonal in  $S$ , with each block given by

$$\rho_S^{m,n} = \sum_{M,M'} D_{S,M,M'}^{m,n} |S, M\rangle\langle S, M'|, \quad (3.18)$$

where  $D_{S,M,M'}$  are density matrix elements for the symmetry type  $S$ . There are  $n_S$  ways for  $N$  spins to construct the basis for each  $S$ , so that  $\sum_S (2S+1)n_S = 2^N$ , *i.e.* the Hilbert space dimension [4]. To find  $n_S$ , we note that  $|S, M\rangle$  forms a basis of the  $(2S+1)$ -dimensional irreducible representation of the  $SU(2)$  group. Determining  $n_S$  is accomplished with the help of the Young tableau of the  $SU(2)$  group, where one can obtain the number of equivalent representations iteratively. Fig. 3.1(a) shows the Young tableau for the  $N = 4$  case. A corresponding tabular method for evaluating  $n_S$  for any  $N$  is shown in Fig. 3.1(b), which contains about one half of Pascal's triangle.

With this in mind, one can now derive a systematic algorithm for obtaining density matrix elements  $D_{S,M,M'}^{m,n}$  given  $SU(4)$  expansion coefficients  $C_{q,q_3,\sigma_3}^{m,n}$ . The procedure is outlined as follows. For each layer of the pyramid [cf. Fig. 3.1(c)], one may start with a corner element ( $M$  and  $M'$  maximal) and fill out the matrix by successive application of the angular momentum lowering operator  $\hat{J}_- = \sum_{j=1}^N \sigma_j^-$  (noting that  $\rho \hat{J}_- = (\mathcal{U}_+ + \mathcal{V}_+) \rho$ ) to recursively fill out each row, and  $\hat{J}_- \rho$  (or Hermiticity of  $\rho$ ) to fill out each column. The layers are filled upwards from the base, starting

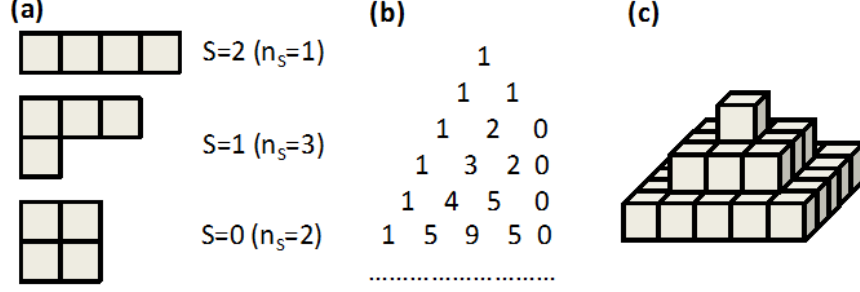


Figure 3.1: (a) Young tableau for determining the irreducible representations contained in the direct product representation of the  $SU(2)$  group for  $N=4$ . The dimension for  $S=2, 1, 0$  is  $5, 3, 1$  respectively, and  $n_s = 1, 3, 2$ , so the total Hilbert space dimension is  $5 \times 1 + 3 \times 3 + 1 \times 2 = 2^4$  as expected. (b) “Pascal’s triangle” to evaluate  $n_s$  in an iterative way for any  $N$  (the case considered in (a) is the fourth row down from the top). (c) Pyramid representation of the density operator in the  $|S, M\rangle$  representation for  $N=4$ . Each layer of the pyramid represents the block matrix for each  $S$ .

with  $D_{N/2, N/2, N/2}^{m, n} = C_{N/2, N/2, 0}^{m, n}$  as the corner element of the lowest layer, and finding the corner element of higher layers by Gaussian elimination from the trace constraint Eq. (3.14). In Appendix C, we demonstrate explicit application to 3 atoms, with extrapolation to higher  $N$  straightforward.

Being able to express the density operator in the  $|S, M\rangle$  representation makes easy the calculation of functionals, such as the purity  $\text{Tr}[\rho^2]$ , or the von Neumann entropy

$$-\text{Tr}(\rho \ln \rho) = -\sum_j \lambda_j \ln \lambda_j, \quad (3.19)$$

where  $\lambda_j$  are eigenvalues of  $\rho$ . The point is that, because the density matrix is block diagonal in the  $|S, M\rangle$  representation, we do not need to diagonalize the whole density matrix, which would be a daunting task. Instead, we only need to diagonalize a series of  $\lfloor N/2 \rfloor + 1$  blocks of dimension  $2S + 1$ .

Therefore, we have developed powerful methods to transform the density operator in the  $SU(4)$  basis representation to the  $|S, M\rangle$  representation. This has enabled us to efficiently diagonalize the whole density matrix and thus provided complete information about the system, including state information and functional properties of the density operator.

### 3.5 Further simplifying: $U(1)$ symmetry and quantum jump

We have formulated and applied a  $SU(4)$  theory to numerically solve the quantum master equation, which has reduced the exponential scaling of the problem to cubic in  $N$ . It turns out that it is possible to further simplify the problem by applying  $U(1)$  symmetry and by using the quantum jump method.

Let us first discuss applying the  $U(1)$  symmetry. By inspecting the laser equation Eq. (2.13), we find that it has global  $U(1)$  symmetry. By performing the following transformation

$$\begin{aligned} \hat{a} &\rightarrow \hat{a}e^{-i\varphi} \quad , \quad \hat{a}^\dagger \rightarrow \hat{a}^\dagger e^{i\varphi} \quad , \\ \hat{\sigma}_j^- &\rightarrow \hat{\sigma}_j^- e^{-i\varphi} \quad , \quad \hat{\sigma}_j^+ \rightarrow \hat{\sigma}_j^+ e^{i\varphi} \quad , \end{aligned} \quad (3.20)$$

where  $\varphi$  is an arbitrary phase, Eq. (2.13) is invariant. As a result, if the initial state of the system is phase invariant, the time evolution of the system will remain phase invariant. This will simplify the expansion of the density matrix in Eq. (3.13), where five quantum numbers  $q, q_3, \sigma_3, m, n$  are needed. In the case of phase-invariant states, the following condition must be satisfied

$$2\sigma_3 = n - m. \quad (3.21)$$

Therefore, only four quantum numbers are needed. This reduces the numerical complexity with respect to the atom number from  $N^3$  to  $N^2$ . This tremendous reduction should be compared with the full dimensionality of the Liouville space given by  $4^N$ . Therefore, it enables us to obtain numerical solutions up to a few hundred pseudospins and tens of photons.

Now let us extend the  $SU(4)$  method by using quantum jump [24, 33, 104]—a standard method in quantum optics. As will be shown, this allows us to simulate systems with a moderate number of photons and atoms. The unusual feature here is that the unraveling is performed in Liouville space rather than in Hilbert space, because it is in Liouville space that the  $SU(4)$  method operates.

According to Eq. (3.13), the dimension of the density matrix grows as the square of the photon number. This would impose great difficulties in numerical simulations of the laser region

due to the large number of photons. To overcome this difficulty, we unravel the master equation into Monte-Carlo trajectories in Liouville space enabling us to eliminate the photon basis from the simulation. The essential idea behind the method is that we are able to deduce the photon state by keeping track of the total number of quanta  $N_q$  in the system.

The quantum Monte Carlo method decomposes the density operator evolution into a set of quantum trajectories where, between applications of random jumps into random channels, the system evolves under an effective Hamiltonian [24, 33, 104]. The random jumps are chosen with probabilities such that the correct density operator evolution is obtained when an average is taken over trajectories. To construct a single trajectory, we first need to identify the jump operators. In our problem, there are four decay channels: repumping, spontaneous emission, dephasing, and cavity decay. The corresponding jump operators  $\mathcal{J}_i$  are

$$\begin{aligned}
\mathcal{J}_1 \hat{\rho} &= w \sum_{j=1}^N (\sigma_j^+ \hat{\rho} \sigma_j^-) = w \mathcal{Q}_+ \hat{\rho}, \\
\mathcal{J}_2 \hat{\rho} &= \gamma \sum_{j=1}^N (\sigma_j^- \hat{\rho} \sigma_j^+) = \gamma \mathcal{Q}_- \hat{\rho}, \\
\mathcal{J}_3 \hat{\rho} &= \frac{1}{2T_2} \sum_{j=1}^N (\sigma_j^z \hat{\rho} \sigma_j^z) \\
&= \frac{1}{2T_2} (4\mathcal{M}_3 - 2\mathcal{Q}_3 - 2\Sigma_3) \hat{\rho}, \\
\mathcal{J}_4 \hat{\rho} &= \kappa a \hat{\rho} a^\dagger.
\end{aligned} \tag{3.22}$$

When a repumping quantum jump occurs,  $N_q$  increases by one. When a spontaneous emission or a cavity-decay quantum jump happens,  $N_q$  decreases by one. The dephasing quantum jumps leave  $N_q$  unchanged. Therefore, during the evolution of a single trajectory,  $N_q$  is uniquely determined at every time step by keeping track of the numbers of jumps of the different types. With knowledge of  $N_q$ , the photon number does not need to be treated as an independent variable but is determined from the number of excited atoms. In Appendix C we have shown that

$$\begin{aligned}
\hat{J}_z P_{q,q_3,\sigma_3}^{(s)} &= (q_3 + \sigma_3) P_{q,q_3,\sigma_3}^{(s)}, \\
P_{q,q_3,\sigma_3}^{(s)} \hat{J}_z &= (q_3 - \sigma_3) P_{q,q_3,\sigma_3}^{(s)},
\end{aligned} \tag{3.23}$$

where  $\hat{J}_z = \sum_{j=1}^N \sigma_j^z/2$  is the collective spin operator. Therefore, the atomic state for a particular fully symmetrical atomic basis state in terms of the number of excited atoms is  $|q_3 + \sigma_3 + N/2\rangle\langle q_3 - \sigma_3 + N/2|$ . And thus the corresponding photon state is

$$|m\rangle\langle n| = |N_q - (q_3 + \sigma_3 + N/2)\rangle\langle N_q - (q_3 - \sigma_3 + N/2)|. \quad (3.24)$$

The simulation of jump times and decay channels is completely analogous to the wave-function Monte Carlo method. The effective evolution of the system is governed by the master equation excluding the above jump operators. As a result, under the effective evolution, the trace of the density operator is no longer conserved, but decreases as a function of time. This is analogous to the decay of the norm of the wavefunction in the wave function Monte Carlo method. A jump occurs when the trace of the density operator is less than a random number uniformly distributed in the interval  $[0, 1]$ . When a decay occurs we stochastically determine the channel  $i$  into which the system decays according to the probability distribution,

$$\mathcal{P}_i^{\text{jump}} = \frac{\text{Tr}[\mathcal{J}_i \hat{\rho}]}{\sum_{k=1}^4 \text{Tr}[\mathcal{J}_k \hat{\rho}]} . \quad (3.25)$$

Finally, in order to get the density operator at each time step, an ensemble average of many quantum trajectories is required. Then, various observables can be calculated according to Section 3.3. It is also worth noting that if one is only interested in the steady state density operator, a time average in the steady state can be applied instead of the ensemble average.

## Chapter 4

### A new perspective on steady state superradiance

In this chapter, we demonstrate a new perspective on the superradiant laser. We show that the cavity-mediated dissipative coupling between atoms in a superradiant laser acts to synchronize their phases. With this new perspective, we investigate Ramsey spectroscopy performed on a synchronized ensemble of two-level atoms. We show that, in principle, with this synchronized system it is possible to observe Ramsey fringes indefinitely, even in the presence of spontaneous emission and other sources of individual-atom dephasing. This could have important consequences for atomic clocks and a wide range of precision metrology applications.

#### 4.1 Synchronization of atomic dipoles

Synchronization is an emergent phenomenon that describes coupled objects spontaneously phase-locking to a common frequency in spite of differences in their natural frequencies [121]. It was famously observed by Huygens, the seventeenth century clock maker, in the antiphase synchronization of two maritime pendulum clocks [59]. Dynamical synchronization is now recognized as ubiquitous behavior occurring in a broad range of physical, chemical, biological, and mechanical engineering systems [16, 103, 121].

Theoretical treatments of this phenomenon are often based on the study of phase models [1, 71], and as such have been applied to an abundant variety of classical systems, including the collective blinking of fireflies, the beating of heart cells, and audience clapping [16, 103, 121]. The concept can be readily extended to systems with an intrinsic quantum mechanical origin such as

nanomechanical resonators [23, 50], optomechanical arrays [47], Josephson junctions [57, 130], and viscous collective atomic recoil lasing [110, 123]. When the number of coupled oscillators is large, it has been demonstrated that the onset of classical synchronization is analogous to a thermodynamic phase transition [135] and exhibits similar scaling behavior [68].

It turns out that in the superradiant laser regime, an effective synchronization model for the laser equation Eq. (2.13) can be derived under the mean-field approximation [140]. According to the model, we find that bad-cavity mediated coupling between atoms acts to synchronize the phase of atomic dipoles.

First of all, in an extreme regime of bad-cavity, the cavity field is slaved to the atomic field and can be adiabatically eliminated [13]. This requires  $\kappa \gg \sqrt{N}g, w, T_1^{-1}, T_2^{-1}$ . In a recent  $^{87}\text{Sr}$  lattice clock experiment at JILA [9] ( $T_1 \approx 160\text{s}$ ,  $T_2 \sim 1\text{s}$ ), this condition can be satisfied very well. Consider typical values of  $\kappa = 10^7\text{s}^{-1}$  and  $C = 0.16$ , then  $g = 10^2\text{s}^{-1}$  and  $\Gamma_C = C/T_1 = 10^{-3}\text{s}^{-1}$ . Even for  $N = 10^6$  atoms,  $\sqrt{N}g = 10^5\text{s}^{-1}$ , and  $w < N\Gamma_C = 10^3\text{s}^{-1}$ . The role of the cavity field then is to simply provide a source for a dissipative collective coupling for the atoms. The effective evolution is given by a quantum master equation containing only atoms:

$$\frac{d\rho}{dt} = -\frac{i}{2}\Delta\nu \sum_{j=1}^N [\hat{\sigma}_j^z, \rho] + \Gamma_C \mathcal{L}[\hat{J}^-]\rho + \sum_{j=1}^N \left( w\mathcal{L}[\hat{\sigma}_j^+] + \gamma\mathcal{L}[\hat{\sigma}_j^-] + \frac{1}{2T_2}\mathcal{L}[\hat{\sigma}_j^z] \right) \rho, \quad (4.1)$$

where  $\Delta\nu$  is the difference between the cavity frequency (in resonant with atomic frequency) and an external frequency (*e.g.* the frequency of a local oscillator). The collective decay rate can be taken to be small, *i.e.*  $\Gamma_C \ll \Gamma_S$ , where  $\Gamma_S = (T_1^{-1} + 2T_2^{-1})/2$  is the single-atom decoherence rate. This is because  $C$  is a dimensionless geometric cavity parameter that for real systems is typically much less than 1. For a current generation  $^{87}\text{Sr}$  optical clock experiment [9],  $\Gamma_S \sim 1\text{s}^{-1}$ , while  $\Gamma_C$  can be as small as  $10^{-3}\text{s}^{-1}$  for  $C \approx 0.16$ .

To derive the effective synchronization model, we first make the mean-field ansatz that the density matrix in Eq. (4.1) is a product of density matrices for each atom, *i.e.*,  $\rho = \prod_j \rho_j$ . We have checked that this ansatz is accurate to  $O(1/N)$ . Plugging this ansatz into Eq. (3) in the paper, we

obtain the equation of motion for  $j$ -th atom by tracing out all other atoms:

$$\begin{aligned} \frac{d\rho_j}{dt} = & \frac{1}{i} \left[ \frac{\Delta\nu}{2} \hat{\sigma}_j^z, \rho_j \right] + \sum_{j=1}^N \left( w \mathcal{L}[\hat{\sigma}_j^+] + \left( \frac{1}{T_1} + \Gamma_C \right) \mathcal{L}[\hat{\sigma}_j^-] + \frac{1}{4T_2} \mathcal{L}[\hat{\sigma}_j^z] \right) \rho_j \\ & + \frac{\Gamma_C}{2} (\hat{\sigma}_j^- \rho_j - \rho_j \hat{\sigma}_j^-) \mathcal{O} + \frac{\Gamma_C}{2} (\rho_j \hat{\sigma}_j^+ - \hat{\sigma}_j^+ \rho_j) \mathcal{O}^*, \end{aligned} \quad (4.2)$$

where  $\mathcal{O} = \sum_{m \neq j} \langle \sigma_m^+ \rangle$ . Eq. (4.2) is self-consistent since the effect of all the other atoms is approximated by a mean field  $\mathcal{O}$ .  $\mathcal{O}$  acts as an order parameter for the synchronization phase transition: in the absence of synchronization, or phase correlation between atoms,  $|\mathcal{O}| = 0$ , while  $|\mathcal{O}| > 0$  in the synchronized phase, breaking the  $U(1)$  symmetry of Eq. (4.1).

There are two factors at work in Eq. (4.2), the interaction with the mean field [resulting from the dissipative coupling in Eq. (4.1)] and quantum noises on individual atoms. We can see this from the quantum Langevin equation for  $\hat{\sigma}_j^+$ ;

$$\frac{d}{dt} \hat{\sigma}_j^+ = i\Delta\nu \hat{\sigma}_j^+ - \frac{1/T_1 + 1/T_2 + w + \Gamma_C}{2} \hat{\sigma}_j^+ + \frac{\Gamma_C}{2} \mathcal{O} \hat{\sigma}_j^z + \mathcal{F}(t), \quad (4.3)$$

where  $\mathcal{F}(t)$  is the quantum noise contributed by spontaneous emission, inhomogeneous dephasing, repumping and collective decay. The quantum noises randomize the phase of individual atoms, and thus inhibit phase locking between atoms. To find the effect of the dissipative coupling between atoms, we parameterize  $\langle \hat{\sigma}_j^+ \rangle$  as  $\alpha_j e^{-i\phi_j}$  and derive the equation of motion for  $\phi_j$ ,

$$\frac{d}{dt} \phi_j = -\Delta\nu + \frac{\Gamma_C}{2} \frac{\langle \hat{\sigma}_j^z \rangle}{\alpha_j} \sum_m \alpha_m \sin(\phi_m - \phi_j). \quad (4.4)$$

Eq. (4.4) is equivalent to the well-known Kuramoto model [70, 120] for describing the phase synchronization. In the case of  $\langle \hat{\sigma}_j^z \rangle > 0$ , the coupling gives rise to phase attraction between atoms.

## 4.2 Probing the synchronization with Ramsey spectroscopy

Ramsey spectroscopy offers an unambiguous way to show the synchronization dynamics of atoms in a superradiant laser. As shown in Fig. 4.1(b), Ramsey spectroscopy consists of three steps: (i) initial preparation of a coherent superposition between two quantum states, (ii) accumulation of a phase difference between the atoms and a local oscillator reference over an interrogation time

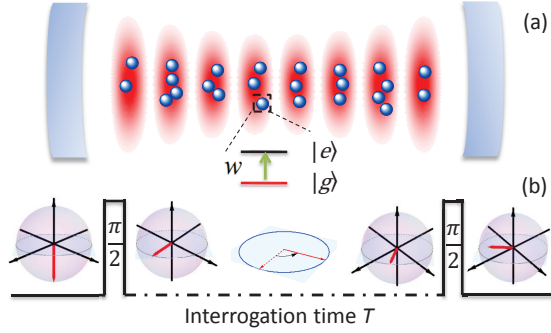


Figure 4.1: (a) Ramsey spectroscopy where atoms are coupled collectively to a cavity and pumped individually with incoherent rate  $w$ . (b) Ramsey sequence showing preparation in state  $|g\rangle$  (pseudospins pointing down to the south pole of the Bloch sphere), the  $\pi/2$   $y$ -axis rotation from the south pole to the equator, precession around the equator, and second  $\pi/2$   $x$ -axis rotation, after which the  $z$ -axis projection carries information about the cosine of the accumulated phase.

$T$ , and (iii) mapping of the phase difference to a population readout. The population measurement gives the well-known Ramsey fringes [105]. Due to the atomic decoherence, the visibility of Ramsey fringes decay as a function of  $T$ .

It is worth to point out that conventional Ramsey spectroscopy is based on independent-atom physics, with the role of a large number of atoms entering only through improving the signal by statistical averaging. Here, however, Ramsey spectroscopy is performed over atoms that are coupled collectively to a cavity. Conventional Ramsey spectroscopy is recovered by setting  $\Gamma_C = 0$  and  $w = 0$  in Eq. (4.1), with the result that the Ramsey fringe visibility then decays exponentially with the single-atom decoherence rate  $\Gamma_S$  [see Fig. 4.2(a)].

According to Eq. (4.4), the dissipative coupling between atoms will phase lock the atomic phases. Thus, we expect that the decay of Ramsey fringe visibility will be slower than that of conventional Ramsey spectroscopy. Indeed, Fig. 4.2(a) shows that the fringe visibility decays much slower than that of conventional Ramsey spectroscopy under the same  $T_1$  and  $T_2$  decoherences, demonstrating the robustness to individual-atom decoherence. When compared to conventional Ramsey spectroscopy with independent atoms, the principal difference here is that strong spin-spin correlations between atoms  $\langle \hat{\sigma}_j^+ \hat{\sigma}_k^- \rangle$  ( $j \neq k$ ) develop due to the dissipative coupling, as shown in Fig. 4.2(b). This feature is a characteristic of phase-locking [72, 93]. After a brief initial transient

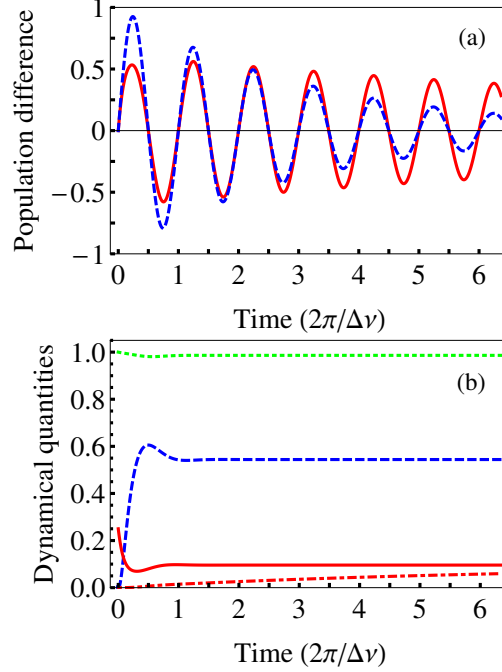


Figure 4.2: Calculations of Eq. (4.1) using  $SU(4)$  theory in Chapter 3 with  $N = 250$ ,  $\Gamma_C = 0.2/T_1$ ,  $T_2 = T_1$ , and  $w = N\Gamma_C/2$ . (a) Ramsey fringes with synchronized atoms (red solid line) versus  $T$ . Conventional Ramsey fringes (blue dashed line) for the same  $T_1$  and  $T_2$ . (b) During the interrogation time, the atomic inversion  $\langle \hat{\sigma}_j^z \rangle$  (blue dashed line), spin-spin correlation  $\langle \hat{\sigma}_j^+ \hat{\sigma}_k^- \rangle$  (red solid line),  $\langle \hat{\sigma}_j^+ \hat{\sigma}_k^- \rangle - \langle \hat{\sigma}_j^+ \rangle \langle \hat{\sigma}_k^- \rangle$  (red dotdashed line) and  $\langle \hat{\sigma}_j^+ \hat{\sigma}_k^z \rangle / (\langle \hat{\sigma}_j^+ \rangle \langle \hat{\sigma}_k^z \rangle)$  (green dotted line).

evolution, the fringe fits well to an exponentially decaying *sine* function, *i.e.*,  $Ae^{-\lambda t} \sin \Delta\nu t$ , where  $\lambda$  is the decay rate of the fringe visibility and  $A$  is an amplitude (we derive this behavior later.)

Intuitively, one may expect that in order to effectively phase-lock the atoms, it should be necessary for the dissipative coupling that provides rephasing to dominate over the ‘random-walk’ due to quantum noises that destroy phase correlations. Because of the all-to-all nature of the interaction of atoms through the cavity mode, the dissipative coupling strength scales with  $N$  and is given by  $N\Gamma_C/2$ . We show the effect of this in the inset of Fig. 4.3. For small atom number, the individual quantum noises dominate over the rephasing, and the fringe envelope decays more rapidly than in conventional Ramsey spectroscopy, *i.e.*  $\lambda > \Gamma_S$ . As  $N$  increases, the dissipative coupling increases, and we reach the regime  $\lambda < \Gamma_S$ . For large atom number, we find  $\lambda$  approaches  $\Gamma_C$ . The  $\Gamma_C$  limit arises from quantum fluctuations associated with the collective pseudospin decay

through the cavity.

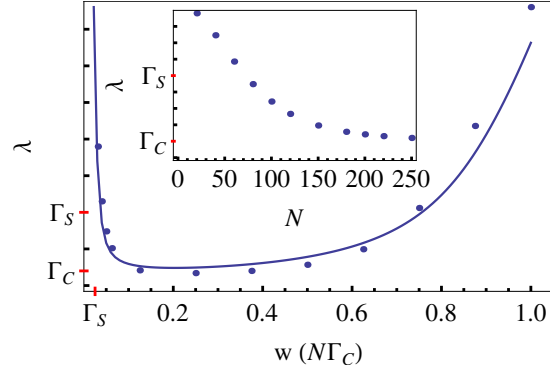


Figure 4.3: The decay rate  $\lambda$  of the visibility of Ramsey fringes at  $\Gamma_C = 0.2/T_1$  and  $T_2 = T_1$  as a function of repumping for  $N = 200$  and as a function of  $N$  for  $w = N\Gamma_C/2$  (Inset). The dots are numerical solutions of Eq. (4.1), and the solid blue line is the semiclassical approximation for comparison.

Therefore, due to the synchronization effect, the coherence time of atoms in steady-state superradiance is significantly longer than the single-atom coherence time and is essentially independent of single atom decoherences. A valid question to consider is: Why does the large incoherent repumping rate  $w$  not destroy the synchronization? One may have thought that the repumping would simply give rise to additional decoherence channels, on top of the usual  $T_1$  and  $T_2$  processes, and cause the Ramsey fringe visibility to decay more rapidly. Somewhat paradoxically, repumping is crucial for building up phase correlations among atoms. In Fig. 4.3, we show the effect of  $w$  on the decay rates of the Ramsey fringe visibility  $\lambda$ . When the repumping rate is too small or too large we find  $\lambda > \Gamma_S$ , so that the system performs worse than conventional Ramsey spectroscopy. This can be understood since the effective Kuramoto model Eq. (4.4) shows that population inversion of the pseudospins is a necessary condition for phase synchronization. The repumping strength must be large enough that there is more probability for the atoms to be in the excited state than in the ground state. However, if the repumping rate is too large, the associated quantum noise destroys the phase correlations before they can develop. As has also been seen in the case of the superradiant laser [93], the most coherent system is realized at an intermediate pump strength.

We emphasize that there are three timescales here. At short times, quantum correlations

develop as the atoms synchronize. This can be seen in the initial transient part of the evolution of the observables shown in Fig. 4.2(b), and is characterized by the timescale  $w^{-1}$ . This phase-locking time should be less than the atomic coherence time  $\Gamma_S^{-1}$  in order to observe high-visibility fringes. There is also a long timescale provided by the collective decay time  $\Gamma_C^{-1}$ . It is important to operate in the parameter regime in which  $w \gg \Gamma_S \gg \Gamma_C$ .

It is possible to develop an accurate semiclassical approximation to get analytical expression of  $\lambda$ . The approximation is valid in the case of large numbers of atoms. Taking advantage of the fact that all expectation values are symmetric with respect to atom exchange, we find from Eq. (4.1),

$$\frac{d}{dt}\langle\hat{\sigma}_j^+\rangle = i\Delta\nu\langle\hat{\sigma}_j^+\rangle - \frac{\Gamma_t}{2}\langle\hat{\sigma}_j^+\rangle + \frac{\Gamma_C}{2}(N-1)\langle\hat{\sigma}_j^+\hat{\sigma}_k^z\rangle, \quad (4.5)$$

where  $j \neq k$  and  $\Gamma_t = 2\Gamma_S + w + \Gamma_C$  is the total decay rate of the atomic coherence. We first point out that instead of calculating the population difference measured at the end of the Ramsey sequence, it is equivalent to calculate  $2\text{Im}[\langle\hat{\sigma}_j^+\rangle]$  just before the second  $\pi/2$  pulse. The decay rate of  $\langle\hat{\sigma}_j^+\rangle$  during the interrogation time  $T$  is therefore the same as that of the Ramsey fringe visibility. As seen in Fig. 4.2(b), the quantities  $\alpha(t) = \langle\hat{\sigma}_j^+\hat{\sigma}_k^z\rangle/(\langle\hat{\sigma}_j^+\rangle\langle\hat{\sigma}_k^z\rangle)$  and  $\langle\hat{\sigma}_j^z(t)\rangle$  rapidly approach steady state on the short timescale of the phase-locking,  $w^{-1}$ . We therefore substitute the steady-state values  $\alpha_{\text{ss}}$  and  $\langle\hat{\sigma}_j^z\rangle_{\text{ss}}$  into Eq. (4.5). This produces the exponentially decaying *sine* function solution noted earlier with decay constant

$$\lambda = \frac{1}{2} [\Gamma_t - (N-1)\Gamma_C\alpha_{\text{ss}}\langle\hat{\sigma}_j^z\rangle_{\text{ss}}]. \quad (4.6)$$

Furthermore  $\alpha_{\text{ss}} \approx 1$ , see Fig. 4.2(b). At the level of mean-field,  $\langle\hat{\sigma}_j^z\rangle_{\text{ss}} \approx \Gamma_t/(N-1)\Gamma_c$  giving the trivial result  $\lambda = 0$ . It is therefore necessary to develop a semiclassical expression for  $\langle\hat{\sigma}_j^z\rangle_{\text{ss}}$  that goes beyond mean-field.

To find  $\langle\hat{\sigma}_j^z\rangle_{\text{ss}}$ , we employ the cumulant approximation method [91, 92, 93]. Expectation values of the atoms are expanded in terms of  $\langle\hat{\sigma}_j^z\rangle$  and  $\langle\hat{\sigma}_j^+\hat{\sigma}_k^-\rangle$ . Their equation of motion can then

be found from Eq. (4.1) in the paper,

$$\begin{aligned}\frac{d}{dt}\langle\hat{\sigma}_j^z\rangle &= -(\Gamma_C + \frac{1}{T_1})(\langle\hat{\sigma}_j^z\rangle + 1) - w(\langle\hat{\sigma}_j^z\rangle - 1) - 2\Gamma_C(N-1)\langle\hat{\sigma}_j^+\hat{\sigma}_k^-\rangle \\ \frac{d}{dt}\langle\hat{\sigma}_j^+\hat{\sigma}_k^-\rangle &\approx -\Gamma_t\langle\hat{\sigma}_j^+\hat{\sigma}_k^-\rangle + \frac{\Gamma_C}{2}\langle\hat{\sigma}_j^z\rangle(1 + \langle\hat{\sigma}_j^z\rangle) + \Gamma_C(N-2)\langle\hat{\sigma}_j^+\hat{\sigma}_k^-\rangle\langle\hat{\sigma}_j^z\rangle.\end{aligned}$$

where we have factorized  $\langle\hat{\sigma}_j^z\hat{\sigma}_k^z\rangle \approx \langle\hat{\sigma}_j^z\rangle^2$  and  $\langle\hat{\sigma}_j^+\hat{\sigma}_k^-\hat{\sigma}_l^z\rangle \approx \langle\hat{\sigma}_j^+\hat{\sigma}_k^-\rangle\langle\hat{\sigma}_l^z\rangle$ .  $\langle\hat{\sigma}_j^z\rangle_{ss}$  can then be found by setting the time derivatives to zero, and the resulting algebraic equations form a close set and can be solved exactly.

Fig. 4.3 compares  $\lambda$  from the semiclassical expression with the quantum master equation solution, showing good agreement over the full range of pumping rates.

### 4.3 Robustness of the synchronization

In the above discussion, the atom-cavity coupling strength  $g$  is assumed to be identical for all atoms. In principle, this could be achieved by trapping the atoms at the antinodes of the cavity mode by an optical lattice in the Lamb-Dicke regime. Even so, there is still weak inhomogeneity of  $g$ . In this section, we show that the synchronization of atoms is robust against spatial variations of the atom-photon coupling strength,  $g$ .

We calculate the decay rate of the visibility of Ramsey fringes,  $\lambda$ , under an inhomogeneous  $g$  factor. As shown in Fig. 4.4(a),  $\lambda$  will increase slowly when the spread in  $g$  ( $\Delta g$ ) increases. However, this can be interpreted as a reduced effective atom number. Fig. 4.4(b) shows that given the inhomogeneity of  $g$ ,  $\lambda$  will approach  $\Gamma_C$  simply by increasing the number of atoms. This is precisely due to the fact that the collective dissipative coupling strength is given by  $N\Gamma_C/2$ . As long as the dissipative coupling can be made to dominate the individual-atom quantum noises, which can be done by increasing  $N$ , the spread in  $g$  does not play an important role.

### 4.4 Conditional Ramsey spectroscopy with synchronized atoms

The performance of conventional Ramsey spectroscopy is limited by the atomic coherence time, which causes decay of the fringe visibility as a function of  $T$ . Due to this decay, an optimal

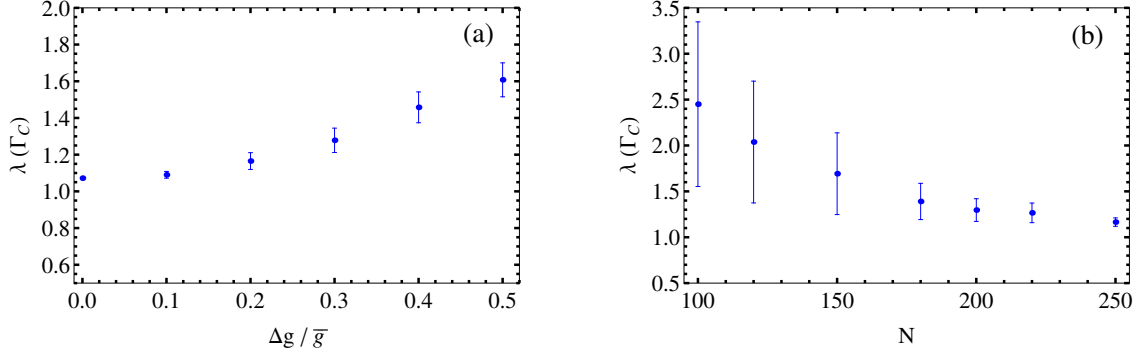


Figure 4.4: (a) The decay rate of the visibility of the Ramsey fringes as a function of standard deviation of the  $g$  factor at  $\Gamma_C = 0.2/T_1$ ,  $T_2 = T_1$ , and  $w = N\Gamma_C/5$  for  $N = 250$  atoms. (b) The decay rate of the visibility of the Ramsey fringes as a function of number of atoms at  $\Gamma_C = 0.2/T_1$ ,  $T_2 = T_1$ ,  $w = N\Gamma_C/5$ , and  $\Delta g/\bar{g} = 0.2$ .  $\Gamma_C$  in both (a) and (b) is defined using the mean of the  $g$  distribution,  $\bar{g}$ . Statistics are accumulated by sampling  $g$  from a Gaussian distribution. The dots are average values for 100 runs, and error bars represent the standard deviations.

strategy is typically used that involves setting  $T$  to be of the order of the coherence time, and filling up the total measurement interval  $\tau$  by repeated Ramsey cycles [54]. This gives an uncertainty in the frequency difference between the atoms and local oscillator that scales as  $1/(\sqrt{N}\tau)$ , with the  $\sqrt{N}$  coming from the quantum projection noise at each readout. This scaling  $\tau^{-1/2}$  is much worse than the fundamental Fourier limit  $\tau^{-1}$ .

There are two paths to improving on the standard limit for Ramsey spectroscopy, apart from simply increasing  $N$ . Firstly, the projection noise can be reduced by preparing spin-squeezed states [66, 132, 133]. Pursuing this direction, there have been numerous efforts to produce spin-squeezing in various physical situations [3, 19, 34, 41, 76, 107, 115]. It is worth pointing out that entangled states are often fragile and sensitive to decoherence processes, which may limit their potential for providing significant improvements to the sensitivity [2, 55]. Secondly, one can increase the coherence time of atoms. One approach has been to increase the dephasing time of magnetically and optically trapped atomic ensembles by spin self-rephasing induced by the exchange interaction between two identical particles [27, 67]. In recent lattice clock experiments [9], the atomic dephasing time  $T_2$  has been pushed to  $\sim 1$ s. Even if further technical improvements are

made, there is a fundamental upper limit to the atomic coherence time provided by the lifetime,  $T_1$ , of the long-lived excited clock state ( $\sim 160$ s for  $^{87}\text{Sr}$ ) [100].

In this section, we propose that Ramsey Spectroscopy using synchronized atoms is potentially more robust against decoherence [140]. We show that synchronized atoms undergo only a collective quantum phase diffusion. However, the collective phase can be continuously monitored by observing the cavity output field. Consequently, this system provides a kind of conditional Ramsey spectroscopy, conditioned on the cavity output, where fringes of high visibility may be observed indefinitely.

We have shown that with synchronized atoms the Ramsey fringe decays extremely slowly with rate  $\Gamma_C$ . This results from a statistical average of independent trials. The decay of the fringe visibility is really due to the averaging itself, as we will now see. In each trial, the quantum phase is diffusing as a function of interrogation time. This means that as time goes on, different trials begin to add out of phase, and so the fringe visibility decays.

This motivates us to consider the properties of a single experimental run, where the behavior is qualitatively different. Although in a single run, the fringe undergoes a quantum phase diffusion, it does so with non-decaying visibility. This quantum phase diffusion has a simple physical interpretation in terms of quantum measurements. Since the cavity field follows the atomic coherence through adiabatic elimination, measuring the phase of the cavity output field, for example by homodyne measurement, is equivalent to a continuous non-destructive measurement on which information is gathered about the evolving collective atomic phase. The back-action of this measurement introduces fluctuations that cause the collective atomic phase to undergo a random-walk [11].

We demonstrate this in Fig. 4.5(a), where we show a typical Ramsey fringe for a single experimental trial by using the method of quantum state diffusion [137, 136] to yield conditional evolution of the system subject to continuous measurements of the cavity field. The phase diffusion of the synchronized atoms is evident from the phase fluctuation of the Ramsey fringe. To find the phase diffusion coefficient, Fig. 4.5(b) shows the statistics of the positions of the zero crossings of the fringe for 4000 trials. They fit well to Gaussian distributions with variance given by  $T\Gamma_C$ ,

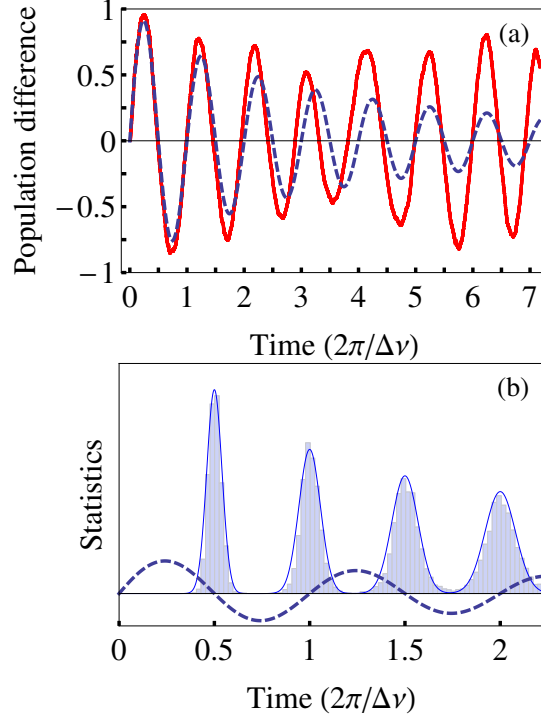


Figure 4.5: Quantum state diffusion calculations of conditional Ramsey fringes subject to continuous homodyne measurement of the cavity output field for  $N = 10$  and  $w = N\Gamma_C/2$ . The blue dashed lines are the ensemble average for reference. (a) A typical Ramsey fringe for a single experimental trial (red solid line). (b) Histograms are the statistics of the positions of zero crossings of each fringe for 4000 trials. The blue solid lines are fitted Gaussian distributions with variance of  $T\Gamma_C$  centered on the zero crossing of the ensemble average.

clearly demonstrating that it is a diffusion process and that the diffusion coefficient is  $\sqrt{\Gamma_C}$ . Note that this is the same mechanism that also sets the quantum limited linewidth in a superradiant laser to be  $\Gamma_C$  [93], observed here in the time rather than frequency domain.

We should emphasize that the quantum phase diffusion does not itself provide a fundamental limit to the performance of conditional Ramsey spectroscopy, since the collective atomic phase can be tracked by measuring the light output from the cavity. This opens up the exciting possibility of observing conditional Ramsey fringes (meaning an experimental trial conditioned on the measurement record of the output field) of near maximum fringe visibility for as long as the atoms can be stored, even in the presence of  $T_1$  and  $T_2$  processes. Of course a practical limit is also set by the length of time for which the local oscillator can remain phase coherent. In principle, if

experimentally achieved, this work could lead to dramatic advances in the sensitivity of Ramsey spectroscopy, since the entire measurement interval could then be used to determine frequency at the Fourier limit.

## Chapter 5

### Quantum synchronization of two ensembles of superradiant atoms

Recently, there has been increasing interest in exploring manifestations of synchronization in the quantum realm [35, 48, 53, 56, 72, 73, 75, 86, 87, 127, 128, 147]. Connections between quantum entanglement and synchronization have been revealed in different systems [72, 73, 87, 147]. Based on Heisenberg uncertainty principle, quantum synchronization measures have been applied to coupled optomechanical cells [87]. The effect of quantum noise has been shown to reduce the synchronization region of a driven self-sustained oscillator [127]. Since the phenomenon is inherently non-equilibrium, all of these systems share the common property of competition between coherent and incoherent driving and dissipative forces.

In this chapter, we propose a modern-day realization of the original Huygens experiment [59]. We consider the synchronization of two active atomic clocks coupled to a common single-mode optical cavity. It has been predicted that in the regime of steady-state superradiance [10, 12, 91, 92, 93] a neutral atom lattice clock could produce an ultracoherent optical field with a quality factor (ratio of frequency to linewidth) that approaches  $10^{18}$ . We show that two such clocks may exhibit a dynamical phase transition [30, 52, 61, 122] from two disparate oscillators to quantum phase-locked dynamics. The onset of synchronization at a critical pump strength is signified by an abruptly increased relative phase diffusion that diverges in the thermodynamic limit. Besides being of fundamental importance in nonequilibrium quantum many-body physics, this work could have broad implications for many practical applications of ultrastable lasers and precision measurements [93].

## 5.1 Setup

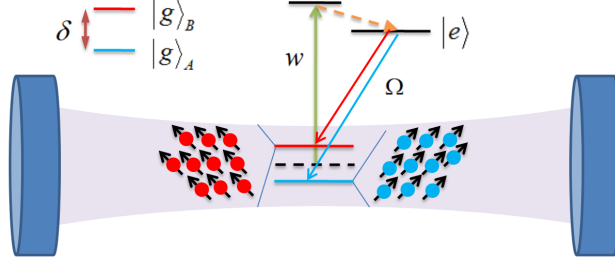


Figure 5.1: Two ensembles of driven two-level atoms coupled to a single-mode cavity field. The atoms in ensemble  $A$  are detuned above the cavity resonance (dashed line). Ensemble  $B$  contains atoms detuned below the cavity resonance by an equivalent amount.

The general setup is shown schematically in Fig. 5.1. Two ensembles, each containing  $N$  two-level atoms with excited state  $|e\rangle$  and ground state  $|g\rangle$ , are collectively coupled to a high-quality optical cavity. The transition frequencies of the atoms in ensembles  $A$  and  $B$  are detuned from the cavity resonance by  $\delta/2$  and  $-\delta/2$  respectively. This could be achieved by spatially separating the ensembles and applying an inhomogeneous magnetic field to induce a differential Zeeman shift. The atoms in both ensembles are pumped incoherently to the excited state as in the steady-state superradiance [10, 12].

This system is described by the Hamiltonian in the rotating frame of the cavity field:

$$\hat{H} = \frac{\hbar\delta}{2}(\hat{J}_A^z - \hat{J}_B^z) + \frac{\hbar g}{2}(\hat{a}^\dagger \hat{J}_A^- + \hat{J}_A^+ \hat{a} + \hat{a}^\dagger \hat{J}_B^- + \hat{J}_B^+ \hat{a}), \quad (5.1)$$

where  $g$  is the atom-cavity coupling. Here  $\hat{J}_{A,B}^z = \frac{1}{2} \sum_{j=1}^N \hat{\sigma}_{(A,B)j}^z$  and  $\hat{J}_{A,B}^\pm = \sum_{j=1}^N \hat{\sigma}_{(A,B)j}^\pm$  are the collective atomic spin operators, written in terms of the Pauli operators for the two-level system  $\hat{\sigma}_{(A,B)j}^z$  and  $\hat{\sigma}_{(A,B)j}^\pm = (\hat{\sigma}_{(A,B)j}^\pm)^\dagger$ .

In addition to the coherent atom-cavity coupling, incoherent processes are critical and include: the cavity intensity decay at rate  $\kappa$ , the pump rate  $w$ , the free-space spontaneous emission rate  $\gamma$ , and a background dephasing of the  $|e\rangle$ - $|g\rangle$  transition at rate  $T_2^{-1}$ . The total system is then described using a master equation for the reduced density operator  $\rho$ :

$$\frac{d\rho}{dt} = \frac{1}{i\hbar}[\hat{H}, \rho] + \kappa \mathcal{L}[\hat{a}] \rho + \sum_{\mathcal{T}=A,B} \sum_{j=1}^N \left( \gamma \mathcal{L}[\hat{\sigma}_{\mathcal{T}j}^-] + w \mathcal{L}[\hat{\sigma}_{\mathcal{T}j}^+] + \frac{1}{2T_2} \mathcal{L}[\hat{\sigma}_{\mathcal{T}j}^z] \right) \rho. \quad (5.2)$$

Again, the regime of steady-state superradiance is defined by the cavity decay being much faster than all other incoherent processes [10, 12, 91, 93]. In this regime, the cavity can be adiabatically eliminated, resulting in a field that is slaved to the collective atomic dipole of the two ensembles of atoms:

$$\hat{a} \simeq -\frac{ig}{\kappa + i\delta} \hat{J}_A^- - \frac{ig}{\kappa - i\delta} \hat{J}_B^- \quad (5.3)$$

For small detuning on the scale of the cavity linewidth,  $\delta \ll \kappa$ , Eq. (5.3) reduces to  $\hat{a} \simeq -ig\hat{J}^-/\kappa$ , where  $\hat{J}^- = \hat{J}_A^- + \hat{J}_B^-$  is the total collective spin-lowering operator. In this limit, the net effect of the cavity is to provide a collective decay channel for the atoms, with rate  $\gamma_C = C\gamma$ . This collective decay should be dominant over other atomic decay processes, *i.e.*,  $N\gamma_C \gg \gamma, T_2^{-1}$ , so that the time evolution is effectively given by a superradiance master equation containing only atoms:

$$\frac{d\rho}{dt} = \frac{\delta}{2i\hbar} [J_A^z - J_B^z, \rho] + \gamma_C \mathcal{L}[\hat{J}^-] \rho + w \sum_{j=1}^N (\mathcal{L}[\hat{\sigma}_{A_j}^+] + \mathcal{L}[\hat{\sigma}_{B_j}^+]) \rho. \quad (5.4)$$

With this system we naturally provide the three necessary ingredients for quantum synchronization; a controllable difference between the oscillation frequencies of two mesoscopic ensembles, a dissipative coupling generated by the emission of photons into the same cavity mode, and a driving force produced by optical pumping.

## 5.2 Mean-field picture

It is possible to understand a great deal about the synchronization of the proposed system with a simple mean-field treatment. Starting from Eq. (5.4), we make the mean-field ansatz that the density matrix is a product of density matrices for each atom, *i.e.*,  $\rho = \bigotimes_j \rho_{A_j} \otimes \rho_{B_j}$ . Substituting this ansatz into the master equation, we obtain the equation of motion for the  $j$ -th atom in each ensemble by tracing out all other atoms, *i.e.*

$$\begin{aligned} \frac{d}{dt} \rho_{A_j} &= -i \left[ \frac{\delta}{2} \hat{\sigma}_{A_j}^z, \rho_{A_j} \right] + w \mathcal{L}[\hat{\sigma}_{A_j}^+] \rho_{A_j} + \frac{\gamma_C}{2} (\hat{\sigma}_{A_j}^- \rho_{A_j} - \rho_{A_j} \hat{\sigma}_{A_j}^-) \mathcal{O} + \frac{\gamma_C}{2} (\rho_{A_j} \hat{\sigma}_{A_j}^+ - \hat{\sigma}_{A_j}^+ \rho_{A_j}) \mathcal{O}^*, \\ \frac{d}{dt} \rho_{B_j} &= -i \left[ -\frac{\delta}{2} \hat{\sigma}_{B_j}^z, \rho_{B_j} \right] + w \mathcal{L}[\hat{\sigma}_{B_j}^+] \rho_{B_j} + \frac{\gamma_C}{2} (\hat{\sigma}_{B_j}^- \rho_{B_j} - \rho_{B_j} \hat{\sigma}_{B_j}^-) \mathcal{O} + \frac{\gamma_C}{2} (\rho_{B_j} \hat{\sigma}_{B_j}^+ - \hat{\sigma}_{B_j}^+ \rho_{B_j}) \mathcal{O}^*, \end{aligned}$$

where  $\mathcal{O} = \sum_j \langle \hat{\sigma}_{A_j}^+ \rangle + \langle \hat{\sigma}_{B_j}^+ \rangle$  is the mean-field.

The above mean-field equation enables us to obtain an analogous two-component phase model to the well-known Kuramoto model for studying synchronization. To this end, we first derive the equation of motion for  $\langle \hat{J}_A^- \rangle$  and  $\langle \hat{J}_B^- \rangle$ ,

$$\frac{d}{dt} \begin{pmatrix} \langle \hat{J}_A^- \rangle \\ \langle \hat{J}_B^- \rangle \end{pmatrix} = M \begin{pmatrix} \langle \hat{J}_A^- \rangle \\ \langle \hat{J}_B^- \rangle \end{pmatrix} = \begin{pmatrix} -i\frac{\delta}{2} - \frac{w}{2} + \frac{\gamma_C}{2} \langle \hat{J}_A^z \rangle & \frac{\gamma_C}{2} \langle \hat{J}_A^z \rangle \\ \frac{\gamma_C}{2} \langle \hat{J}_B^z \rangle & i\frac{\delta}{2} - \frac{w}{2} + \frac{\gamma_C}{2} \langle \hat{J}_B^z \rangle \end{pmatrix} \begin{pmatrix} \langle \hat{J}_A^- \rangle \\ \langle \hat{J}_B^- \rangle \end{pmatrix}. \quad (5.5)$$

By parameterizing  $\langle \hat{J}_A^- \rangle$  as  $\alpha \exp(i\theta_A)$  and  $\langle \hat{J}_B^- \rangle$  as  $\beta \exp(i\theta_B)$ , we have

$$\frac{d}{dt} \theta_A = -\frac{\delta}{2} + \frac{\gamma_C}{2} \frac{\beta}{\alpha} \langle \hat{J}_A^z \rangle \sin(\theta_B - \theta_A), \quad \frac{d}{dt} \theta_B = \frac{\delta}{2} + \frac{\gamma_C}{2} \frac{\alpha}{\beta} \langle \hat{J}_B^z \rangle \sin(\theta_A - \theta_B). \quad (5.6)$$

From Eq. (5.6), we find a phase attraction between the two ensembles of atoms that exists as long as the atoms are repumped so that the atomic population inversion  $\langle \hat{J}_{A,B}^z \rangle$  is positive. It is the phase attraction resulting from the dissipative coupling that gives rise to the synchronization.

We may identify the synchronization transition within the mean-field theory. In the synchronized phase, the frequencies of the atoms are locked to the cavity frequency, leading to a non-oscillatory steady state in Eq. (4.2). In this case, it is easy to calculate the steady state value of  $\langle \hat{J}_{A,B}^z \rangle$  to be  $(w^2 + \delta^2)/(2w\gamma_C)$ . However, as  $\delta > w$ , the matrix  $M$  in Eq. (5.5) acquires complex (non-real) eigenvalues, indicating oscillations and therefore a precession of the relative phase. We refer to this as the unsynchronized parameter region.

The photons emitted by the cavity provide directly measurable observables. Synchronization is evident in the properties of the photon spectra. In the case of two independent ensembles in the unsynchronized phase, each ensemble radiates photons at its own distinct transition frequency. This leads to two Lorentzian peaks that are typically well-separated. In the synchronized phase, all of the atoms radiate at a common central frequency resulting in a single peak.

### 5.3 Quantum signatures of the synchronization

Although the mean-field treatment correctly predicts the phase transition, the associated quantum noises in the open quantum system and quantum correlations between the pseudospins

are absent. These are the aspects that distinguish quantum synchronization from classical synchronization.

To solve this problem quantum mechanically, we use a semiclassical approximation that is applicable to large atom numbers. Cumulants for the expectation values of system operators  $\{\hat{\sigma}_{(A,B)j}^z, \hat{\sigma}_{(A,B)j}^\pm\}$  are expanded to second order [91, 93]. All expectation values are symmetric with respect to exchange of atoms within each ensemble, *i.e.*  $\langle \hat{\sigma}_{B_i}^+ \hat{\sigma}_{B_j}^- \rangle = \langle \hat{\sigma}_{B_1}^+ \hat{\sigma}_{B_2}^- \rangle$ , for all  $i \neq j$ . Due to the  $U(1)$  symmetry,  $\langle \hat{\sigma}_{(A,B)j}^\pm \rangle = 0$ . Therefore, all nonzero observables can be expressed in terms of  $\langle \hat{\sigma}_{(A,B)j}^z \rangle$ ,  $\langle \hat{\sigma}_{(A,B)i}^+ \hat{\sigma}_{(A,B)j}^- \rangle$ , and  $\langle \hat{\sigma}_{(A,B)i}^z \hat{\sigma}_{(A,B)j}^z \rangle$ . Expectation values involving only one ensemble are the same for both ensembles and for these cases we omit the superfluous  $A, B$  subscripts. The equations of motion can then be found from Eq. (5.4):

$$\begin{aligned} \frac{d}{dt} \langle \hat{\sigma}_1^z \rangle &= -\gamma_C (\langle \hat{\sigma}_1^z \rangle + 1) - w (\langle \hat{\sigma}_1^z \rangle - 1) \\ &\quad - 2\gamma_C (N-1) \langle \hat{\sigma}_1^+ \hat{\sigma}_2^- \rangle - \gamma_C N (\langle \hat{\sigma}_{A_1}^+ \hat{\sigma}_{B_1}^- \rangle + \text{c.c.}), \end{aligned} \quad (5.7)$$

$$\begin{aligned} \frac{d}{dt} \langle \hat{\sigma}_1^+ \hat{\sigma}_2^- \rangle &= -(w + \gamma_C) \langle \hat{\sigma}_1^+ \hat{\sigma}_2^- \rangle + \frac{\gamma_C}{2} (\langle \hat{\sigma}_1^z \hat{\sigma}_2^z \rangle + \langle \hat{\sigma}_1^z \rangle) \\ &\quad + \gamma_C (N-2) \langle \hat{\sigma}_1^z \rangle \langle \hat{\sigma}_1^+ \hat{\sigma}_2^- \rangle \\ &\quad + \frac{\gamma_C}{2} N \langle \hat{\sigma}_1^z \rangle (\langle \hat{\sigma}_{A_1}^+ \hat{\sigma}_{B_1}^- \rangle + \text{c.c.}), \end{aligned} \quad (5.8)$$

$$\begin{aligned} \frac{d}{dt} \langle \hat{\sigma}_{A_1}^+ \hat{\sigma}_{B_1}^- \rangle &= -(w + \gamma_C - i\delta) \langle \hat{\sigma}_{A_1}^+ \hat{\sigma}_{B_1}^- \rangle + \frac{\gamma_C}{2} (\langle \hat{\sigma}_{A_1}^z \hat{\sigma}_{B_1}^z \rangle + \langle \hat{\sigma}_1^z \rangle) \\ &\quad + \gamma_C (N-1) \langle \hat{\sigma}_1^z \rangle (\langle \hat{\sigma}_{A_1}^+ \hat{\sigma}_{B_1}^- \rangle + \langle \hat{\sigma}_1^+ \hat{\sigma}_2^- \rangle), \end{aligned} \quad (5.9)$$

describing population inversion, spin-spin coherence within each ensemble, and correlation between ensembles, respectively. In deriving Eq. (5.8) and (5.9), we have dropped third order cumulants. We also factorize  $\langle \hat{\sigma}_{(A,B)i}^z \hat{\sigma}_{(A,B)j}^z \rangle \approx \langle \hat{\sigma}_1^z \rangle^2$ , which we find to be valid outside the regime of very weak pumping where a non-factorizable subradiant dark state plays an important role [91]. After making these approximations, Eq. (5.7) to (5.9) form a closed set of equations. The steady state is found by setting the time derivatives to zero and the resulting algebraic equations can be solved exactly.

We have validated Eq. (5.7) to (5.9) by comparison with exact numerical solutions of the

quantum master equation based on applying the  $SU(4)$  group theory (see Chapter 3). As shown in Fig. 5.2, the comparison is very good even for small system size of 30 atoms in each ensemble. Due to the presence of multiple ensembles it is difficult to implement exact calculations for more than about 50 atoms.

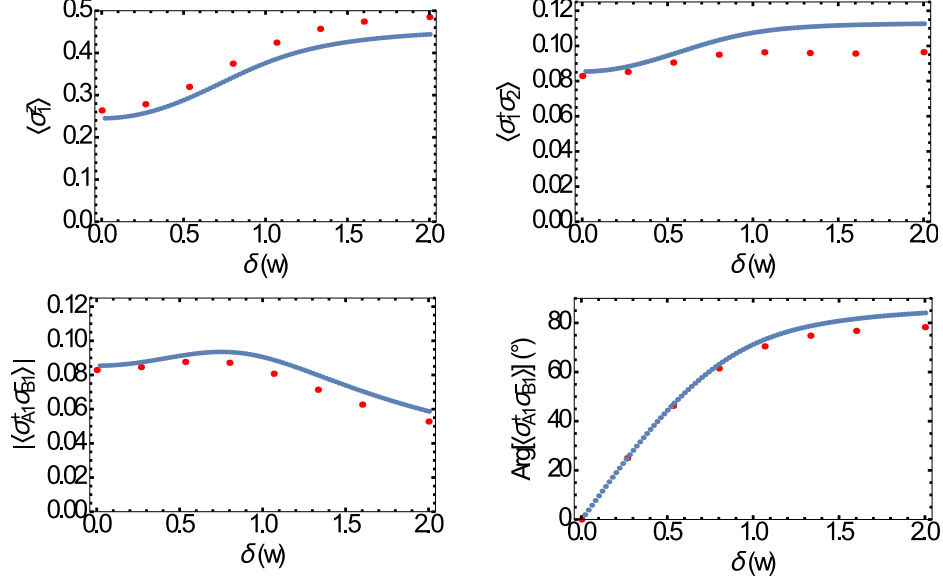


Figure 5.2: Steady state value of population inversion  $\langle \hat{\sigma}_1^z \rangle$ , spin-spin coherence within each ensemble  $\langle \hat{\sigma}_1^+ \hat{\sigma}_2^- \rangle$  and correlation between ensembles  $\langle \hat{\sigma}_{A1}^+ \hat{\sigma}_{B1}^- \rangle$  as a function of detuning. Red dots are exact numerical calculation by applying the  $SU(4)$  group theory. Blue lines are semiclassical results based on solutions to Eq. (5.7) to (5.9).

In order to calculate the photon spectrum, we employ the quantum regression theorem [95] to obtain the two-time correlation function of the light field,  $\langle \hat{a}^\dagger(\tau) \hat{a}(0) \rangle$ , where time 0 denotes an arbitrary time-origin in steady-state. In the limit  $\delta \ll \kappa$ , according to Eq. (5.3), the phase diffusion of the atoms and light are the same, *i.e.*  $\langle \hat{a}^\dagger(\tau) \hat{a}(0) \rangle \sim \langle \hat{J}^+(\tau) \hat{J}^-(0) \rangle$ . We begin by deriving equations of motion for  $\langle \hat{\sigma}_{A1}^+(\tau) \hat{\sigma}_{B1}^-(0) \rangle$  and  $\langle \hat{\sigma}_{B1}^+(\tau) \hat{\sigma}_{B2}^-(0) \rangle$ :

$$\frac{d}{d\tau} \begin{pmatrix} \langle \hat{\sigma}_{A1}^+(\tau) \hat{\sigma}_{B1}^-(0) \rangle \\ \langle \hat{\sigma}_{B1}^+(\tau) \hat{\sigma}_{B2}^-(0) \rangle \end{pmatrix} = \frac{1}{2} \begin{pmatrix} X & Y \\ Y & X^* \end{pmatrix} \begin{pmatrix} \langle \hat{\sigma}_{A1}^+(\tau) \hat{\sigma}_{B1}^-(0) \rangle \\ \langle \hat{\sigma}_{B1}^+(\tau) \hat{\sigma}_{B2}^-(0) \rangle \end{pmatrix}, \quad (5.10)$$

where  $X = \gamma_C(N - 1)\langle\hat{\sigma}_1^z(0)\rangle - \gamma_C - w + i\delta$ ,  $Y = \gamma_CN\langle\hat{\sigma}_1^z(0)\rangle$ . We have systematically factorized:

$$\begin{aligned}\langle\hat{\sigma}_1^z(\tau)\hat{\sigma}_{A1}^+(\tau)\hat{\sigma}_{B1}^-(0)\rangle &\approx \langle\hat{\sigma}_1^z(0)\rangle\langle\hat{\sigma}_{A1}^+(\tau)\hat{\sigma}_{B1}^-(0)\rangle, \\ \langle\hat{\sigma}_1^z(\tau)\hat{\sigma}_{B1}^+(\tau)\hat{\sigma}_{B2}^-(0)\rangle &\approx \langle\hat{\sigma}_1^z(0)\rangle\langle\hat{\sigma}_{B1}^+(\tau)\hat{\sigma}_{B2}^-(0)\rangle.\end{aligned}\quad (5.11)$$

Similarly, one finds that  $\langle\hat{\sigma}_{A1}^+(\tau)\hat{\sigma}_{A2}^-(0)\rangle$  and  $\langle\hat{\sigma}_{B1}^+(\tau)\hat{\sigma}_{A1}^-(0)\rangle$  satisfy the same equation of motion as Eq. (5.10). The solution of this coupled set is straightforward and shows that both  $\langle\hat{\sigma}_{A1}^+(\tau)\hat{\sigma}_{B1}^-(0)\rangle$  and thus also  $\langle\hat{a}^\dagger(\tau)\hat{a}(0)\rangle$  evolve in proportion to the exponential:

$$\exp\left[-\frac{1}{2}\left(w + \gamma_C - (N - 1)\gamma_C\langle\hat{\sigma}_1^z\rangle - \sqrt{(N\gamma_C\langle\hat{\sigma}_1^z\rangle)^2 - \delta^2}\right)\tau\right], \quad (5.12)$$

which we parametrize by  $\exp[-(\Gamma + i\Delta)\tau/2]$ , where  $\Gamma$  represents the decay of the first-order correlation and  $\Delta$  the modulation frequency. Laplace transformation yields the photon spectrum which consists of Lorentzians of halfwidth  $\Gamma/2$  centered at frequencies  $\pm\Delta/2$ .

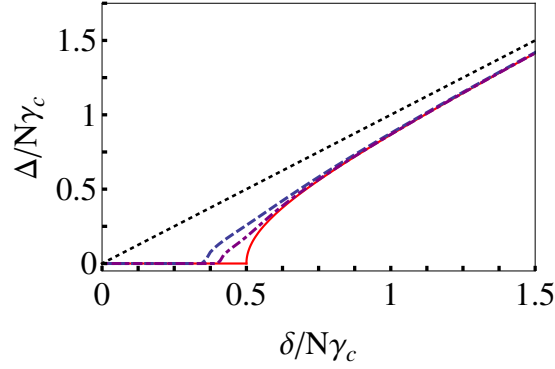


Figure 5.3: Steady-state relative phase precession for two ensembles as a function of detuning at  $w = N\gamma_C/2$  for  $N = 100$  (blue dashed line),  $N = 500$  (purple dot dashed line) and  $N = 10^6$  (red solid line). The straight dotted line is  $\delta = \Delta$ .

The importance of the two-time correlation function is that it provides direct access to the correlated phase dynamics of the two ensembles. The parameter  $\Delta$  physically represents the precession frequency of the phase of the collective mesoscopic dipoles with respect to one another. In Fig. 5.3, we show  $\Delta$  as a function of  $\delta$  at  $w = N\gamma_C/2$  for several values of  $N$ . For large detuning,  $\Delta$  approaches  $\delta$ , indicating that the dipoles precess independently at their uncoupled frequency. Below a critical  $\delta$ , we find  $\Delta$  to be zero, indicating synchronization and phase locking.

There is not yet a generally accepted meaning of the term ‘quantum synchronization’. In general, we believe that in the quantum synchronization case, quantum mechanics introduces two effects. The first is the quantum noise, which is due to the oscillator gaining or losing individual quanta. This can be equivalently viewed as the fundamental fluctuations due to the interaction of the system with its environment. The second effect is that the oscillators can be quantum mechanically correlated.

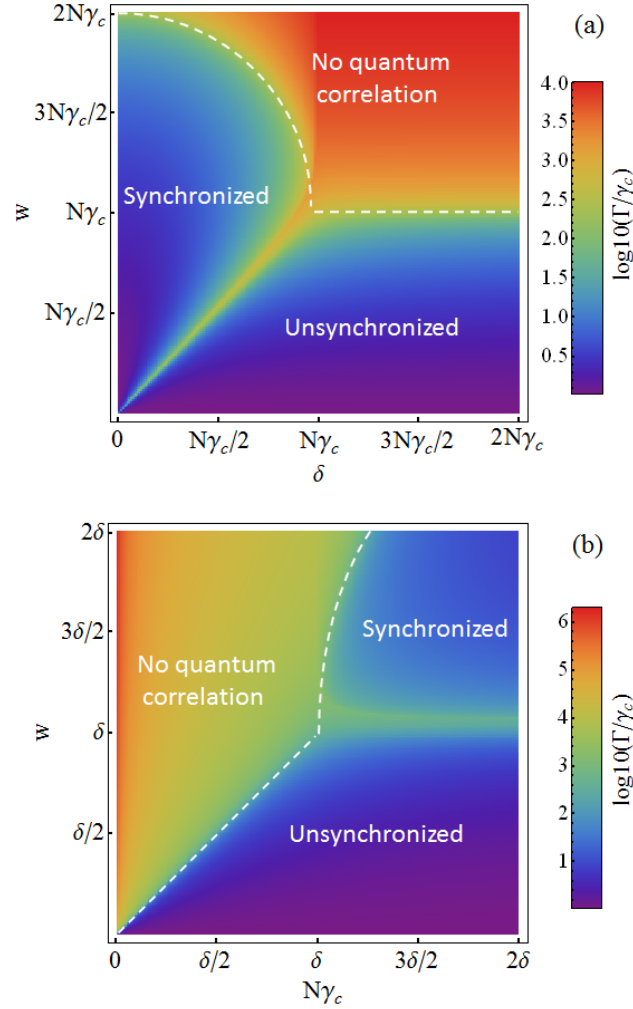


Figure 5.4: (a) Nonequilibrium phase diagram of the quantum synchronization represented by  $\Gamma$  (in units of  $\gamma_C$ ) on the  $w$ - $\delta$  parameter plane, where the dissipative coupling  $N\gamma_C$  ( $N = 10^4$ ) is fixed. An abrupt peak is observed at the boundary between the synchronized and unsynchronized phases. (b) As for (a) but on the  $w$ - $N\gamma_C$  parameter plane.

We first discuss the quantum noise aspect. The fact that this system undergoes a synchro-

nization transition that is fundamentally quantum mechanical is evident in the manifestation of quantum noises associated with the repumping process and the cavity decay. It is shown that quantum noises result in the phase diffusion of the collective atomic dipoles (see Chapter 4), setting the ultimate quantum limit for the linewidth of the superradiant laser to be  $\gamma_C$ . They also give rise to the relative quantum phase diffusion between the two ensembles, as quantified by the linewidth  $\Gamma$  of the Lorentzian peak(s). Therefore,  $\Gamma/\gamma_C$  can be a dimensionless measure of the degree of the synchronization between the two ensembles as normalized by the phase diffusion within each ensemble.

This system has three independent control variables; the detuning  $\delta$ , the dissipative coupling  $N\gamma_C$  and the pumping  $w$ , so we show  $\Gamma/\gamma_C$  on the  $w$ - $\delta$  parameter plane in Fig. 5.4(a) and on the  $w$ - $N\gamma_C$  parameter plane in Fig. 5.4(b). In the region of no quantum correlation, the quantum noise due to pumping destroys the coherences between spins faster than the collective coupling induced by the cavity field can reestablish them. Therefore the mesoscopic dipole is destroyed and the observed spectra are broad. In both the synchronized and unsynchronized regions, spins within each ensemble are well-correlated so that the corresponding Lorentzian peaks have ultranarrow linewidth ( $\sim \gamma_C$ ). As is apparent in Fig. 5.4(a), the two ensembles cannot be synchronized when  $N\gamma_C < \delta$  since then the coherent coupling is not sufficient to overcome the relative precession that arises from the detuning.

For strong coupling,  $N\gamma_C > \delta$ , the synchronization transition occurs as the pump rate passes a critical value. The two phases on either side of the critical region are abruptly separated. As one approaches the synchronized phase from the unsynchronized one by variation of either  $\delta$  or  $w$ , the linewidth increases rapidly, showing amplification of the effect of quantum noise in vicinity of the critical point. After passage of the critical region, the linewidth drops rapidly, leading to rigid phase locking between the two collective dipoles.

We emphasize that the synchronization dynamics shown in Fig. 5.3 and 5.4 is a dynamical phase transition [30, 52, 61, 122] that is reminiscent of a second-order quantum phase transition. To capture features of the quantum criticality, we numerically study the finite size scaling behavior.

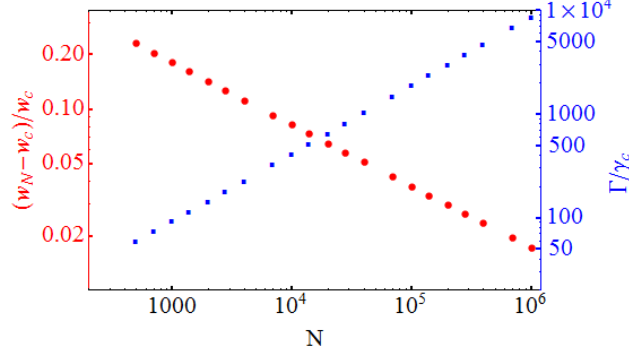


Figure 5.5: Finite size scaling behavior of the quantum criticality for  $\delta = N\gamma_C/2$ . For  $N \rightarrow \infty$ , the critical pump rate is  $w_c = \delta$ . The red dots show the offset between the critical pump rate  $w_N$  for finite  $N$  and  $w_c$ . The blue squares show  $\Gamma$  (in units of  $\gamma_C$ ) at  $w_N$ . Both exhibit linear scalings on the log-log plot.

Fig. 5.5 shows both the critical pump rate  $w_N$  for finite  $N$  and the corresponding  $\Gamma$  at  $w_N$ . The scaling laws of  $(w_N - w_c)/w_c \simeq N^{-0.34}$  and  $\Gamma/\gamma_C \simeq N^{0.66}$  can be identified.

In Hamiltonian systems, a quantum phase transition results from the competition between two noncommuting Hamiltonian components with different symmetries on changing their relative weight. The transition between the two distinct quantum phases can be identified from the nonanalytical behavior of an order parameter, and the scaling behavior of certain correlation functions that diverge at the critical point. By analogy, the synchronization phase transition is caused by the competition between unitary dynamics that is parametrized by  $\delta$  and enters asymmetrically for the two ensembles, and driven-dissipative dynamics parametrized by  $\gamma_C$  that is symmetric. The order parameter  $\Delta$  is zero in the synchronized phase and non-zero in the unsynchronized phase. The critical behavior is encapsulated by the divergence of the relative quantum phase diffusion. It should be emphasized that the treatment given here is quite different to the typical analysis since the transition is embodied by the characteristic features of the two-time correlation functions, rather than the behavior of an energy gap or correlation length.

In the thermodynamic limit, simple expressions for  $\langle \hat{\sigma}_1^z \rangle$  to leading order in  $1/N$  can be

obtained:

$$\langle \hat{\sigma}_1^z \rangle = \begin{cases} \frac{w}{2N\gamma_C}, & \text{if } \delta = 0 \\ \frac{w^2 + \delta^2}{2wN\gamma_C}, & \text{if } 0 < \delta < w \\ \frac{w}{N\gamma_C}, & \text{if } \delta \geq w \end{cases} \quad (5.13)$$

where  $w$  should be such that  $\langle \hat{\sigma}_1^z \rangle < 1$ . A critical point at  $w_c = \delta$  can be found by substituting Eq. (5.13) into Eq. (5.12). In particular,  $\Delta = (\delta^2 - w^2)^{1/2}$  in the unsynchronized phase, which shows an analogous critical exponent to that of a second-order quantum phase transition, *i.e.*,  $\beta = 1/2$ .

As a second point, we provide in-depth detail to quantify the effect of correlations. We do this by a calculation of what is known as the quantum discord. It is worth to point out that the connection between synchronization phenomena and quantum correlations are subtle and subject of current research. Quantum discord can generally be thought of as a measure of the degree of nonclassical correlations between two subsystems. Fig. 5.6 shows the degree of “quantumness” of the correlation presented in our system. We also see that the cumulant expansion provides a good description of the important quantum correlations in the system.

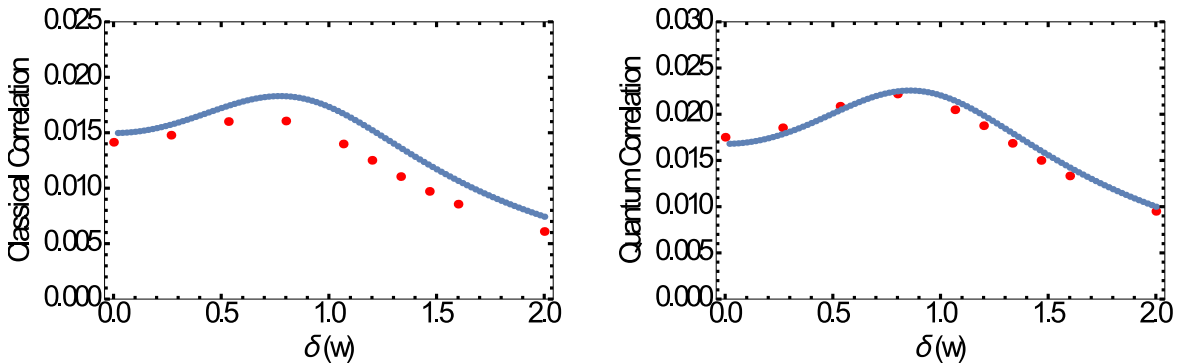


Figure 5.6: Classical correlation and quantum discord between one atom in ensemble A and one atom in ensemble B. The blue dashed line is based on semiclassical approximation described in the paper. The red dots are exact numerical calculations. There are 30 atoms in each ensemble. The comparison between these two lines indicates the “quantumness” of correlations present in our system.

We have presented a system that exhibits quantum synchronization as a modern analogue of the Huygens experiment but is implemented using state-of-the-art neutral atom lattice clocks of the

highest precision. It sheds lights on the ongoing efforts of understanding the quantum aspects of synchronization. It will be intriguing in future work to study the many possible extensions that are inspired by these results, such as the effect of an atom number imbalance on the synchronization dynamics, and the sensitivity of the phase-locking to external perturbation.

## Chapter 6

### Supercooling of atoms based on steady-state superradiance

In the previous discussion of steady-state superradiance, the external motions of atoms were assumed to be frozen. Therefore, the mechanical effects of cavity-photon atom interaction was neglected. In this chapter, we investigate the motional effects on atoms in steady-state superradiance. We focus on how the novel features of steady-state superradiance can be used for efficient cooling of the atoms. We demonstrate that when atomic dipoles are synchronized in the regime of steady-state superradiance, the motion of the atoms may be subject to a giant frictional force leading to potentially very low temperatures. The ultimate temperature limits are determined by a modified atomic linewidth, which can be orders of magnitude smaller than the cavity linewidth. The cooling rate is enhanced by the superradiant emission into the cavity mode allowing reasonable cooling rates even for dipolar transitions with ultranarrow linewidth.

#### 6.1 Cavity cooling in the strong coupling regime

The discovery of laser cooling [129] has enabled new areas of quantum gas physics and quantum state engineering [8]. Laser cooling is an essential technology in many fields, including precision measurements, quantum optics, and quantum information processing [83, 126, 131]. Doppler laser cooling [45, 134] relies on repeated cycles of electronic excitation by lasers followed by spontaneous relaxation, reaching temperature limits determined by the atomic linewidth. Only specific atomic species can be Doppler cooled because they should possess an internal level structure that allows for closed cycling transitions.

Cavity-assisted laser cooling [32, 108] utilizes the decay of an optical resonator instead of atomic spontaneous emission for energy dissipation. It is based on the preferential coherent scattering of laser photons into an optical cavity [51, 125]. Temperatures that can be achieved in this way are limited by the cavity linewidth. Since the particle properties enter only through the coherent scattering amplitude, cavity-assisted cooling promises to be applicable to any polarizable object [63, 78, 79, 89, 90, 96, 97, 116, 139], including molecules [79, 97] and even mesoscopic systems such as nanoparticles [63, 96]. The requirement of cavity cooling [51, 125] is that the single-atom cooperativity parameter  $C$  should be much greater than 1, since we want the atom to scatter light mostly into the cavity rather than the free space.

In this section, I provide a simple model to illustrate the underlying mechanism of cavity cooling. Consider that an atom is confined within a standing-wave resonator and is illuminated by a transverse laser (see Fig. 6.1). A dipolar transition of the atom couples far-detuned with the laser fields and scatters photons from the laser into the cavity. Therefore, the cavity is effectively

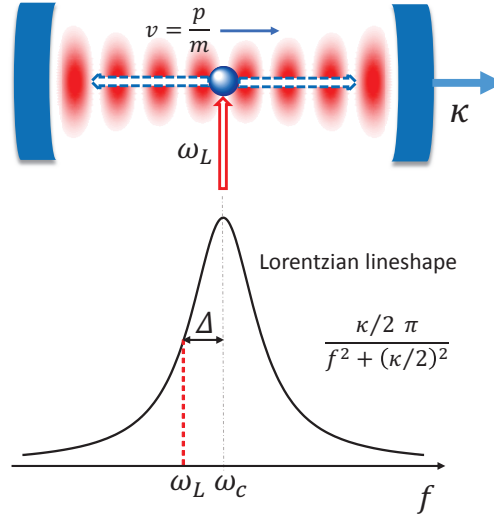


Figure 6.1: An atom with velocity  $v$  is moving freely along the cavity axis. The atom coherently scatters the photons of the transverse laser into the cavity mode. The frequency of the laser  $\omega_L$  is red detuned from the cavity resonance frequency  $\omega_c$  by  $\Delta_c$ . Due to Doppler effect, the atom will scatter more photons into the direction along which it moves.

pumped by laser photons. The effective Hamiltonian of the cavity-atom system is [117]

$$\hat{H} = \frac{\hat{p}^2}{2m} + \hbar \frac{S_d}{2} (\hat{a} + \hat{a}^\dagger) \cos(k\hat{x}) + \hbar \Delta_c \hat{a}^\dagger \hat{a}, \quad (6.1)$$

where  $S_d$  is the effective pumping rate of the cavity and  $\Delta_c$  is the detuning between the cavity frequency and laser frequency. Here, the motion of the atom is restricted to the cavity axis ( $x$ -axis). The position and canonically conjugated momentum of the atom are given by  $\hat{x}$  and  $\hat{p}$  with  $[\hat{x}, \hat{p}] = i\hbar$ . Note that the shift of the cavity frequency due to the interaction with the atom is neglected in Eq. (6.1) since it is much smaller than  $\Delta_c$  [117].

In the regime  $C \gg 1$ , spontaneous emission of the atom can be neglected [117]. Therefore, the only decay channel of the system is the cavity decay and the system can be described by the quantum master equation for the density matrix  $\rho$ ,

$$\frac{d}{dt}\rho = \frac{1}{i\hbar} [\hat{H}, \rho] + \kappa \mathcal{L}[\hat{a}]\rho. \quad (6.2)$$

Let us focus on the condition under which the motion of the atom can be treated semiclassically. This requires that

$$\hbar k \ll \Delta p, \quad (6.3)$$

where  $\hbar k$  is the photon momentum and  $\Delta p$  is the momentum width of the atom.

In the parameter regime of interest, the cavity linewidth is much larger than the atomic motion,

$$k \frac{\Delta p}{m} \ll |\kappa + i\Delta_c|. \quad (6.4)$$

Note that when the recoil frequency  $\omega_r = \hbar k^2/2m$  is much less than  $\kappa$ , this condition is consistent with Eq. (6.3). Therefore, the cavity field can be adiabatically eliminated. In order to correctly encapsulate the cavity cooling mechanism, the adiabatic elimination of the cavity field has to be expanded beyond the leading order. Specifically, the retardation effects between the cavity field and atomic variables should be included.

The Langevin equation of motion for the cavity field is

$$\frac{d}{dt}\hat{a} = -\frac{\kappa}{2}\hat{a} - i\Delta_c\hat{a} - i\frac{S_d}{2}\cos(kx) - \sqrt{\kappa}\hat{\xi}_\kappa(t), \quad (6.5)$$

where  $x$  is now the semiclassical position and  $\hat{\xi}_\kappa$  is the quantum white noise originating from the cavity output with  $\langle \hat{\xi}_\kappa(t)\hat{\xi}_\kappa^\dagger(t') \rangle = \delta(t-t')$ . Following the procedure of doing adiabatic elimination (see Appendix A), we have

$$\begin{aligned} \hat{a} &\approx \int_0^t ds e^{-(\kappa/2+i\Delta_c)s} \left( -i\frac{S_d}{2} \cos(kx) - \sqrt{\kappa}\hat{\xi}_\kappa \right) \\ &\approx \frac{-i\frac{S_d\kappa}{4} \cos(kx)}{\kappa^2/4 + \Delta_c^2} - \frac{\frac{S_d\Delta_c}{2} \cos(kx)}{\kappa^2/4 + \Delta_c^2} + \frac{\kappa\Delta_c \frac{S_d}{2} \frac{d}{dt} \cos(kx)}{(\kappa^2/4 + \Delta_c^2)^2} + \frac{i\frac{S_d}{2}(\kappa^2/4 - \Delta_c^2) \frac{d}{dt} \cos(kx)}{(\kappa^2/4 + \Delta_c^2)^2} - \frac{\sqrt{\kappa}\hat{\xi}_\kappa}{\kappa/2 + i\Delta_c}. \end{aligned} \quad (6.6)$$

We can see from Eq. (6.6) that the retardation between the cavity field and the atomic motion has been included to the second order in  $1/\kappa$ .

The total force on the atom is given by the derivative of the Hamiltonian

$$f = -\nabla H = \hbar k \sin(kx) \frac{S_d}{2} (\hat{a} + \hat{a}^\dagger) \quad (6.7)$$

By plugging Eq. (6.6) into Eq. (6.7), we find the conservative force to be

$$f^c = -\hbar k \sin(kx) \frac{S_d}{2} \frac{S_d\Delta_c}{\kappa^2/4 + \Delta_c^2} \cos(kx), \quad (6.8)$$

the frictional force to be

$$f^f = \hbar k \sin(kx) \frac{S_d}{2} \frac{\kappa\Delta_c S_d \frac{d}{dt} \cos(kx)}{(\kappa^2/4 + \Delta_c^2)^2} = -\hbar k \sin^2(kx) \frac{\kappa S_d^2/4}{\kappa^2/4 + \Delta_c^2} \frac{2\Delta_c k/m}{\kappa^2/4 + \Delta_c^2} p, \quad (6.9)$$

and the diffusion force has the correlation matrix

$$\langle dpdp \rangle = \hbar^2 k^2 \frac{\kappa S_d^2/4}{\kappa^2/4 + \Delta_c^2} \sin^2(kx) dt \quad (6.10)$$

The final cooling temperature  $T$  for the atom is

$$k_B T = \frac{\langle p^2 \rangle}{m} = \frac{D}{2m\alpha} = \hbar \frac{\Delta_c^2 + \kappa^2/4}{4\Delta_c}, \quad (6.11)$$

since from Eq. (6.10) and Eq. (6.9), the diffusion and friction coefficient,  $D$  and  $\alpha$ , are given by

$$\begin{aligned} D &= \hbar^2 k^2 \sin^2(kx) \frac{\kappa S_d^2/4}{\kappa^2/4 + \Delta_c^2}, \\ \alpha &= \hbar k \sin^2(kx) \frac{\kappa S_d^2/4}{\kappa^2/4 + \Delta_c^2} \frac{2\Delta_c k/m}{\Delta_c^2 + (\kappa/2)^2}. \end{aligned} \quad (6.12)$$

According to Eq. (6.11), the minimum temperature that can be achieved by cavity cooling is  $k_B T = \hbar\kappa/4$  at  $\Delta_c = \kappa/2$ .

The many-atom effects of cavity-assisted cooling were theoretically discussed by Ritsch and collaborators [31] and experimentally reported [5, 17]. It is shown that the many-atom case exhibits a threshold, which is mainly determined by the intensity of the transverse laser. Below the threshold, the atoms distribute homogeneously along the cavity axis. The physics is the same as the single-atom case discussed above. Above threshold, self-organized atomic structure (Bragg gratings) form, which superradiantly scatters photons into the cavity. Recently, it has been shown that the long-range nature of the cavity-mediated interaction between atoms gives rise to interesting prethermalization behavior [118]. In spite of the intrinsic many-body nature, the underlying cooling mechanism shares much with the single-atom case, and indeed the final temperature observed in these systems is limited by the cavity linewidth.

## 6.2 Supercooling

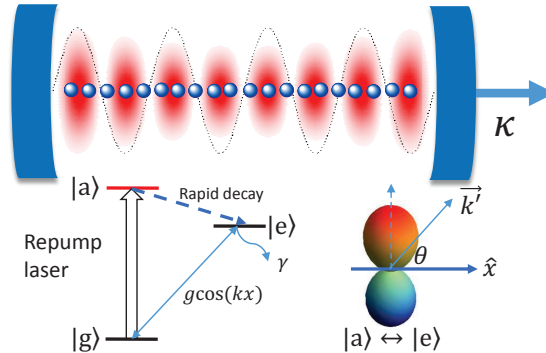


Figure 6.2: Atoms with ultranarrow transition  $|g\rangle \leftrightarrow |e\rangle$  are confined to the axis of a standing-wave mode of an optical cavity. Different implementations of pumping may be considered [12, 93]. In the simplest scenario shown, a transition is driven from the ground state  $|g\rangle$  to an auxiliary state  $|a\rangle$  that rapidly decays to the excited state  $|e\rangle$ . In this way  $|a\rangle$  can be adiabatically eliminated and a two-state pseudospin description in the  $\{|g\rangle, |e\rangle\}$  subspace used, with repumping corresponding to an effective rate  $w$  from  $|g\rangle$  to  $|e\rangle$ . If the repumping laser is directed normal to the cavity axis, the absorption does not modify the momentum. Momentum recoil is induced by the on-axis component of the wavevector  $\vec{k}'$  of the dipole radiation pattern for the  $|a\rangle \leftrightarrow |e\rangle$  transition.

In this section, we demonstrate that the mechanical action of the atom-cavity coupling takes

on a dramatically new character for atoms in the regime of steady-state superradiance [11, 12, 91, 93, 140, 142]. Specifically, the frictional force on a single atom is significantly enhanced, and the final temperature is much lower than the temperature that can be achieved in cavity-assisted cooling [51, 125]. Furthermore, as the atom number increases, the cooling may become faster due to the increasing rate of superradiant collective emission. We show that ability to achieve much lower temperatures than for single-atom cavity-assisted cooling derives from the emergence of atom-atom dipole correlations in the many-body atomic ensemble.

We now consider a specific situation of an ensemble of  $N$  point-like two-level atoms with transition frequency  $\omega_a$  and natural linewidth  $\gamma$ , interacting with a single-mode cavity with resonance frequency  $\omega_c$  and linewidth  $\kappa$ , as shown in Fig. 6.2. The atoms are restricted to move freely along the direction of the cavity axis ( $x$ -axis), a situation that can be realized by tightly confining the atoms in the other two directions. The atom-cavity coupling strength is given by  $g \cos(kx)$ , where  $g$  is the vacuum Rabi frequency at the field maximum and  $\cos(kx)$  describes the one-dimensional cavity mode function. The atoms are incoherently repumped at rate  $w$ , thus providing the source of photons.

The Hamiltonian describing the atom-cavity system in the rotating frame of the atomic transition frequency is given by,

$$\hat{H} = \hbar\Delta\hat{a}^\dagger\hat{a} + \sum_{j=1}^N \frac{\hat{p}_j^2}{2m} + \hbar\frac{g}{2} \sum_{j=1}^N (\hat{a}^\dagger\hat{\sigma}_j^- + \hat{\sigma}_j^+\hat{a}) \cos(k\hat{x}_j), \quad (6.13)$$

where  $\Delta = \omega_c - \omega_a$ . We have introduced the bosonic annihilation and creation operators,  $\hat{a}$  and  $\hat{a}^\dagger$ , for cavity photons. The  $j$ -th atom is represented by Pauli pseudospin operators,  $\hat{\sigma}_j^z$  and  $\hat{\sigma}_j^- = (\hat{\sigma}_j^+)^\dagger$ , and position and momentum  $\hat{x}_j$  and  $\hat{p}_j$ , respectively.

In the presence of dissipation, the evolution of the system is described by the Born-Markov quantum master equation for the density matrix  $\hat{\rho}$  for the cavity and atoms,

$$\frac{d}{dt}\hat{\rho} = \frac{1}{i\hbar} [\hat{H}, \hat{\rho}] + \kappa\mathcal{L}[\hat{a}]\rho + w \sum_{j=1}^N \int_{-1}^1 du N(u) \mathcal{L}[\hat{\sigma}_j^+ e^{iuk'\hat{x}_j}]\rho, \quad (6.14)$$

The term proportional to  $\kappa$  describes the cavity decay. The repumping is the term proportional to  $w$  and is modeled by spontaneous absorption with recoil [44]. The recoil is parametrized by the

normalized emission pattern  $N(u)$  and wavevector  $k'$ . It will generally be a good approximation to neglect the effect of free-space spontaneous emission of the atoms outside of the cavity, since the natural linewidth  $\gamma$  is assumed to be extremely small for atoms with an ultraweak-dipole transition.

The typical relaxation time of the cavity mode is of the order of  $T_C \sim |\kappa + i\Delta|^{-1}$ , while the one of the atoms is given by  $T_A \sim \left( \max \left\{ \sqrt{N\bar{n}}g, w, k\sqrt{\langle p^2 \rangle}/m \right\} \right)^{-1}$ , where  $\bar{n}$  is the mean photon number in the cavity. In steady state superradiance, the relaxation time of the cavity is assumed to be much shorter than the timescale on which the atoms are evolving, namely  $T_A \gg T_C$ . Therefore, the cavity field can be quasiadiabatically eliminated as in Section 6.1. To this end, we start with the quantum Langevin equation for the cavity field according to the quantum master equation Eq. (6.14),

$$\frac{d}{dt}\hat{a} = -\frac{\kappa}{2}\hat{a} - i\Delta\hat{a} - i\frac{g}{2}\hat{J}^- + \sqrt{\kappa}\hat{\xi}_\kappa(t), \quad (6.15)$$

where  $\hat{J}^- = \sum_{j=1}^N \hat{\sigma}_j^- \cos(k\hat{x}_j)$  is redefined in this case to include the atomic position and  $\hat{\xi}_\kappa$  is again the quantum white noise originating from the cavity output with  $\langle \hat{\xi}_\kappa(t)\hat{\xi}_\kappa^\dagger(t') \rangle = \delta(t-t')$ .

The formal solution to Eq. (6.15) is

$$\hat{a}(t) = e^{-(\kappa/2+i\Delta)\Delta t}\hat{a}(t_0) - i\frac{g}{2}\int_0^{\Delta t} ds e^{-(\kappa/2+i\Delta)s}\hat{J}^-(t-s) + \hat{\mathcal{F}}(t), \quad (6.16)$$

where  $\hat{\mathcal{F}}(t) = \sqrt{\kappa}\int_0^{\Delta t} ds e^{-(\kappa/2+i\Delta)s}\hat{\xi}_\kappa(t-s)$  is the noise term and  $\Delta t = t - t_0$ . Under the approximation of coarse graining ( $T_A \gg \Delta t \gg T_C$ ), the first term on the right-hand side (RHS) of Eq. (6.16) vanishes, and it is shown in Appendix A that

$$\langle \hat{\mathcal{F}}(t)\hat{\mathcal{F}}^\dagger(t') \rangle \approx \frac{\kappa}{\kappa^2/4 + \Delta^2}\delta(t-t'). \quad (6.17)$$

It would be convenient to choose  $\hat{\mathcal{F}}(t) = -i\frac{\sqrt{\gamma_C}}{g/2}\hat{\xi}(t)$ , with

$$\gamma_C = \frac{g^2\kappa/4}{\kappa^2/4 + \Delta^2}. \quad (6.18)$$

Furthermore, the integral in Eq. (6.16) can be expanded in powers of  $1/(\kappa/2 + i\Delta)$  (see Appendix A). As a result we obtain

$$\hat{a}(t) \approx \frac{-i\frac{g}{2}\hat{J}^-}{\kappa/2 + i\Delta} - \frac{\frac{d}{dt}(-i\frac{g}{2}\hat{J}^-)}{(\kappa/2 + i\Delta)^2} + \hat{\mathcal{F}}(t) + \mathcal{O}[(\kappa/2 + i\Delta)^{-3}]. \quad (6.19)$$

As can be seen from Eq. (6.19), the retardation effects between the cavity field and atomic variables are included.

The force on the  $j$ -th atom  $\hat{F}_j$  is given by

$$\hat{F}_j = \frac{d}{dt}\hat{p}_j = \hbar k \sin(k\hat{x}_j) \frac{g}{2} (\hat{\sigma}_j^+ \hat{a} + \hat{a}^\dagger \hat{\sigma}_j^-) + \hat{\mathcal{N}}_j^{\text{pump}}, \quad (6.20)$$

where  $\hat{\mathcal{N}}_j^{\text{pump}}$  represents the random force due to recoil of the incoherent pumping process. Substituting Eq. (6.19) into the above equation, we have

$$\begin{aligned} \frac{d}{dt}\hat{p}_j &\approx \hbar k \sin(k\hat{x}_j) \frac{\gamma_C}{2} \left( -i\hat{\sigma}_j^+ \hat{J}^- + i\hat{J}^+ \hat{\sigma}_j^- \right) \\ &\quad - \hbar k \sin(k\hat{x}_j) \frac{\gamma_\Delta}{2} \sum_{l=1}^N \cos(kx_l) \left( \hat{\sigma}_j^+ \hat{\sigma}_l^- + \hat{\sigma}_l^+ \hat{\sigma}_j^- - \beta_1 \hat{\sigma}_j^+ \frac{d}{dt} \hat{\sigma}_l^- - \beta_1^* \frac{d}{dt} \hat{\sigma}_l^+ \hat{\sigma}_j^- \right) \\ &\quad - \sin(k\hat{x}_j) \frac{\gamma_C}{2} \sum_{l=1}^N \frac{\eta}{2} [\sin(k\hat{x}_l), \hat{p}_l]_+ \left( \hat{\sigma}_j^+ \hat{\sigma}_l^- + \hat{\sigma}_l^+ \hat{\sigma}_j^- + \beta_2 \hat{\sigma}_j^+ \hat{\sigma}_l^- + \beta_2^* \hat{\sigma}_l^+ \hat{\sigma}_j^- \right) + \hat{\mathcal{N}}_j, \end{aligned} \quad (6.21)$$

where  $[\hat{A}, \hat{B}]_+ = \hat{A}\hat{B} + \hat{B}\hat{A}$  is the anticommutator and the coefficients are

$$\gamma_\Delta = \frac{g^2 \Delta / 2}{\kappa^2 / 4 + \Delta^2}, \beta_1 = \frac{\kappa}{\kappa^2 / 4 + \Delta^2} + i \frac{\kappa^2 / 4 - \Delta^2}{\Delta (\kappa^2 / 4 + \Delta^2)}, \beta_2 = i \frac{\kappa^2 / 4 - \Delta^2}{\kappa \Delta}, \eta = \frac{4\omega_r \Delta}{\kappa^2 / 4 + \Delta^2}. \quad (6.22)$$

Here  $\hat{\mathcal{N}}_j = \hat{\mathcal{N}}_j^{\text{cav}} + \hat{\mathcal{N}}_j^{\text{pump}}$  is the sum of the noise processes originating from the cavity output  $\hat{\mathcal{N}}_j^{\text{cav}}$  and repumping  $\hat{\mathcal{N}}_j^{\text{pump}}$ . In the first line of equation (6.21) we neglect  $\beta_1$  because in the steady state superradiance regime it holds that  $|\beta_1| \langle \hat{\sigma}_j^+ \frac{d}{dt} \hat{\sigma}_l^- \rangle \sim \frac{w}{\kappa} \langle \hat{\sigma}_j^+ \hat{\sigma}_l^- \rangle \ll \langle \hat{\sigma}_j^+ \hat{\sigma}_l^- \rangle$ . This has also been checked numerically. Therefore we get

$$\frac{d}{dt}\hat{p}_j = \frac{d}{dt}\hat{p}_j^0 + \hat{\mathcal{N}}_j, \quad (6.23)$$

where we define the force without noise as

$$\begin{aligned} \frac{d}{dt}\hat{p}_j^0 &\approx \hbar k \sin(k\hat{x}_j) \frac{\gamma_C}{2} \left( -i\hat{\sigma}_j^+ \hat{J}^- + i\hat{J}^+ \hat{\sigma}_j^- \right) - \hbar k \sin(k\hat{x}_j) \frac{\gamma_\Delta}{2} \sum_{l=1}^N \cos(kx_l) \left( \hat{\sigma}_j^+ \hat{\sigma}_l^- + \hat{\sigma}_l^+ \hat{\sigma}_j^- \right) \\ &\quad - \sin(k\hat{x}_j) \frac{\gamma_C}{2} \sum_{l=1}^N \frac{\eta}{2} [\sin(k\hat{x}_l), \hat{p}_l]_+ \left( \hat{\sigma}_j^+ \hat{\sigma}_l^- + \hat{\sigma}_l^+ \hat{\sigma}_j^- + \beta_2 \hat{\sigma}_j^+ \hat{\sigma}_l^- + \beta_2^* \hat{\sigma}_l^+ \hat{\sigma}_j^- \right). \end{aligned} \quad (6.24)$$

We work at the detuning  $\Delta = \kappa/2$  so that  $\eta$  is maximized and  $\beta_2$  vanishes. Note that at  $\Delta = \kappa/2$ ,

$\gamma_C = g^2/2\kappa = \Gamma_C/2$ . As a result we obtain

$$\begin{aligned} \frac{d}{dt}\hat{p}_j^0 &\approx \hbar k \sin(k\hat{x}_j) \frac{\gamma_C}{2} \left( -i\hat{\sigma}_j^+ \hat{J}^- + i\hat{J}^+ \hat{\sigma}_j^- - \hat{\sigma}_j^+ \hat{J}^- - \hat{J}^+ \hat{\sigma}_j^- \right) \\ &- \sin(k\hat{x}_j) \frac{\gamma_C}{2} \sum_{l=1}^N \frac{\eta}{2} [\sin(k\hat{x}_l), \hat{p}_l]_+ \left( \hat{\sigma}_j^+ \hat{\sigma}_l^- + \hat{\sigma}_l^+ \hat{\sigma}_j^- \right). \end{aligned} \quad (6.25)$$

The first term on the RHS of Eq. (6.25) represents forces originating from the adiabatic component of the cavity field, while the second term represents the frictional force arising from retardation effects. The noise term  $\hat{\mathcal{N}}_j$  in equation (6.23) gives rise to momentum diffusion due to quantum noises associated with incoherent processes. So we derive the equations of motion for the second moments of momenta,

$$\frac{d}{dt} \langle \hat{p}_j \hat{p}_l \rangle = \left\langle \hat{p}_j^0 \frac{d\hat{p}_l^0}{dt} \right\rangle + \left\langle \frac{d\hat{p}_j^0}{dt} \hat{p}_l^0 \right\rangle + \gamma_C \hbar^2 k^2 \langle \sin(k\hat{x}_j) \sin(k\hat{x}_l) \hat{\sigma}_j^+ \hat{\sigma}_l^- \rangle + w \delta_{jl} \hbar^2 k'^2 \overline{u^2} \langle \hat{\sigma}_j^- \hat{\sigma}_l^+ \rangle, \quad (6.26)$$

where  $\delta_{jl}$  is the Kronecker delta, and  $\overline{u^2}$  is the second moment of the dipole radiation pattern, *i.e.*,

$$\overline{u^2} = \int_{-1}^1 du N(u) u^2 = \frac{2}{5}, \quad (6.27)$$

where we have taken the dipole pattern  $N(u) = \frac{3}{2}|u|\sqrt{1-u^2}$ .

We treat the external atomic motion classically under the assumption that the momentum width of the particles  $\sqrt{\langle p^2 \rangle}$  is larger than the single photon recoil  $\hbar k$  [Eq. (6.3)]. So we make the mapping  $\langle \hat{p}_j \rangle \rightarrow p_j$  and  $\langle \hat{x}_j \rangle \rightarrow x_j$ . As a result this leads to

$$\frac{d}{dt} p_j = \frac{d}{dt} p_j^0 + \xi_j^p, \quad (6.28)$$

with

$$\frac{d}{dt} p_j^0 = \hbar k \sin(kx_j) \gamma_C \left( \text{Im}[\langle \hat{\sigma}_j^+ \hat{J}^- \rangle] - \text{Re}[\langle \hat{\sigma}_j^+ \hat{J}^- \rangle] \right) - \sin(kx_j) \gamma_C \sum_{l=1}^N \eta \text{Re}[\langle \hat{\sigma}_j^+ \hat{\sigma}_l^- \rangle] \sin(kx_l) p_l, \quad (6.29)$$

where  $\xi_j^p$  is the classical noise acting on the momentum of  $j$ -th atom and  $\langle \xi_j^p(t) \xi_l^p(t') \rangle = D^{jl} \delta(t-t')$ .

The diffusion matrix  $D^{jl}$  can be computed by making quantum-classical correspondence for the second moments. According to Eq. (6.28),

$$\frac{d}{dt} \langle p_j p_l \rangle = \left\langle p_j^0 \frac{d p_l^0}{dt} \right\rangle + \left\langle \frac{d p_j^0}{dt} p_l^0 \right\rangle + D^{jl}. \quad (6.30)$$

We use symmetric ordering of quantum operators for the quantum-classical correspondence, *i.e.*,  $\frac{1}{2} \left\langle \left[ \hat{p}_j, \frac{d\hat{p}_l}{dt} \right]_+ \right\rangle \rightarrow \left\langle p_j \frac{dp_l}{dt} \right\rangle$ . Matching Eq. (6.26) and Eq. (6.30), we get

$$D^{jl} = \gamma_C \hbar^2 k^2 \sin(kx_j) \sin(kx_l) \text{Re}[\langle \hat{\sigma}_l^+ \hat{\sigma}_j^- \rangle] + w \delta_{jl} \hbar^2 k'^2 \overline{u^2} \langle \hat{\sigma}_j^- \hat{\sigma}_l^+ \rangle. \quad (6.31)$$

Therefore, we could simulate the external motion of atoms with Eq. (6.28) and the equation of motion for  $x_j$

$$\frac{d}{dt} x_j = \frac{p_j}{m}. \quad (6.32)$$

The classical noises  $\xi_j^p$  with diffusion matrix  $D^{jl}$  make sure that we have the right second order moments for momenta.

To begin with, we first consider the case in which the effect of recoil associated with the repumping is neglected, *i.e.* we set  $k' = 0$ . This will determine the ultimate temperature limit imposed by the vacuum noise due to the cavity output. For the simple one-atom (labeled by 1) case, we can then directly find the friction ( $\alpha_1$ ) and diffusion ( $D_1$ ) coefficient from Eq. (6.28) and Eq. (6.31). The steady-state temperature  $T$  for the single atom is

$$k_B T = \frac{\langle p_1^2 \rangle}{m} = \frac{D_1}{2m\alpha_1} = \frac{\hbar\kappa}{4}, \quad (6.33)$$

since

$$\begin{aligned} D_1 &= \hbar^2 k^2 \gamma_C \sin^2(kx_1) \langle \hat{\sigma}_1^+ \hat{\sigma}_1^- \rangle, \\ \alpha_1 &= \eta \gamma_C \sin^2(kx_1) \langle \hat{\sigma}_1^+ \hat{\sigma}_1^- \rangle. \end{aligned} \quad (6.34)$$

Note that this is precisely the same temperature limit previously found in the cavity-assisted cooling case in Section 6.1. Here the rate of the decay into the cavity mode is proportional to  $\gamma_C \langle \hat{\sigma}_1^+ \hat{\sigma}_1^- \rangle$ , which is applicable to the weak coupling regime of cavity QED [95]. In Fig. 6.3(a), we show a numerical simulation of the cooling trajectory of a single atom as a function of time. As expected, the final temperature  $k_B T$  asymptotes to  $\hbar\kappa/4$  and the cooling rate is well approximated by  $R_S = \eta \gamma_C \langle \hat{\sigma}_1^+ \hat{\sigma}_1^- \rangle$ .

The cooling in the many-atom case exhibits a distinctly different character. A feature of this model is the pseudospin-to-motion coupling of the atoms. In order to close the evolution equations

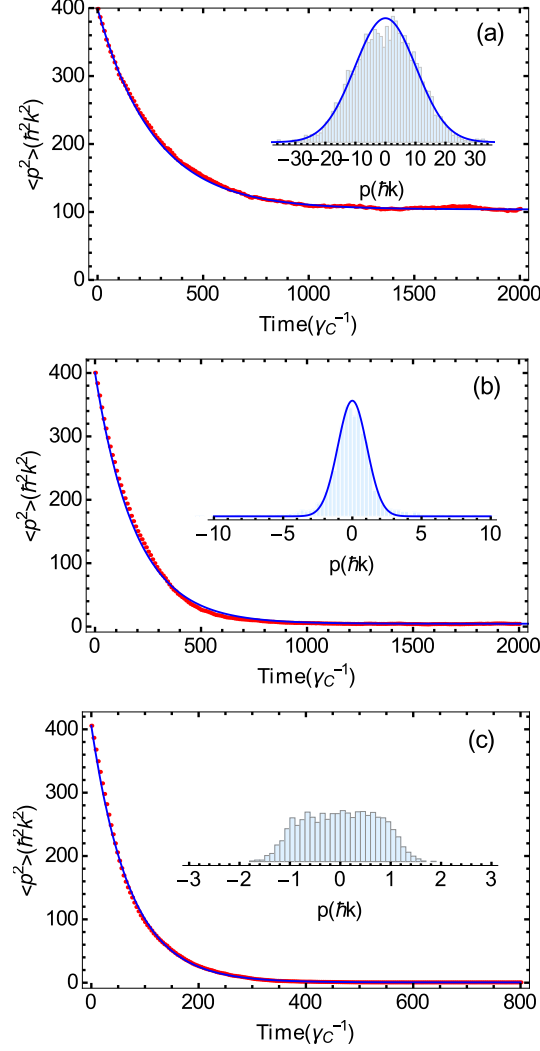


Figure 6.3: Time evolution of the average momentum square (red dots) evaluated from 4000 trajectories simulated by integrating Eqs. (6.28) and (6.32) for 1 atom (a), 20 atoms (b), and 60 atoms (c). The blue solid line is a fit to an exponential decay. The parameters are  $\Delta = \kappa/2 = 100$ ,  $\gamma_C = 0.1$ , and  $\omega_r = 0.25$ . The repumping rates are chosen such that the average atomic population inversion in all cases is the same [ $w = 0.15$  (a), 0.28 (b), 1.3 (c)]. Insets show the momentum statistics. The blue solid line is a fit to a Gaussian distribution.

of the atomic motion as described by Eq. (6.28) and Eq. (6.32), it is also necessary to solve for the dynamics of the pseudospins. For this purpose, we derive the effective quantum master equation for the pseudospins.

For the internal dynamics of atoms in a superradiant laser, it is sufficient to keep the first

order term in Eq. (6.19),

$$\hat{a}(t) \approx -i\frac{\gamma_C}{g}\hat{J}^- - \frac{\gamma_\Delta}{g}\hat{J}^- + \hat{\mathcal{F}}(t). \quad (6.35)$$

Here, retardation effects are not included because they give rise to corrections that are of higher order and their contribution is negligible. The adiabatic elimination of the cavity field leads to an effective quantum master equation for the atomic spins only

$$\frac{d}{dt}\rho = \frac{1}{i\hbar}[\hat{H}_{\text{eff}}, \rho] + \gamma_C\mathcal{L}[\hat{J}^-]\rho + w\sum_{j=1}^N\int_{-1}^1 du N(u)\mathcal{L}[\hat{\sigma}_j^+ e^{i\vec{k}'\cdot\vec{x}_j}]\rho, \quad (6.36)$$

where the Hamiltonian  $\hat{H}_{\text{eff}} = -\frac{\hbar\gamma_C}{2}\hat{J}^+\hat{J}^-$  describes the coherent coupling between each pair of atoms, and the collective decay [term  $\gamma_C\mathcal{L}[\hat{J}^-]$  in Eq. (6.36)] leads to dissipative coupling. We want to emphasize that this atomic master equation is not sufficient for the external degrees of freedom, for which retardation effects are not negligible.

The spin degrees of freedom of atoms scale exponentially with the number of atoms. To solve Eq. (6.36), we thus use a semiclassical approximation that is applicable to large atom numbers in the steady-state superradiance [91, 92]. Cumulants for the expectation values of spin operators are expanded to second order. Because of the  $U(1)$  symmetry,  $\langle\hat{\sigma}_j^\pm\rangle = 0$ . Therefore, all nonzero observables are expanded in terms of  $\langle\hat{\sigma}_j^+\hat{\sigma}_j^-\rangle$  and  $\langle\hat{\sigma}_j^+\hat{\sigma}_l^-\rangle$  ( $j \neq l$ ). Their equations of motion can then be found from the effective master equation,

$$\begin{aligned} \frac{d}{dt}\langle\hat{\sigma}_j^+\hat{\sigma}_j^-\rangle &= w(1 - \langle\hat{\sigma}_j^+\hat{\sigma}_j^-\rangle) - \frac{1}{2}(\gamma_C + i\gamma_\Delta)\cos(k\hat{x}_j)\langle\hat{J}^+\hat{\sigma}_j^-\rangle - \frac{1}{2}(\gamma_C - i\gamma_\Delta)\cos(k\hat{x}_j)\langle\hat{\sigma}_j^+\hat{J}^-\rangle, \\ \frac{d}{dt}\langle\hat{\sigma}_j^+\hat{\sigma}_l^-\rangle &= -w\langle\hat{\sigma}_j^+\hat{\sigma}_l^-\rangle + \frac{1}{2}(\gamma_C + i\gamma_\Delta)\cos(k\hat{x}_j)\langle\hat{J}^+\hat{\sigma}_l^-\hat{\sigma}_j^z\rangle + \frac{1}{2}(\gamma_C - i\gamma_\Delta)\cos(k\hat{x}_l)\langle\hat{\sigma}_l^z\hat{\sigma}_j^+\hat{J}^-\rangle \\ &\approx -\left(w + (\gamma_C + i\gamma_\Delta)\cos^2(k\hat{x}_j)\langle\hat{\sigma}_j^+\hat{\sigma}_j^-\rangle + (\gamma_C - i\gamma_\Delta)\cos^2(k\hat{x}_l)\langle\hat{\sigma}_l^+\hat{\sigma}_l^-\rangle\right)\langle\hat{\sigma}_j^+\hat{\sigma}_l^-\rangle \\ &\quad + \frac{1}{2}(\gamma_C + i\gamma_\Delta)\cos(k\hat{x}_j)(2\langle\hat{\sigma}_j^+\hat{\sigma}_j^-\rangle - 1)\langle\hat{J}^+\hat{\sigma}_l^-\rangle + \frac{1}{2}(\gamma_C - i\gamma_\Delta)\cos(k\hat{x}_l)(2\langle\hat{\sigma}_l^+\hat{\sigma}_l^-\rangle - 1)\langle\hat{\sigma}_j^+\hat{J}^-\rangle, \end{aligned} \quad (6.37)$$

describing the population inversion and spin-spin correlation respectively. In deriving Eq. (6.37), we have dropped the third-order cumulants. In the simulations we integrate (6.28), (6.32) and (6.37) simultaneously.

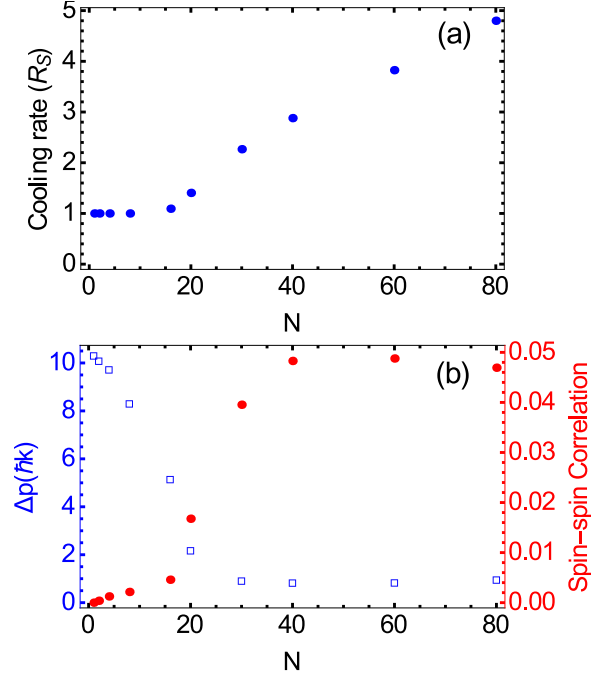


Figure 6.4: (a) Cooling rate (in units of the single atom cooling rate  $R_S$ ) as a function of atom number. (b) Final momentum width ( $\Delta p = \sqrt{\langle p^2 \rangle}$ , blue squares) and spin-spin correlation (red dots) as a function of atom number. The parameters are the same as those in Fig. 6.3.

Simulations of the cooling dynamics for many atoms are shown in Figs. 6.3(b) and (c). Remarkably, we find the collective atomic effects to lead to a more rapid cooling rate, and simultaneously to generate a lower final temperature. Figure 6.4 shows the cooling rate (a) and the final momentum width (b) as a function of the atom number. We note that the cooling rate exhibits two kinds of behavior, hinting towards the existence of a  $N$ -dependent threshold, see Fig. 6.4(a). For  $N \lesssim 20$ , the cooling rate is independent of  $N$ , while for  $N \gtrsim 20$ , it increases monotonously. Correspondingly, in this regime, the momentum width has reached a minimum which is independent of  $N$ , see Fig. 6.4(b). Note that when the final temperature gets closer to the recoil temperature, the momentum distribution is not Gaussian anymore, rendering the notion of temperature invalid. The semiclassical treatment predicts a uniform distribution in the momentum interval  $[-\hbar k, \hbar k]$  corresponding to the recoil limit, as shown in the inset of Fig. 6.3(c). We note that sub-Doppler temperatures for a similar setup have been reported in Refs. [112], where spontaneous decay was

assumed to be the fastest incoherent process. Differing from that regime, the recoil limit is here reached thanks to the small spontaneous decay rate. When the temperature approaches the recoil temperature, however, the validity of the semiclassical treatment of atomic motion is questionable and a full quantum model is necessary in order to determine the asymptotic energy. These results demonstrate that for atoms in the steady-state superradiant regime, not only is the cooling more efficient due to the rapid rate of superradiant light emission, but also the final temperature is determined by the relaxation rate of the atomic dipole, and not the cavity linewidth.

The principal new feature here is that spin-spin correlations between atoms develop due to the cavity-mediated coupling. In order to measure the extent of this effect, we introduce  $\langle \hat{\sigma}^+ \hat{\sigma}^- \rangle_E$  defined as averaged spin-spin correlations,

$$\langle \hat{\sigma}^+ \hat{\sigma}^- \rangle_E = \left( \langle \hat{J}^+ \hat{J}^- \rangle - \sum_{j=1}^N \langle \hat{\sigma}_j^+ \hat{\sigma}_j^- \rangle \cos^2(kx_j) \right) / [N(N-1)]. \quad (6.38)$$

Fig. 6.4(b) shows  $\langle \hat{\sigma}^+ \hat{\sigma}^- \rangle_E$  as a function of the number of atoms. The equilibrium temperature is seen to decrease as the collective spin-spin correlation emerges. This is reminiscent of the linewidth of the superradiant laser, where the synchronization of spins leads to a significant reduction of the linewidth to the order of  $\gamma_C$  [93, 140]. The establishment of spin-spin correlations is a competition between dephasing due to both cavity output noise and repumping, and the dissipative coupling between atoms which tends to synchronize the dipoles [140]. Since the coupling strength scales with  $N$ , a sufficient atom number is required to establish strong spin-spin correlations [140].

Further characterizing the ultimate temperature limits, Fig. 6.5(a) shows the final momentum width as a function of  $\gamma_C$ . We see that as  $\gamma_C$  is decreased, the final temperature reduces in proportion to  $\gamma_C$  until it hits the recoil limit. This effect is consistent with a significantly increased friction coefficient providing a reduction of the order of the final temperature from the one to many atom case from  $\kappa$  to  $\gamma_C$ .

In the large atom number limit, we are able to derive analytically the average frictional force on a single atom moving in a large ensemble of atoms that are in steady-state superradiance.

We start by finding the steady state of the large ensemble of atoms in equilibrium. In the

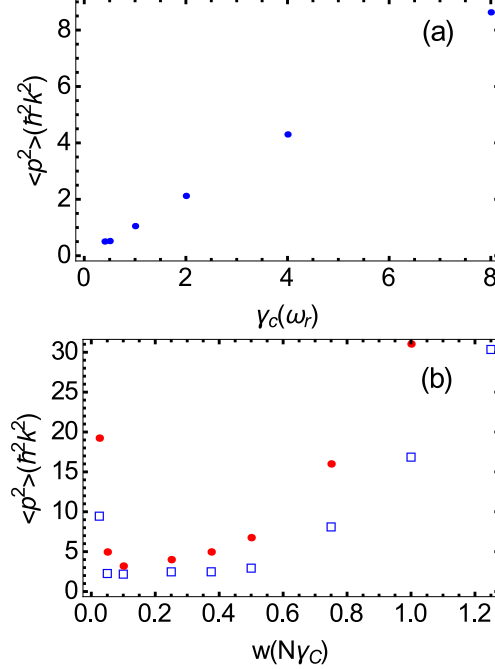


Figure 6.5: (a) Final momentum width as a function of  $\gamma_C$  for 40 atoms. The parameters are  $\Delta = \kappa/2 = 200$ ,  $w = N\gamma_C/4$ , and  $\omega_r = 0.25$ . (b) Final momentum width as a function of repumping strength for 40 atoms without ( $k' = 0$ , blue squares) and with recoil associated with repumping ( $k' = k$ , red dots). The parameters are  $\Delta = \kappa/2 = 200$ ,  $\gamma_C = 0.5$ , and  $\omega_r = 0.25$ .

moving frame of atoms, the master equation for the system [Eq. (6.14)] becomes

$$\frac{d}{dt}\rho = \frac{1}{i\hbar} \left[ \hbar \frac{g}{2} \sum_{j=1}^N (\hat{a}^\dagger \hat{\sigma}_j^- + \hat{\sigma}_j^+ \hat{a}) \cos(\delta_j t), \rho \right] + \kappa \mathcal{D}[\hat{a}]\rho + w \sum_{j=1}^N \int_{-1}^1 du N(u) \mathcal{D}[\hat{\sigma}_j^+ e^{ik' \cdot \vec{x}_j}] \rho, \quad (6.39)$$

where  $\delta_j = kp_j/m$  is the Doppler frequency for  $j$ -th atom. Following the cumulant expansion method developed in Ref. [93], we get a set of closed equations from the above master equation,

$$\begin{aligned} \frac{d}{dt} \langle \hat{a}^\dagger \hat{\sigma}_l^- \rangle &\approx -(\kappa' - i\Delta) \langle \hat{a}^\dagger \hat{\sigma}_l^- \rangle + i \frac{g}{2} \cos(\delta_l t) \left( \langle \hat{a}^\dagger \hat{a} \rangle \langle \hat{\sigma}_l^z \rangle + \frac{1 + \langle \hat{\sigma}_l^z \rangle}{2} \right) \\ &\quad + i \frac{g}{2} \sum_{j \neq l} \cos(\delta_j t) \langle \hat{\sigma}_j^+ \hat{\sigma}_l^- \rangle, \end{aligned} \quad (6.40a)$$

$$\frac{d}{dt} \langle \hat{\sigma}_j^+ \hat{\sigma}_l^- \rangle = -w \langle \hat{\sigma}_j^+ \hat{\sigma}_l^- \rangle + i \frac{g}{2} \left( \cos(\delta_l t) \langle \hat{\sigma}_l^z \rangle \langle \hat{\sigma}_j^+ \hat{a} \rangle - \cos(\delta_j t) \langle \hat{\sigma}_j^z \rangle \langle \hat{a}^\dagger \hat{\sigma}_l^- \rangle \right), \quad (6.40b)$$

$$\frac{d}{dt} \langle \hat{\sigma}_l^z \rangle = w(1 - \langle \hat{\sigma}_l^z \rangle) + ig(\mathcal{X}_l - \mathcal{X}_l^*), \quad (6.40c)$$

$$\frac{d}{dt} \langle \hat{a}^\dagger \hat{a} \rangle = -\kappa \langle \hat{a}^\dagger \hat{a} \rangle - i \frac{g}{2} \sum_j (\mathcal{X}_j - \mathcal{X}_j^*), \quad (6.40d)$$

where  $\mathcal{X}_j = \langle \hat{a}^\dagger \hat{\sigma}_j^- \rangle \cos(\delta_j t)$  and  $\kappa' = (\kappa + w)/2$ . In the adiabatic region where  $w \gg \delta_j$ , we obtain from Eq. (6.40b) the spin-spin correlation

$$\langle \hat{\sigma}_j^+ \hat{\sigma}_l^- \rangle \approx i \frac{g}{2w} \left( \cos(\delta_l t) \langle \hat{\sigma}_l^z \rangle \mathcal{X}_j^* / \cos(\delta_j t) - \cos(\delta_j t) \langle \hat{\sigma}_j^z \rangle \mathcal{X}_l / \cos(\delta_l t) \right). \quad (6.41)$$

Plugging it into Eq. (6.40a) in the steady state,

$$\mathcal{X}_l \approx \sum_{j \neq l} \frac{g^2}{4w(\kappa' - i\Delta)} \left( \cos^2(\delta_j t) \langle \hat{\sigma}_j^z \rangle \mathcal{X}_l - \cos^2(\delta_l t) \langle \hat{\sigma}_l^z \rangle \mathcal{X}_j^* \right), \quad (6.42)$$

where we have dropped the single-atom terms in Eq. (6.40a), because the collective terms dominate in the steady-state superradiance for many atoms [93].

For further simplification, we define the average of a quantity  $q$  in terms of ensemble average  $\langle q \rangle_E = \sum_{j=1}^N q_j / N$  and time average in steady state  $\bar{q}$ . By assuming the ergodicity of the system,  $\langle q \rangle_E = \bar{q}$ . Performing time average on both sides of Eq. (6.42), we end up with a simple equation

$$\langle \mathcal{X} \rangle_E \approx \frac{Ng^2 \langle \hat{\sigma}^z \rangle_E}{8w(\kappa' - i\Delta)} (\langle \mathcal{X} \rangle_E - \langle \mathcal{X}^* \rangle_E). \quad (6.43)$$

The approximation employed here is that

$$\begin{aligned} \langle \cos^2(\delta_j t) \langle \hat{\sigma}_j^z \rangle \rangle_E &= \sum_{j=1}^N \cos^2(\delta_j t) \langle \hat{\sigma}_j^z \rangle / N \approx \frac{1}{2} \langle \hat{\sigma}^z \rangle_E, \\ \overline{\cos^2(\delta_l t) \langle \hat{\sigma}_l^z \rangle} &\approx \frac{1}{2} \langle \hat{\sigma}^z \rangle_E, \end{aligned} \quad (6.44)$$

assuming homogeneous density distribution of atoms. Furthermore, from Eq. (6.40c), we have

$$w(\langle \hat{\sigma}^z \rangle_E - 1) = ig(\langle \mathcal{X} \rangle_E - \langle \mathcal{X}^* \rangle_E). \quad (6.45)$$

For convenience, we introduce a real quantity  $\langle \hat{\sigma}^+ \hat{\sigma}^- \rangle_E$ ,

$$\langle \mathcal{X} \rangle_E = \frac{iNg}{2} \frac{1}{\kappa' - i\Delta} \langle \hat{\sigma}^+ \hat{\sigma}^- \rangle_E. \quad (6.46)$$

Solving Eq. (6.43) and Eq. (6.45), we finally obtain in the steady state

$$\langle \hat{\sigma}^z \rangle_E = \frac{2w\kappa}{Ng^2} \frac{\kappa'^2 + \Delta^2}{\kappa'^2} \approx \frac{2w}{N\gamma_C}, \quad \langle \hat{\sigma}^+ \hat{\sigma}^- \rangle_E \approx \frac{1}{4} \langle \hat{\sigma}^z \rangle_E (1 - \langle \hat{\sigma}^z \rangle_E), \quad \langle \hat{a}^\dagger \hat{a} \rangle = \frac{N^2 \gamma_C \langle \hat{\sigma}^+ \hat{\sigma}^- \rangle_E}{\kappa}. \quad (6.47)$$

$\langle \hat{\sigma}^+ \hat{\sigma}^- \rangle_E$  can be understood as the averaged spin-spin correlation, because

$$\langle \hat{\sigma}^+ \hat{\sigma}^- \rangle_E = \langle \hat{J}^+ \hat{J}^- \rangle / N^2. \quad (6.48)$$

We now proceed to calculate the average frictional force on a single atom (labeled by 1) moving in a large ensemble of atoms in steady state. From Eq. (6.39), this force is

$$f_1 = \hbar k g \text{Re}[(\mathcal{S} - \mathcal{R})/2i]. \quad (6.49)$$

where  $\mathcal{S} = \langle \hat{a}^\dagger \hat{\sigma}_1^- \rangle e^{i\delta_1 t}$  and  $\mathcal{R} = \langle \hat{a}^\dagger \hat{\sigma}_1^- \rangle e^{-i\delta_1 t}$ . The equation of motion for  $\mathcal{S}$  is

$$\frac{d}{dt} \mathcal{S} = i\delta_1 \mathcal{S} + e^{i\delta_1 t} \frac{d}{dt} \langle \hat{a}^\dagger \hat{\sigma}_j^- \rangle \approx i\delta_1 \mathcal{S} - (\kappa' - i\Delta) \mathcal{S} + i\frac{g}{2} \sum_{j \neq l} \cos(\delta_j t) e^{i\delta_1 t} \langle \hat{\sigma}_j^+ \hat{\sigma}_1^- \rangle, \quad (6.50)$$

where we once again omit the single-atom terms. Since we only care about the average frictional force in the steady state, this would require that  $e^{i\delta_1 t} \langle \hat{\sigma}_j^+ \hat{\sigma}_1^- \rangle$  is in steady state, *i.e.*

$$0 = \frac{d}{dt} \langle \hat{\sigma}_j^+ \hat{\sigma}_1^- \rangle e^{i\delta_1 t} = -(w - i\delta_1) \langle \hat{\sigma}_j^+ \hat{\sigma}_1^- \rangle e^{i\delta_1 t} + e^{i\delta_1 t} i\frac{g}{2} \left( \cos(\delta_1 t) \langle \hat{\sigma}_1^z \rangle \mathcal{X}_j^* / \cos(\delta_j t) - \cos(\delta_j t) \langle \hat{\sigma}_j^z \rangle x_1 / \cos(\delta_1 t) \right). \quad (6.51)$$

Solving the above equation for  $\langle \hat{\sigma}_j^+ \hat{\sigma}_1^- \rangle e^{i\delta_1 t}$  and plugging the result into Eq. (6.50), we can get

$$\frac{d}{dt} \mathcal{S} = -(\kappa' - i\Delta - i\delta_1) \mathcal{S} + \frac{g^2}{4(w - i\delta_1)} \sum_{j \neq l} \cos^2(\delta_j t) \langle \hat{\sigma}_j^z \rangle \mathcal{S} - e^{i\delta_1 t} \cos(\delta_1 t) \langle \hat{\sigma}_1^z \rangle \mathcal{X}_j^*. \quad (6.52)$$

Invoking the approximation in Eq. (6.44), we end up with a simple equation for  $\mathcal{S}$

$$(\kappa' - i\Delta - i\delta_1) \mathcal{S} \approx \frac{Ng^2 \langle \hat{\sigma}^z \rangle_E}{8(w - i\delta_1)} (\mathcal{S} - \langle \mathcal{X}^* \rangle_E). \quad (6.53)$$

Similarly, for  $\mathcal{R}$

$$(\kappa' - i\Delta + i\delta_1) \mathcal{R} \approx \frac{Ng^2 \langle \hat{\sigma}^z \rangle_E}{8(w + i\delta_1)} (\mathcal{R} - \langle \mathcal{X}^* \rangle_E). \quad (6.54)$$

Plugging  $\mathcal{S}$  and  $\mathcal{R}$  into Eq. (6.49),

$$f_1 \approx -\hbar k g^2 \frac{\delta_1 \Delta \kappa' / 2}{(\kappa'^2 + \Delta^2)^2} \frac{4\kappa'}{w} N \langle \hat{\sigma}^+ \hat{\sigma}^- \rangle_E. \quad (6.55)$$

In deriving the above equation, we only keep terms to the first order in  $\delta_1/w$ . Recall the one-atom friction coefficient  $\alpha_1$  in Eq. (6.34)

$$\alpha_1 = \gamma_C \sin^2(kx_1) \eta \langle \hat{\sigma}_1^+ \hat{\sigma}_1^- \rangle. \quad (6.56)$$

Therefore, the average  $\langle \alpha_1 \rangle = \gamma_C \eta \langle \hat{\sigma}_1^+ \hat{\sigma}_1^- \rangle / 2$ , and

$$f_1 \approx -\langle \alpha_1 \rangle p_1 \cdot \frac{\kappa}{w} \frac{N \langle \hat{\sigma}^+ \hat{\sigma}^- \rangle_E}{\langle \hat{\sigma}_1^+ \hat{\sigma}_1^- \rangle / 2}, \quad (6.57)$$

where we can identify a significant enhancement of the friction by a factor  $\frac{\kappa}{w} \frac{N \langle \hat{\sigma}^+ \hat{\sigma}^- \rangle_E}{\langle \hat{\sigma}_1^+ \hat{\sigma}_1^- \rangle}$ . Because

$$\frac{N \langle \hat{\sigma}^+ \hat{\sigma}^- \rangle_E}{\langle \hat{\sigma}_1^+ \hat{\sigma}_1^- \rangle / 2} = \frac{\gamma_C \langle \hat{J}^+ \hat{J}^- \rangle / N}{\gamma_C \langle \hat{\sigma}_1^+ \hat{\sigma}_1^- \rangle / 2}, \quad (6.58)$$

the enhancement is due to increased single-atom photon emission rate by superradiance and the factor  $\kappa/w$ . Plugging in  $w$ , we immediately see a great increase of the average frictional force on a single atom by a factor of order  $\kappa/\gamma_C$ . Note also that  $\langle \hat{\sigma}^+ \hat{\sigma}^- \rangle_E$  should have finite value, or else there would be no superradiant emission.

From Eq. (6.57), we find a significantly increased friction coefficient for the many-atom laser cooling case due to both the increased photon emission rate due to superradiance (*i.e.*  $N \langle \hat{\sigma}^+ \hat{\sigma}^- \rangle_E \gg \langle \hat{\sigma}_1^+ \hat{\sigma}_1^- \rangle / 2$ ) and the large ratio  $\kappa/w$ . The friction coefficient is enhanced by a factor of  $\kappa/\gamma_C$  compared to the one-atom case. This is consistent with the reduction of the order of the final temperature from the one to many atom case from  $\kappa$  to  $\gamma_C$ .

So far our discussion has neglected the recoil associated with repumping. We have done that because its effect on the final temperature will depend crucially on specifics of its implementation, including factors such as the polarizations and directions of repump lasers, the atomic system, and the transitions used. However, in the specific repumping model shown in Fig. 6.2, the magnitude of  $k'$  controls the recoil effect of the repumping on the momentum diffusion. Fig. 6.5(b) shows the final momentum width as a function of repumping for  $k' = 0$  and  $k' = k$ . Again, in the region of small and large repumping, where spin-spin correlations are very small, the final temperature is high. When the recoil due to repumping is included, the final temperature becomes higher and is eventually determined by  $w\bar{u}^2$ . However for weak repumping, with  $w$  not significantly larger than  $\gamma_C$  it is still possible to achieve temperatures not much higher than that predicted when pump recoil was neglected. This is especially promising for the implementation of supercooling in realistic experimental systems. Note that  $k = k'$  is more or less a worst case scenario, since by

using a dipole allowed transition for the relaxation from the auxiliary state to the excited state, one could in principle use a much reduced frequency with correspondingly small recoil.

To summarize, we have proposed supercooling of the atomic motion along the axis of an optical cavity. The superradiant emission was observed to lead to an enhanced cooling rate and extremely low final temperature. The ultimate temperatures were constrained by the relaxation of the atomic dipole, and may be orders of magnitude lower than for single atom cooling where temperatures are limited by the cavity linewidth. From a broader viewpoint, we have demonstrated an example of many-body laser cooling in which all motional degrees of freedom of a collective system are simultaneously cooled and in which macroscopic spin-spin correlations are essential and must develop for the cooling mechanism to work.

## Chapter 7

### Summary and outlook

Time and frequency are the most accurately measured physical quantities so far. State-of-the-art optical lattice clocks achieve accuracy in the realm of  $10^{-18}$  [9, 49]. Up to now, all these high-precision optical clocks are passive frequency standards, where the frequency of a narrow linewidth laser (local oscillator), stabilized to an ultrastable optical resonator, is used for the interrogation of trapped ions or neutral atoms [60]. In these systems, the optical resonator undergoes unavoidable thermal vibrations of the dielectric coatings on the cavity mirrors [65], giving rise to frequency fluctuations of the local oscillator. Instability of the local oscillator is one of the main limiting factors for the short-term stability of modern optical clocks [83]. Improvement may be attained by minimizing the thermal vibration of the reference cavity [22] or by locking the local oscillator to another reference that is more stable than the reference cavity. A promising candidate for this reference is an active optical frequency standard. For example, in the microwave domain, the Hydrogen maser is used as a flywheel for the Caesium timekeeping system. In the optical domain, there is still no working system whose stability could compete with the stability provided by the reference cavity [60]. The steady-state superradiant laser offers such potential, which is supported by what we have done in this thesis. The synchronization and supercooling mechanism revealed in this thesis lay the theoretical foundation for an active frequency standard. Combined with the recent demonstration of Dicke superradiance on the clock transition of strontium atoms in an optical cavity [99], an eventual experimental realization of the superradiant laser may be on the horizon.

## Bibliography

- [1] J. A. Acebrón, L. L. Bonilla, C. J. Pérez Vicente, F. Ritort, and R. Spigler. The kuramoto model: A simple paradigm for synchronization phenomena. Rev. Mod. Phys., 77:137–185, Apr 2005.
- [2] A. André, A. S. Sørensen, and M. D. Lukin. Stability of atomic clocks based on entangled atoms. Phys. Rev. Lett., 92:230801, Jun 2004.
- [3] J. Appel, P. J. Windpassinger, D. Oblak, U. B. Hoff, N. Kjørgaard, and E. S. Polzik. Mesoscopic atomic entanglement for precision measurements beyond the standard quantum limit. Proceedings of the National Academy of Sciences, 106(27):10960–10965, 2009.
- [4] F. T. Arecchi, E. Courtens, R. Gilmore, and H. Thomas. Atomic coherent states in quantum optics. Phys. Rev. A, 6:2211–2237, Dec 1972.
- [5] K. J. Arnold, M. P. Baden, and M. D. Barrett. Self-organization threshold scaling for thermal atoms coupled to a cavity. Phys. Rev. Lett., 109:153002, Oct 2012.
- [6] A. Bauch. Caesium atomic clocks: function, performance and applications. Measurement Science and Technology, 14(8):1159, 2003.
- [7] C. Benkert, M. O. Scully, J. Bergou, L. Davidovich, M. Hillery, and M. Orszag. Role of pumping statistics in laser dynamics: Quantum langevin approach. Phys. Rev. A, 41:2756–2765, Mar 1990.
- [8] I. Bloch, J. Dalibard, and W. Zwerger. Many-body physics with ultracold gases. Rev. Mod. Phys., 80:885–964, Jul 2008.
- [9] B. J. Bloom, T. L. Nicholson, J. R. Williams, S. L. Campbell, M. Bishof, X. Zhang, W. Zhang, S. L. Bromley, and J. Ye. An optical lattice clock with accuracy and stability at the  $10^{-18}$  level. Nature, 506:71–75, Feb 2014.
- [10] J. G. Bohnet, Z. Chen, J. M. Weiner, K. C. Cox, and J. K. Thompson. Relaxation oscillations, stability, and cavity feedback in a superradiant raman laser. Phys. Rev. Lett., 109:253602, Dec 2012.
- [11] J. G. Bohnet, Z. Chen, J. M. Weiner, K. C. Cox, and J. K. Thompson. Active and passive sensing of collective atomic coherence in a superradiant laser. Phys. Rev. A, 88:013826, Jul 2013.

- [12] J. G. Bohnet, Z. Chen, J. M. Weiner, D. Meiser, M. J. Holland, and J. K. Thompson. A steady-state superradiant laser with less than one intracavity photon. Nature, 484(7392):78–81, Apr 2012.
- [13] R. Bonifacio, P. Schwendimann, and F. Haake. Quantum statistical theory of superradiance: I. Phys. Rev. A, 4:302–313, Jul 1971.
- [14] C. J. Bordé. Base units of the si, fundamental constants and modern quantum physics. Philosophical Transactions of the Royal Society of London A: Mathematical, Physical and Engineering Sciences, 363(1834):2177–2201, 2005.
- [15] J. Borregaard, P. Kómár, E. M. Kessler, A. S. Sørensen, and M. D. Lukin. Heralded quantum gates with integrated error detection in optical cavities. Phys. Rev. Lett., 114:110502, Mar 2015.
- [16] S. Bregni. Synchronization of Digital Telecommunications Networks. Wiley, Chichester, 2002.
- [17] H. W. Chan, A. T. Black, and V. Vuletić. Observation of collective-emission-induced cooling of atoms in an optical cavity. Phys. Rev. Lett., 90:063003, Feb 2003.
- [18] J. Chen. Active optical clock. Chinese Science Bulletin, 54:348–352, 2009.
- [19] Z. Chen, J. G. Bohnet, S. R. Sankar, J. Dai, and J. K. Thompson. Conditional spin squeezing of a large ensemble via the vacuum rabi splitting. Phys. Rev. Lett., 106:133601, Mar 2011.
- [20] C. W. Chou, D. B. Hume, T. Rosenband, and D. J. Wineland. Optical clocks and relativity. Science, 329(5999):1630–1633, 2010.
- [21] Y. Chu and M. D. Lukin. Quantum optics with nitrogen-vacancy centers in diamond. arXiv:1504.05990, Apr 2015.
- [22] G. D. Cole, W. Zhang, M. J. Martin, J. Ye, and M. Aspelmeyer. Tenfold reduction of brownian noise in high-reflectivity optical coatings. Nat Photon, 7(8):644–650, Aug 2013.
- [23] M. C. Cross, A. Zumdieck, Ron Lifshitz, and J. L. Rogers. Synchronization by nonlinear frequency pulling. Phys. Rev. Lett., 93:224101, Nov 2004.
- [24] J. Dalibard, Y. Castin, and K. Mølmer. Wave-function approach to dissipative processes in quantum optics. Phys. Rev. Lett., 68:580–583, Feb 1992.
- [25] E. G. Dalla Torre, J. Otterbach, E. Demler, V. Vuletić, and M. D. Lukin. Dissipative preparation of spin squeezed atomic ensembles in a steady state. Phys. Rev. Lett., 110:120402, Mar 2013.
- [26] A. Derevianko and M. Pospelov. Hunting for topological dark matter with atomic clocks. Nat Phys, 10(12):933–936, Dec 2014.
- [27] C. Deutsch, F. Ramirez-Martinez, C. Lacroûte, F. Reinhard, T. Schneider, J. N. Fuchs, F. Piéchon, F. Laloë, J. Reichel, and P. Rosenbusch. Spin self-rephasing and very long coherence times in a trapped atomic ensemble. Phys. Rev. Lett., 105:020401, Jul 2010.
- [28] R. H. Dicke. Coherence in spontaneous radiation processes. Phys. Rev., 93:99–110, Jan 1954.

- [29] S. Diehl, A. Micheli, A. Kantian, B. Kraus, H. P. Buchler, and P. Zoller. Quantum states and phases in driven open quantum systems with cold atoms. Nat Phys, 4(11):878–883, Nov 2008.
- [30] S. Diehl, A. Tomadin, A. Micheli, R. Fazio, and P. Zoller. Dynamical phase transitions and instabilities in open atomic many-body systems. Phys. Rev. Lett., 105:015702, Jul 2010.
- [31] P. Domokos and H. Ritsch. Collective cooling and self-organization of atoms in a cavity. Phys. Rev. Lett., 89:253003, Dec 2002.
- [32] P. Domokos and H. Ritsch. Mechanical effects of light in optical resonators. J. Opt. Soc. Am. B, 20(5):1098–1130, May 2003.
- [33] R. Dum, P. Zoller, and H. Ritsch. Monte carlo simulation of the atomic master equation for spontaneous emission. Phys. Rev. A, 45:4879–4887, Apr 1992.
- [34] J. Esteve, C. Gross, A. Weller, S. Giovanazzi, and M. K. Oberthaler. Squeezing and entanglement in a bose-einstein condensate. Nature, 455(7217):1216–1219, Oct 2008.
- [35] L. J. Fiderer, M. Kuš, and D. Braun. Quantum-phase synchronization. arXiv:1511.04309v1, Nov 2015.
- [36] C. Gardiner and P. Zoller. Quantum Noise. Springer-Verlag Berlin Heidelberg, 2004.
- [37] A. Goban, C.-L. Hung, J. D. Hood, S.-P. Yu, J. A. Muniz, O. Painter, and H. J. Kimble. Superradiance for atoms trapped along a photonic crystal waveguide. Phys. Rev. Lett., 115:063601, Aug 2015.
- [38] S. Gopalakrishnan, B. L. Lev, and P. M. Goldbart. Emergent crystallinity and frustration with bose-einstein condensates in multimode cavities. Nat Phys, 5(11):845–850, Nov 2009.
- [39] S. Gopalakrishnan, B. L. Lev, and P. M. Goldbart. Frustration and glassiness in spin models with cavity-mediated interactions. Phys. Rev. Lett., 107:277201, Dec 2011.
- [40] P. W. Graham, J. M. Hogan, M. A. Kasevich, and S. Rajendran. New method for gravitational wave detection with atomic sensors. Phys. Rev. Lett., 110:171102, Apr 2013.
- [41] C. Gross, T. Zibold, E. Nicklas, J. Estève, and M. K. Oberthaler. Nonlinear atom interferometer surpasses classical precision limit. Nature, 464(7292):1165–1169, Apr 2010.
- [42] M. Gross and S. Haroche. Superradiance: An essay on the theory of collective spontaneous emission. Physics Reports, 93(5):301 – 396, 1982.
- [43] H. Haken. Theory of intensity and phase fluctuations of a homogeneously broadened laser. Zeitschrift für Physik, 190(3):327–356, Sep 1966.
- [44] H. Haken. Laser Theory. Springer, Berlin, 1984.
- [45] T. W. Hänsch and A. L. Schawlow. Cooling of gases by laser radiation. Optics Communications, 13(1):68 – 69, 1975.
- [46] S. Hartmann. Generalized dicke states. arXiv:1201.1732, Jan 2012.

- [47] G. Heinrich, M. Ludwig, J. Qian, B. Kubala, and F. Marquardt. Collective dynamics in optomechanical arrays. Phys. Rev. Lett., 107:043603, Jul 2011.
- [48] I. Hermoso de Mendoza, L. A. Pachón, J. Gómez-Gardeñes, and D. Zueco. Synchronization in a semiclassical kuramoto model. Phys. Rev. E, 90:052904, Nov 2014.
- [49] N. Hinkley, J. A. Sherman, N. B. Phillips, M. Schioppo, N. D. Lemke, K. Beloy, M. Pizzocaro, C. W. Oates, and A. D. Ludlow. An atomic clock with  $10^{-18}$  instability. Science, 341(6151):1215–1218, 2013.
- [50] C. A. Holmes, C. P. Meaney, and G. J. Milburn. Synchronization of many nanomechanical resonators coupled via a common cavity field. Phys. Rev. E, 85:066203, Jun 2012.
- [51] P. Horak, G. Hechenblaikner, K. M. Gheri, H. Stecher, and H. Ritsch. Cavity-induced atom cooling in the strong coupling regime. Phys. Rev. Lett., 79:4974–4977, Dec 1997.
- [52] B. Horstmann, J. I. Cirac, and G. Giedke. Noise-driven dynamics and phase transitions in fermionic systems. Phys. Rev. A, 87:012108, Jan 2013.
- [53] A. M. Hriscu and Y. V. Nazarov. Quantum synchronization of conjugated variables in a superconducting device leads to the fundamental resistance quantization. Phys. Rev. Lett., 110:097002, Feb 2013.
- [54] S. F. Huelga, C. Macchiavello, T. Pellizzari, A. K. Ekert, M. B. Plenio, and J. I. Cirac. Improvement of frequency standards with quantum entanglement. Phys. Rev. Lett., 79:3865–3868, Nov 1997.
- [55] S. F. Huelga, C. Macchiavello, T. Pellizzari, A. K. Ekert, M. B. Plenio, and J. I. Cirac. Improvement of frequency standards with quantum entanglement. Phys. Rev. Lett., 79:3865–3868, Nov 1997.
- [56] M. R. Hush, W. Li, S. Genway, I. Lesanovsky, and A. D. Armour. Spin correlations as a probe of quantum synchronization in trapped-ion phonon lasers. Phys. Rev. A, 91:061401, Jun 2015.
- [57] A. K. Jain, K. K. Likharev, J. E. Lukens, and J. E. Sauvageau. Mutual phase-locking in josephson junction arrays. Physics Reports, 109(6):309 – 426, 1984.
- [58] L. Jiang, G. K. Brennen, A. V. Gorshkov, K. Hammerer, M. Hafezi, E. Demler, M. D. Lukin, and P. Zoller. Anyonic interferometry and protected memories in atomic spin lattices. Nat Phys, 4(6):482–488, Jun 2008.
- [59] M. Kapitaniak, K. Czolczynski, P. Perlikowski, A. Stefanski, and T. Kapitaniak. Synchronization of clocks. Physics Reports, 517(12):1 – 69, 2012.
- [60] G. A. Kazakov and T. Schumm. Active optical frequency standards using cold atoms: Perspectives and challenges. In European Frequency and Time Forum (EFTF), 2014, pages 411–414, June 2014.
- [61] E. M. Kessler, G. Giedke, A. Imamoglu, S. F. Yelin, M. D. Lukin, and J. I. Cirac. Dissipative phase transition in a central spin system. Phys. Rev. A, 86:012116, Jul 2012.

- [62] E. M. Kessler, S. Yelin, M. D. Lukin, J. I. Cirac, and G. Giedke. Optical superradiance from nuclear spin environment of single-photon emitters. Phys. Rev. Lett., 104:143601, Apr 2010.
- [63] N. Kiesel, F. Blaser, U. Delić, D. Grass, R. Kaltenbaek, and M. Aspelmeyer. Cavity cooling of an optically levitated submicron particle. Proceedings of the National Academy of Sciences, 110(35):14180–14185, 2013.
- [64] H. J. Kimble. Strong interactions of single atoms and photons in cavity qed. Physica Scripta, 1998(T76):127, 1998.
- [65] H. J. Kimble, Benjamin L. Lev, and Jun Ye. Optical interferometers with reduced sensitivity to thermal noise. Phys. Rev. Lett., 101:260602, Dec 2008.
- [66] M. Kitagawa and M. Ueda. Squeezed spin states. Phys. Rev. A, 47:5138–5143, Jun 1993.
- [67] G. Kleine Büning, J. Will, W. Ertmer, E. Rasel, J. Arlt, C. Klempt, F. Ramirez-Martinez, F. Piéchon, and P. Rosenbusch. Extended coherence time on the clock transition of optically trapped rubidium. Phys. Rev. Lett., 106:240801, Jun 2011.
- [68] O. Kogan, J. L. Rogers, M. C. Cross, and G. Refael. Renormalization group approach to oscillator synchronization. Phys. Rev. E, 80:036206, Sep 2009.
- [69] M. I. Kolobov, L. Davidovich, E. Giacobino, and C. Fabre. Role of pumping statistics and dynamics of atomic polarization in quantum fluctuations of laser sources. Phys. Rev. A, 47:1431–1446, Feb 1993.
- [70] Y. Kuramoto. International Symposium on Mathematical Problems in Theoretical Physics, volume 39. Springer-Verlag, Berlin, 1975.
- [71] Y. Kuramoto. Chemical Oscillations, Waves and Turbulence. Courier Dover Publications, 2003.
- [72] T. E. Lee, C.-K. Chan, and S. Wang. Entanglement tongue and quantum synchronization of disordered oscillators. Phys. Rev. E, 89:022913, Feb 2014.
- [73] T. E. Lee and M. C. Cross. Quantum-classical transition of correlations of two coupled cavities. Phys. Rev. A, 88:013834, Jul 2013.
- [74] T. E. Lee, H. Häffner, and M. C. Cross. Collective quantum jumps of rydberg atoms. Phys. Rev. Lett., 108:023602, Jan 2012.
- [75] T. E. Lee and H. R. Sadeghpour. Quantum synchronization of quantum van der pol oscillators with trapped ions. Phys. Rev. Lett., 111:234101, Dec 2013.
- [76] D. Leibfried, M. D. Barrett, T. Schaetz, J. Britton, J. Chiaverini, W. M. Itano, J. D. Jost, C. Langer, and D. J. Wineland. Toward heisenberg-limited spectroscopy with multiparticle entangled states. Science, 304(5676):1476–1478, 2004.
- [77] D. Leibfried, R. Blatt, C. Monroe, and D. Wineland. Quantum dynamics of single trapped ions. Rev. Mod. Phys., 75:281–324, Mar 2003.
- [78] D. R. Leibbrandt, J. Labaziewicz, V. Vuletić, and I. L. Chuang. Cavity sideband cooling of a single trapped ion. Phys. Rev. Lett., 103:103001, Aug 2009.

- [79] B. L. Lev, A. Vukics, E. R. Hudson, B. C. Sawyer, P. Domokos, H. Ritsch, and J. Ye. Prospects for the cavity-assisted laser cooling of molecules. Phys. Rev. A, 77:023402, Feb 2008.
- [80] G. Lindblad. On the generators of quantum dynamical semigroups. Comm. Math. Phys., 48(2):119–130, 1976.
- [81] W. H. Louisell. Quantum statistical properties of radiation. John Wiley & Sons Canada, Limited, 1973.
- [82] E. Lucero, R. Barends, Y. Chen, J. Kelly, M. Mariantoni, A. Megrant, P. O’Malley, D. Sank, A. Vainsencher, J. Wenner, T. White, Y. Yin, A. N. Cleland, and J. M. Martinis. Computing prime factors with a josephson phase qubit quantum processor. Nat Phys, 8(10):719–723, Oct 2012.
- [83] A. D. Ludlow, M. M. Boyd, J. Ye, E. Peik, and P. O. Schmidt. Optical atomic clocks. Rev. Mod. Phys., 87:637–701, Jun 2015.
- [84] X.-S. Ma, T. Herbst, T. Scheidl, D. Wang, S. Kropatschek, W. Naylor, B. Wittmann, A. Mech, J. Kofler, E. Anisimova, V. Makarov, T. Jennewein, R. Ursin, and A. Zeilinger. Quantum teleportation over 143 kilometres using active feed-forward. Nature, 489(7415):269–273, Sep 2012.
- [85] T. H. Maiman. Stimulated optical radiation in ruby. Nature, 187(4736):493–494, Aug 1960.
- [86] G. Manzano, F. Galve, G. L. Giorgi, E. Hernández-García, and R. Zambrini. Synchronization, quantum correlations and entanglement in oscillator networks. Scientific Reports, 3:1439, Mar 2013.
- [87] A. Mari, A. Farace, N. Didier, V. Giovannetti, and R. Fazio. Measures of quantum synchronization in continuous variable systems. Phys. Rev. Lett., 111:103605, Sep 2013.
- [88] M. J. Martin, M. Bishof, M. D. Swallows, X. Zhang, C. Benko, J. von Stecher, A. V. Gorshkov, A. M. Rey, and Jun Ye. A quantum many-body spin system in an optical lattice clock. Science, 341(6146):632–636, 2013.
- [89] P. Maunz, T. Puppe, I. Schuster, N. Syassen, P. W. H. Pinkse, and G. Rempe. Cavity cooling of a single atom. Nature, 428(6978):50–52, Mar 2004.
- [90] J. McKeever, J. R. Buck, A. D. Boozer, A. Kuzmich, H.-C. Nägerl, D. M. Stamper-Kurn, and H. J. Kimble. State-insensitive cooling and trapping of single atoms in an optical cavity. Phys. Rev. Lett., 90:133602, Apr 2003.
- [91] D. Meiser and M. J. Holland. Intensity fluctuations in steady-state superradiance. Phys. Rev. A, 81:063827, Jun 2010.
- [92] D. Meiser and M. J. Holland. Steady-state superradiance with alkaline-earth-metal atoms. Phys. Rev. A, 81:033847, Mar 2010.
- [93] D. Meiser, Jun Ye, D. R. Carlson, and M. J. Holland. Prospects for a millihertz-linewidth laser. Phys. Rev. Lett., 102:163601, Apr 2009.

- [94] I. B. Mekhov, C. Maschler, and H. Ritsch. Probing quantum phases of ultracold atoms in optical lattices by transmission spectra in cavity quantum electrodynamics. *Nat Phys*, 3(5):319–323, May 2007.
- [95] P. Meystre and M. Sargent III. *Elements of Quantum Optics*. Springer, New York, 1998.
- [96] J. Millen, P. Z. G. Fonseca, T. Mavrogordatos, T. S. Monteiro, and P. F. Barker. Cavity cooling a single charged levitated nanosphere. *Phys. Rev. Lett.*, 114:123602, Mar 2015.
- [97] G. Morigi, P. W. H. Pinkse, M. Kowalewski, and R. de Vivie-Riedle. Cavity cooling of internal molecular motion. *Phys. Rev. Lett.*, 99:073001, Aug 2007.
- [98] D. Nagy, G. Szirmai, and P. Domokos. Critical exponent of a quantum-noise-driven phase transition: The open-system dicke model. *Phys. Rev. A*, 84:043637, Oct 2011.
- [99] M. A. Norcia, M. N. Winchester, J. R. K. Cline, and J. K. Thompson. Superradiance on the millihertz linewidth strontium clock transition. arXiv:1603.05671, Mar 2016.
- [100] L. Ostermann, H. Ritsch, and C. Genes. Protected state enhanced quantum metrology with interacting two-level ensembles. *Phys. Rev. Lett.*, 111:123601, Sep 2013.
- [101] W. Pfeifer. *The Lie algebras SU(N)*. Birkhäuser Verlag, 2003.
- [102] H. Pichler, T. Ramos, A. J. Daley, and P. Zoller. Quantum optics of chiral spin networks. *Phys. Rev. A*, 91:042116, Apr 2015.
- [103] A. Pikovsky, M. Rosenblum, and J. Kurths. *Synchronization: A Universal Concept in Nonlinear Sciences*. Cambridge University Press, Cambridge, England, 2001.
- [104] M. B. Plenio and P. L. Knight. The quantum-jump approach to dissipative dynamics in quantum optics. *Rev. Mod. Phys.*, 70:101–144, Jan 1998.
- [105] N. F. Ramsey. *Molecular Beams*. Oxford University, New York, 1956.
- [106] A. M. Rey, A. V. Gorshkov, C. V. Kraus, M. J. Martin, M. Bishof, M. D. Swallows, X. Zhang, C. Benko, J. Ye, N. D. Lemke, and A. D. Ludlow. Probing many-body interactions in an optical lattice clock. *Annals of Physics*, 340(1):311 – 351, 2014.
- [107] M. F. Riedel, P. Böhi, Y. Li, T. W. Hänsch, A. Sinatra, and P. Treutlein. Atom-chip-based generation of entanglement for quantum metrology. *Nature*, 464(7292):1170–1173, Apr 2010.
- [108] H. Ritsch, P. Domokos, F. Brennecke, and T. Esslinger. Cold atoms in cavity-generated dynamical optical potentials. *Rev. Mod. Phys.*, 85:553–601, Apr 2013.
- [109] S. Ritter, C. Nolleke, C. Hahn, A. Reiserer, A. Neuzner, M. Uphoff, M. Mücke, E. Figueroa, J. Bochmann, and G. Rempe. An elementary quantum network of single atoms in optical cavities. *Nature*, 484(7393):195–200, Apr 2012.
- [110] G. R. M. Robb, N. Piovella, A. Ferraro, R. Bonifacio, Ph. W. Courteille, and C. Zimmermann. Collective atomic recoil lasing including friction and diffusion effects. *Phys. Rev. A*, 69:041403, Apr 2004.

- [111] T. Rosenband, D. B. Hume, P. O. Schmidt, C. W. Chou, A. Brusch, L. Lorini, W. H. Oskay, R. E. Drullinger, T. M. Fortier, J. E. Stalnaker, S. A. Diddams, W. C. Swann, N. R. Newbury, W. M. Itano, D. J. Wineland, and J. C. Bergquist. Frequency ratio of  $\text{al}^+$  and  $\text{hg}^+$  single-ion optical clocks; metrology at the 17th decimal place. Science, 319(5871):1808–1812, 2008.
- [112] T. Salzburger and H. Ritsch. Lasing and cooling in a finite-temperature cavity. Phys. Rev. A, 74:033806, Sep 2006.
- [113] A. L. Schawlow and C. H. Townes. Infrared and optical masers. Phys. Rev., 112:1940–1949, Dec 1958.
- [114] M. Scheibner, T. Schmidt, L. Worschech, A. Forchel, G. Bacher, T. Passow, and D. Hommel. Superradiance of quantum dots. Nat Phys, 3(2):106–110, Feb 2007.
- [115] M. H. Schleier-Smith, I. D. Leroux, and V. Vuletić. States of an ensemble of two-level atoms with reduced quantum uncertainty. Phys. Rev. Lett., 104:073604, Feb 2010.
- [116] M. H. Schleier-Smith, I. D. Leroux, H. Zhang, M. A. Van Camp, and V. Vuletić. Optomechanical cavity cooling of an atomic ensemble. Phys. Rev. Lett., 107:143005, Sep 2011.
- [117] S. Schütz, H. Habibian, and G. Morigi. Cooling of atomic ensembles in optical cavities: Semiclassical limit. Phys. Rev. A, 88:033427, Sep 2013.
- [118] S. Schütz and G. Morigi. Prethermalization of atoms due to photon-mediated long-range interactions. Phys. Rev. Lett., 113:203002, Nov 2014.
- [119] P. Strack and S. Sachdev. Dicke quantum spin glass of atoms and photons. Phys. Rev. Lett., 107:277202, Dec 2011.
- [120] S. H. Strogatz. From kuramoto to crawford: exploring the onset of synchronization in populations of coupled oscillators. Physica D: Nonlinear Phenomena, 143(14):1 – 20, 2000.
- [121] S. H. Strogatz. Sync: The Emerging Science of Spontaneous Order. Hyperion, New York, 2003.
- [122] A. Tomadin, S. Diehl, and P. Zoller. Nonequilibrium phase diagram of a driven and dissipative many-body system. Phys. Rev. A, 83:013611, Jan 2011.
- [123] C. von Cube, S. Slama, D. Kruse, C. Zimmermann, Ph. W. Courteille, G. R. M. Robb, N. Piovella, and R. Bonifacio. Self-synchronization and dissipation-induced threshold in collective atomic recoil lasing. Phys. Rev. Lett., 93:083601, Aug 2004.
- [124] J. Vuckovic. Quantum optics and cavity qed with quantum dots in photonic crystals. arXiv:1402.2541, Feb 2014.
- [125] V. Vuletić and S. Chu. Laser cooling of atoms, ions, or molecules by coherent scattering. Phys. Rev. Lett., 84:3787–3790, Apr 2000.
- [126] I. A. Walmsley. Quantum optics: Science and technology in a new light. Science, 348(6234):525–530, 2015.
- [127] S. Walter, A. Nunnenkamp, and C. Bruder. Quantum synchronization of a driven self-sustained oscillator. Phys. Rev. Lett., 112:094102, Mar 2014.

- [128] S. Walter, A. Nunnenkamp, and C. Bruder. Quantum synchronization of two van der pol oscillators. Annalen der Physik, 527(1-2):131–138, 2015.
- [129] C. E. Wieman, D. E. Pritchard, and D. J. Wineland. Atom cooling, trapping, and quantum manipulation. Rev. Mod. Phys., 71:S253–S262, Mar 1999.
- [130] K. Wiesenfeld, P. Colet, and S. H. Strogatz. Synchronization transitions in a disordered josephson series array. Phys. Rev. Lett., 76:404–407, Jan 1996.
- [131] D. J. Wineland. Nobel lecture: Superposition, entanglement, and raising schrödinger’s cat. Rev. Mod. Phys., 85:1103–1114, Jul 2013.
- [132] D. J. Wineland, J. J. Bollinger, W. M. Itano, and D. J. Heinzen. Squeezed atomic states and projection noise in spectroscopy. Phys. Rev. A, 50:67–88, Jul 1994.
- [133] D. J. Wineland, J. J. Bollinger, W. M. Itano, F. L. Moore, and D. J. Heinzen. Spin squeezing and reduced quantum noise in spectroscopy. Phys. Rev. A, 46:R6797–R6800, Dec 1992.
- [134] D. J. Wineland and Wayne M. Itano. Laser cooling of atoms. Phys. Rev. A, 20:1521–1540, Oct 1979.
- [135] A. T. Winfree. Biological rhythms and the behavior of populations of coupled oscillators. Journal of Theoretical Biology, 16(1):15 – 42, 1967.
- [136] H. M. Wiseman and G. J. Milburn. Interpretation of quantum jump and diffusion processes illustrated on the bloch sphere. Phys. Rev. A, 47:1652–1666, Mar 1993.
- [137] H. M. Wiseman and G. J. Milburn. Quantum theory of field-quadrature measurements. Phys. Rev. A, 47:642–662, Jan 1993.
- [138] H. M. Wiseman and G. J. Milburn. Quantum Measurement and Control. Cambridge University Press, 2009.
- [139] M. Wolke, J. Klinner, H. Keßler, and A. Hemmerich. Cavity cooling below the recoil limit. Science, 337(6090):75–78, 2012.
- [140] Minghui Xu and M. J. Holland. Conditional ramsey spectroscopy with synchronized atoms. Phys. Rev. Lett., 114:103601, Mar 2015.
- [141] Minghui Xu, S. B. Jäger, S. Schütz, J. Cooper, G. Morigi, and M. J. Holland. Supercooling of atoms in an optical resonator. Phys. Rev. Lett., 116:153002, Apr 2016.
- [142] Minghui Xu, D. A. Tieri, E. C. Fine, James K. Thompson, and M. J. Holland. Synchronization of two ensembles of atoms. Phys. Rev. Lett., 113:154101, Oct 2014.
- [143] Minghui Xu, D. A. Tieri, and M. J. Holland. Simulating open quantum systems by applying  $su(4)$  to quantum master equations. Phys. Rev. A, 87:062101, Jun 2013.
- [144] N. Xu, J. Zhu, D. Lu, X. Zhou, X. Peng, and J. Du. Quantum factorization of 143 on a dipolar-coupling nuclear magnetic resonance system. Phys. Rev. Lett., 108:130501, Mar 2012.

- [145] J. Yin, J.-G. Ren, H. Lu, Y. Cao, H.-L. Yong, Y.-P. Wu, C. Liu, S.-K. Liao, F. Zhou, Y. Jiang, X.-D. Cai, P. Xu, G.-S. Pan, J.-J. Jia, Y.-M. Huang, H. Yin, J.-Y. Wang, Y.-A. Chen, C.-Z. Peng, and J.-W. Pan. Quantum teleportation and entanglement distribution over 100-kilometre free-space channels. Nature, 488(7410):185–188, Aug 2012.
- [146] J. Q. You and F. Nori. Atomic physics and quantum optics using superconducting circuits. Nature, 474(7353):589–597, Jun 2011.
- [147] O. V. Zhirov and D. L. Shepelyansky. Quantum synchronization and entanglement of two qubits coupled to a driven dissipative resonator. Phys. Rev. B, 80:014519, Jul 2009.

## Appendix A

### Adiabatic elimination

There is a systematic way to perform adiabatic elimination of fast variables. Suppose we have an differential equation such as

$$\frac{d}{dt}y(t) = -(\kappa/2 + i\Delta)y(t) + x(t). \quad (\text{A.1})$$

The formal solution to it is

$$y(t) = e^{-(\kappa/2+i\Delta)t}y(0) + \int_0^t ds e^{-(\kappa/2+i\Delta)s}x(t-s). \quad (\text{A.2})$$

Under the approximation of coarse graining ( $\kappa$  is large), *i.e.*,  $t \gg \kappa^{-1}$ , we have

$$\begin{aligned} y(t) &\approx \int_0^t ds e^{-(\kappa/2+i\Delta)s}x(t-s) \\ &\approx \int_0^t ds \left[ x(t) - x'(t)s + \frac{1}{2!}x''(t)s^2 \dots \right] e^{-(\kappa/2+i\Delta)s} \\ &= \frac{1}{(\kappa/2 + i\Delta)}x(t) - \frac{1}{(\kappa/2 + i\Delta)^2}x'(t) + \frac{1}{(\kappa/2 + i\Delta)^3}x''(t) + \dots \end{aligned} \quad (\text{A.3})$$

We can see that it is a systematic expansion with respect to  $1/\kappa$ . As a result, we can approximate  $y(t)$  in terms of  $x(t)$  and its time derivatives. To the first order,  $y(t)$  is locked to  $x(t)$ .

When  $x(t)$  contains the noise term such as  $\sqrt{\kappa}\hat{\xi}_\kappa(t)$  with  $\langle \hat{\xi}_\kappa(t)\hat{\xi}_\kappa^\dagger(t') \rangle = \delta(t-t')$ , we need to deal with it separately. Following Eq. (A.3), the noise entering into  $y(t)$  is

$$\hat{\mathcal{F}}(t) = \int_0^t ds e^{-(\kappa/2+i\Delta)s} \sqrt{\kappa}\hat{\xi}_\kappa(t-s) = \int_0^t d\tau e^{-(\kappa/2+i\Delta)(t-\tau)} \sqrt{\kappa}\hat{\xi}_\kappa(\tau). \quad (\text{A.4})$$

It is obvious that  $\langle \hat{\mathcal{F}}(t) \rangle = 0$ . The non-zero second order correlation is

$$\begin{aligned}
\langle \hat{\mathcal{F}}(t) \hat{\mathcal{F}}^\dagger(t') \rangle &= \int_0^t d\tau_1 \int_0^{t'} d\tau_2 e^{-(\kappa/2+i\Delta)(t-\tau_1)} e^{-(\kappa/2-i\Delta)(t'-\tau_2)} \kappa \langle \hat{\xi}_\kappa(\tau_1) \hat{\xi}_\kappa^\dagger(\tau_2) \rangle \\
&= \int_0^t d\tau_1 \int_0^{t'} d\tau_2 e^{-(\kappa/2+i\Delta)(t-\tau_1)} e^{-(\kappa/2-i\Delta)(t'-\tau_2)} \kappa \delta(\tau_1 - \tau_2), \\
&= e^{-\kappa(t+t')/2-i\Delta(t-t')} \int_0^t d\tau_1 \int_0^{t'} d\tau_2 \kappa e^{\kappa/2(\tau_1+\tau_2)+i\Delta(\tau_1-\tau_2)} \delta(\tau_1 - \tau_2) \\
&\approx e^{-\kappa|t'-t|/2-i\Delta(t-t')}
\end{aligned} \tag{A.5}$$

Let us now examine the function  $f(\tau) = e^{-\kappa|\tau|/2-i\Delta\tau}$ . We first notice that

$$\int_{-\infty}^{\infty} d\tau f(\tau) = \frac{1}{\kappa/2+i\Delta} + \frac{1}{\kappa/2-i\Delta} = \frac{\kappa}{\kappa^2/4+\Delta^2}. \tag{A.6}$$

Therefore,

$$\frac{\kappa^2/4+\Delta^2}{\kappa} e^{-\kappa|\tau|/2-i\Delta\tau} = \delta(\tau), \quad \kappa \gg \tau^{-1}. \tag{A.7}$$

As a result,

$$\langle \hat{\mathcal{F}}(t) \hat{\mathcal{F}}^\dagger(t') \rangle = \frac{\kappa}{\kappa^2/4+\Delta^2} \delta(t-t'). \tag{A.8}$$

We can then choose

$$\hat{\mathcal{F}}(t) = \frac{e^{i\theta} \sqrt{\kappa}}{\kappa/2+i\Delta} \hat{\xi}(t), \tag{A.9}$$

where  $\theta$  is an arbitrary phase and  $\hat{\xi}(t)$  is the normal white noise satisfying  $\langle \hat{\xi}(t) \hat{\xi}^\dagger(t') \rangle = \delta(t-t')$ .

## Appendix B

### $SU(4)$ generators and $\lambda$ -matrices

The hermitian  $4 \times 4$  matrix generators of  $SU(4)$  group, analogous to the Pauli matrices of  $SU(2)$  group are [101]:

$$\begin{aligned} \lambda_1 &= \begin{pmatrix} 0 & 1 & 0 & 0 \\ 1 & 0 & 0 & 0 \\ 0 & 0 & 0 & 0 \\ 0 & 0 & 0 & 0 \end{pmatrix}, & \lambda_2 &= \begin{pmatrix} 0 & -i & 0 & 0 \\ i & 0 & 0 & 0 \\ 0 & 0 & 0 & 0 \\ 0 & 0 & 0 & 0 \end{pmatrix}, & \lambda_3 &= \begin{pmatrix} 1 & 0 & 0 & 0 \\ 0 & -1 & 0 & 0 \\ 0 & 0 & 0 & 0 \\ 0 & 0 & 0 & 0 \end{pmatrix}, \\ \lambda_4 &= \begin{pmatrix} 0 & 0 & 1 & 0 \\ 0 & 0 & 0 & 0 \\ 1 & 0 & 0 & 0 \\ 0 & 0 & 0 & 0 \end{pmatrix}, & \lambda_5 &= \begin{pmatrix} 0 & 0 & -i & 0 \\ 0 & 0 & 0 & 0 \\ i & 0 & 0 & 0 \\ 0 & 0 & 0 & 0 \end{pmatrix}, & \lambda_6 &= \begin{pmatrix} 0 & 0 & 0 & 0 \\ 0 & 0 & 1 & 0 \\ 0 & 1 & 0 & 0 \\ 0 & 0 & 0 & 0 \end{pmatrix}, \\ \lambda_7 &= \begin{pmatrix} 0 & 0 & 0 & 0 \\ 0 & 0 & -i & 0 \\ 0 & i & 0 & 0 \\ 0 & 0 & 0 & 0 \end{pmatrix}, & \lambda_8 &= \frac{1}{\sqrt{3}} \begin{pmatrix} 1 & 0 & 0 & 0 \\ 0 & 1 & 0 & 0 \\ 0 & 0 & -2 & 0 \\ 0 & 0 & 0 & 0 \end{pmatrix}, & \lambda_9 &= \begin{pmatrix} 0 & 0 & 0 & 1 \\ 0 & 0 & 0 & 0 \\ 0 & 0 & 0 & 0 \\ 1 & 0 & 0 & 0 \end{pmatrix}, \end{aligned}$$

$$\begin{aligned}
\lambda_{10} &= \begin{pmatrix} 0 & 0 & 0 & -i \\ 0 & 0 & 0 & 0 \\ 0 & 0 & 0 & 0 \\ i & 0 & 0 & 0 \end{pmatrix}, & \lambda_{11} &= \begin{pmatrix} 0 & 0 & 0 & 0 \\ 0 & 0 & 0 & 1 \\ 0 & 0 & 0 & 0 \\ 0 & 1 & 0 & 0 \end{pmatrix}, & \lambda_{12} &= \begin{pmatrix} 0 & 0 & 0 & 0 \\ 0 & 0 & 0 & -i \\ 0 & 0 & 0 & 0 \\ 0 & i & 0 & 0 \end{pmatrix}, \\
\lambda_{13} &= \begin{pmatrix} 0 & 0 & 0 & 0 \\ 0 & 0 & 0 & 0 \\ 0 & 0 & 0 & 1 \\ 0 & 0 & 1 & 0 \end{pmatrix}, & \lambda_{14} &= \begin{pmatrix} 0 & 0 & 0 & 0 \\ 0 & 0 & 0 & 0 \\ 0 & 0 & 0 & -i \\ 0 & 0 & i & 0 \end{pmatrix}, & \lambda_{15} &= \frac{1}{\sqrt{6}} \begin{pmatrix} 1 & 0 & 0 & 0 \\ 0 & 1 & 0 & 0 \\ 0 & 0 & 1 & 0 \\ 0 & 0 & 0 & -3 \end{pmatrix}.
\end{aligned}$$

The  $\lambda$  matrices are traceless, orthogonal and satisfy

$$\text{Tr}(\lambda_\mu)^2 = 2, \quad \mu = 1, \dots, 15.$$

## Appendix C

### $|S, M\rangle\langle S, M'|$ representation

In order to project the density operator from the  $SU(4)$  basis onto the  $|S, M\rangle\langle S, M'|$  representation, let us first show that  $M$  and  $M'$  are related to the  $P_{q,q_3,\sigma_3}^{(s)}$  by  $q_3 + \sigma_3 = M$  and  $q_3 - \sigma_3 = M'$ . To see this, defining  $\hat{J}_3 = \sum_{j=1}^N \sigma_j^{(3)}/2$ , we could get

$$\begin{aligned}\hat{J}_3 P_{q,q_3,\sigma_3}^{(s)} &= \frac{1}{2}(\alpha + \gamma - \beta - \delta)P_{q,q_3,\sigma_3}^{(s)} = (q_3 + \sigma_3)P_{q,q_3,\sigma_3}^{(s)}, \\ P_{q,q_3,\sigma_3}^{(s)} \hat{J}_3 &= \frac{1}{2}(\alpha + \delta - \beta - \gamma)P_{q,q_3,\sigma_3}^{(s)} = (q_3 - \sigma_3)P_{q,q_3,\sigma_3}^{(s)},\end{aligned}\tag{C.1}$$

and by definition, we have

$$\begin{aligned}\hat{J}_3 |S, M\rangle\langle S, M'| &= M |S, M\rangle\langle S, M'|, \\ |S, M\rangle\langle S, M'| \hat{J}_3 &= M' |S, M\rangle\langle S, M'|.\end{aligned}\tag{C.2}$$

Therefore, the complex coefficients from the  $P_{q,q_3,\sigma_3}^{(s)}$  basis contributing to the matrix element for  $|S, M\rangle\langle S, M'|$  all satisfy  $q_3 + \sigma_3 = M$  and  $q_3 - \sigma_3 = M'$ .

With this in mind, we now describe a systematic algorithm to obtain the density matrix elements  $D_{S,M,M'}^{m,n}$  from the  $SU(4)$  expansion coefficients  $C_{q,q_3,\sigma_3}^{m,n}$ . We illustrate our method by considering in detail the elementary case of three atoms. The density matrix in the  $|S, M\rangle\langle S, M'|$  representation is block diagonal in  $S$ ; the block matrices for all  $S$  can be arranged in the shape of a pyramid as shown in Fig. 3.1(c). For instance, the base layer corresponds to  $S = N/2$ , with the matrix dimension being  $(N + 1)^2$ . The second layer has  $S = N/2 - 1$  and dimension  $(N - 1)^2$ , and so on. Furthermore there are  $n_S$  copies associated with each layer, so that  $\sum_S (2S + 1)n_S = 2^N$ . Taking  $N = 3$  for example, there are two layers,  $S = 3/2$  and  $S = 1/2$  with  $n_{3/2} = 1$  and  $n_{1/2} = 2$ , so that the Hilbert space dimension is  $(3 + 1) + 2 \times (1 + 1) = 2^3$ .

The density matrix needs to be built from the bottom layer upwards. In the bottom layer, we find that the only element contributing to  $|N/2, N/2\rangle\langle N/2, N/2|$  is  $P_{N/2, N/2, 0}^{(s)}$ . So the top left corner is  $D_{N/2, N/2, N/2}^{m, n} = C_{N/2, N/2, 0}^{m, n}$ . We next apply the lowering operator  $\hat{J}_- = \sum_{j=1}^N \sigma_j^-$  to iteratively generate  $D_{N/2, N/2, M}^{m, n}$ , with  $M = N/2 - 1, \dots, -N/2$ . To do this, we need the recursion relation

$$\begin{aligned} D_{S, M, M'-1}^{m, n} &= \langle S, M | \rho^{m, n} \hat{J}_- | S, M' \rangle = \frac{\langle S, M | \rho^{m, n} \hat{J}_- | S, M' \rangle}{\sqrt{(S+M')(S-M'+1)}} \\ &= \frac{\langle S, M | (\mathcal{U}_+ + \mathcal{V}_+) \rho^{m, n} | S, M' \rangle}{\sqrt{(S+M')(S-M'+1)}}. \end{aligned} \quad (\text{C.3})$$

Therefore, with the actions of the raising and lowering operators [Eq. (3.12)], we can derive all  $D_{N/2, N/2, M'}^{m, n}$ , *i.e.* the first row of the bottom layer. Using the fact that the density matrix is Hermitian and  $C_{q, q_3, \sigma_3}^{m, n} = (C_{q, q_3, -\sigma_3}^{m, n})^*$ , we could get all the elements for the first column by  $D_{N/2, M', N/2}^{m, n} = (D_{N/2, N/2, M'}^{m, n})^*$ . By repeatedly applying the recursion relation [Eq. (C.3)] in each row, we then construct the full base layer. As an explicit example, we have constructed the bottom layer, *i.e.*  $S = 3/2$  for the three atom case,

$$\begin{array}{l} \left. \begin{array}{l} |\frac{3}{2}, \frac{3}{2}\rangle \\ |\frac{3}{2}, \frac{1}{2}\rangle \\ |\frac{3}{2}, -\frac{1}{2}\rangle \\ |\frac{3}{2}, -\frac{3}{2}\rangle \end{array} \right\} \left( \begin{array}{cccc} \langle \frac{3}{2}, \frac{3}{2} | & \langle \frac{3}{2}, \frac{1}{2} | & \langle \frac{3}{2}, -\frac{1}{2} | & \langle \frac{3}{2}, -\frac{3}{2} | \\ C_{3/2, 3/2, 0}^{m, n} & \frac{C_{1, 1, 1/2}^{m, n}}{\sqrt{3}} & \frac{C_{1/2, 1/2, 1}^{m, n}}{\sqrt{3}} & C_{0, 0, 3/2}^{m, n} \\ \frac{C_{1, 1, -1/2}^{m, n}}{\sqrt{3}} & \frac{C_{3/2, 1/2, 0}^{m, n} + C_{1/2, 1/2, 0}^{m, n}}{3} & \frac{C_{1, 0, 1/2}^{m, n} + C_{0, 0, 1/2}^{m, n}}{3} & \frac{C_{1/2, -1/2, 1}^{m, n}}{\sqrt{3}} \\ \frac{C_{1/2, 1/2, -1}^{m, n}}{\sqrt{3}} & \frac{C_{1, 0, -1/2}^{m, n} + C_{0, 0, -1/2}^{m, n}}{3} & \frac{C_{3/2, -1/2, 0}^{m, n} + C_{1/2, -1/2, 0}^{m, n}}{3} & \frac{C_{1, -1, 1/2}^{m, n}}{\sqrt{3}} \\ C_{0, 0, -3/2}^{m, n} & \frac{C_{1/2, -1/2, -1}^{m, n}}{\sqrt{3}} & \frac{C_{1, -1, -1/2}^{m, n}}{\sqrt{3}} & C_{3/2, -3/2, 0}^{m, n} \end{array} \right). \quad (\text{C.4}) \end{array}$$

In order to illustrate the use of the recursion relation, we now show how to get  $D_{3/2, 1/2, 1/2}^{m, n}$  from  $D_{3/2, 1/2, 3/2}^{m, n}$ . Because  $\mathcal{V}_+ P_{3/2, 1/2, 0}^{(s)} = P_{1, 1, -1/2}^{(s)}$  and  $\mathcal{U}_+ P_{1/2, 1/2, 0}^{(s)} = P_{1, 1, -1/2}^{(s)}$ , we have  $D_{3/2, 1/2, 1/2}^{m, n} = (C_{3/2, 1/2, 0}^{m, n} + C_{1/2, 1/2, 0}^{m, n})/\sqrt{3}/\sqrt{3}$ .

To construct the next layer, we thus find out the top left matrix element first, and then apply the same procedure as before to determine the rest of the matrix elements. Let us first examine the three atom case. The  $S = 1/2$  layer has two copies, each of which is a  $2 \times 2$  matrix. To find the top left element  $D_{1/2, 1/2, 1/2}^{m, n}$ , noticing the constraint imposed by the trace of the density matrix, we derive  $2D_{1/2, 1/2, 1/2}^{m, n} + D_{3/2, 1/2, 1/2}^{m, n} = C_{3/2, 1/2, 0}^{m, n}$  so that  $D_{1/2, 1/2, 1/2}^{m, n} = (2C_{3/2, 1/2, 0}^{m, n} - C_{1/2, 1/2, 0}^{m, n})/6$ . By

applying the same method as in the bottom layer, we construct the block matrix for  $S = 1/2$  layer

$$\begin{matrix} & \langle \frac{1}{2}, \frac{1}{2} | & \langle \frac{1}{2}, -\frac{1}{2} | \\ \begin{matrix} |\frac{1}{2}, \frac{1}{2}\rangle \\ |\frac{1}{2}, -\frac{1}{2}\rangle \end{matrix} & \begin{pmatrix} \frac{2C_{3/2,1/2,0}^{m,n} - C_{1/2,1/2,0}^{m,n}}{6} & \frac{C_{1,0,1/2}^{m,n} - 2C_{0,0,1/2}^{m,n}}{6} \\ \frac{C_{1,0,-1/2}^{m,n} - 2C_{0,0,-1/2}^{m,n}}{6} & \frac{2C_{3/2,-1/2,0}^{m,n} - C_{1/2,-1/2,0}^{m,n}}{6} \end{pmatrix} \end{matrix}. \quad (\text{C.5})$$

Therefore in general, if we suppose that we have constructed the block matrix for  $S' > S$ , the formula to find the top left matrix element  $D_{S',S,S}^{m,n}$  for layer  $S$  is

$$\sum_{S \leq S' \leq N/2} n_{S'} D_{S',S,S}^{m,n} = C_{N/2,S,0}^{m,n}. \quad (\text{C.6})$$

Having the top left matrix element for each layer  $S$ , we can easily construct the  $(2S+1) \times (2S+1)$  block matrix by applying the recursion relation based on the angular momentum lowering operator. Repeated iteration of these steps systematically fills in all sites of the pyramid.